TECHNISCHE UNIVERSITÄT WIEN
Vienna University of Technology

DISSERTATION

Modelling and simulation of the impact behaviour of fibre reinforced laminates and components

ausgeführt zum Zwecke der Erlangung des akademischen Grades eines Doktors der technischen Wissenschaften unter der Leitung von

Assoc.Prof. Dipl.-Ing. Dr.techn. Heinz Pettermann
E317
Institut für Leichtbau und Struktur-Biomechanik

eingereicht an der Technischen Universität Wien
Fakultät für Maschinenwesen und Betriebswissenschaften

von

Dipl.-Ing. Martin Schwab
Matrikelnummer 0825772
Eduard Pichlerstrasse 3
3860 Heidenreichstein

Wien, im Oktober 2016 Martin Schwab

Acknowledgment

This work was carried out in the course of my employment at the Institute of Lightweight Design and Structural Biomechanics (ILSB) at the Vienna University of Technology. The funding within the framework of the TAKE OFF program by the Austrian Research Promotion Agency (FFG) and the Austrian Federal Ministry for Transport, Innovation and Technology is gratefully acknowledged. The experiments used for the verifications in the present work have been conducted at the Polymer Competence Center Leoben (Leoben, Austria), where the specimens have been provided by FACC AG (Ried im Innkreis, Austria). The valuable collaboration is gratefully acknowledged.

I want to express my deepest gratitude to my thesis advisor, Prof. Heinz Pettermann, for his valuable support during all stages of this work. His positive attitude always encouraged me and the numerous discussions helped me to reflect critically and develop new ideas. Furthermore, I thank Prof. Clara Schuecker and Prof. Thomas Antretter for acting as reviewers of my thesis.

I would like to express my gratitude to all members of the ILSB, and especially to Prof. Helmut J. Böhm and Prof. Franz G. Rammerstorfer as heads of the institute, for creating such a friendly and supportive work environment. Special thanks go to my colleagues Jakob Gager, Martin Springer and Melanie Todt who contributed to this work in many fruitful discussions.

Finally, I want to thank my family and friends for their support and, especially Christina for being part of my life.

Contents

Abstract

The aim of the present work is to develop modelling strategies by means of advanced methods within the framework of the Finite Element Method (FEM), which are capable of predicting the impact behaviour of fabric reinforced laminated composites. Not only the total energy absorption of the laminate, but also the share of energy absorbed by individual mechanisms is predicted, where fibre rupture, matrix cracking, delamination and the accumulation of inelastic strains are considered. Within the present work, mainly high energy impact scenarios with intermediate impact velocities are considered. Hence, a dynamic impact response and penetration of the laminate are expected. Modelling strategies at different geometrical length scales are developed which on the one hand, aim at gaining a detailed insight into the impact behaviour of fabric reinforced laminates and on the other hand, aim at simulating the impact behaviour of entire composite components.

A shell element based modelling strategy, which resolves the fabric topology at the level of individual tows (i.e. impregnated bundles of fibres) is developed. It proves to be efficient enough to conduct simulations of the highly dynamic, nonlinear behaviour of fabric reinforced composite coupon specimens under impact loading within reasonable computational resources. The modelling approach is verified based on experimental drop weight impact tests of carbon/epoxy laminates carried out by co-operation partners. Very good agreement between the simulation results and the experimental data is found. Furthermore, the predictions give detailed insight into the impact behaviour of fabric reinforced composites.

Also, a ply-level based strategy for modelling and simulating the impact behaviour of fabric reinforced laminates up to complete perforation is developed. Special attention is directed towards numerical efficiency in order to open up the possibility for simulating impact on structural components much larger than coupon specimens within reasonable computation time. The modelling approach is verified based on experimental drop weight impact tests of carbon/epoxy laminates carried out by cooperation partners. The predicted damage and failure behaviour is in very close agreement with the experimental observations. Furthermore, the approach is found to be of exceptional numerical efficiency. A detailed comparison of the predicted energy absorption behaviour between the ply-level and the tow-level modelling approach is conducted in order to evaluate the effect of different modelling length scales.

Finally, a modelling approach for simulating the impact behaviour of large laminated composite components impacted by large deformable bodies within reasonable computation time and resources is presented. Another focus is set on the simulation of high energy impact on glass fabric reinforced epoxy laminates up to complete perforation. Thereby, the developed ply-level modelling approach is used in combination with an embedding approach. In a first step, the applicability of the ply-level approach to the simulation of high energy impact on glass/epoxy laminates is verified based on a comparison with experimental drop weight impact tests carried out by cooperation partners. Then, to demonstrate an application, two configurations of a generic composite fan containment casing of a jet engine subjected to fan blade out are investigated, where detailed insight into the components' behaviour during the fan blade out event is gained.

Kurzfassung

Das Ziel dieser Arbeit besteht in der Entwicklung von Modellierungsstrategien mittels fortgeschrittener Methoden im Rahmen der Finiten Elemente Methode, die es ermöglichen, das Ein- und Durchschlagverhalten von gewebeverstärkten laminierten Verbundwerkstoffen vorherzusagen. Dabei soll neben der gesamten Energieabsorption des Laminats auch deren Aufteilung auf einzelne Mechanismen vorhergesagt werden, wobei Faserbruch, Zwischenfaserbruch, Delamination und die Akkumulation inelastischer Verzerrungen betrachtet werden. Innerhalb der vorliegenden Arbeit werden hauptsächlich Hochenergie-Einschläge im mittleren Geschwindigkeitsbereich betrachtet. Folglich werden ein dynamisches Einschlagverhalten und eine Durchdringung des Laminats erwartet. Es werden Modellierungsstrategien auf unterschiedlichen Längenskalen entwickelt um, zum einen, einen detaillierten Einblick in das Ein- und Durchschlagverhalten von gewebeverstärkten Laminaten zu gewinnen und, zum anderen, das Einschlagverhalten von ganzen Bauteilen aus Verbundwerkstoffen zu simulieren.

Es wird eine auf Schalenelementen basierende Modellierungsstrategie entwickelt, welche die Gewebetopologie auf der Ebene einzelner Faserbündel auflöst. Diese erweist sich als effizient genug, um Simulationen des hoch dynamischen, nichtlinearen Verhaltens von gewebeverstärkten Probenkörpern unter Einschlagbelastungen im Rahmen eines vernünftigen Rechenaufwands durchzuführen. Der Modellierungsansatz wird basierend auf experimentellen Fallgewicht-Einschlagtests auf Kohlefaser/Epoxy Laminaten, welche bei Kooperationspartnern durchgeführt werden, verifiziert. Es wird

eine sehr gute Übereinstimmung zwischen den Simulationsergebnissen und den experimentellen Daten festgestellt. Darüberhinaus geben die Vorhersagen einen detaillierten Einblick in das Ein- und Durchschlagverhalten von gewebeverstärkten Verbundwerkstoffen.

Außerdem wird eine auf Ebene der Laminat-Einzellagen basierende Strategie zur Modellierung und Simulation des Ein- und Durchschlagverhaltens von gewebeverstärkten Laminaten bis hin zur kompletten Durchlöcherung entwickelt. Besonderes Augenmerk wird auf die numerische Effizienz gerichtet, um die Möglichkeit der Simulation von Einschlagvorgängen auf strukturelle Bauteile innerhalb vernünftigen Rechenaufwands zu eröffnen. Der Modellierungsansatz wird basierend auf experimentellen Fallgewicht-Einschlagtests auf Kohlefaser/Epoxy Laminaten, welche bei Kooperationspartnern durchgeführt werden, verifiziert. Das vorhergesagte Schädigungs- und Versagensverhalten ist in sehr enger Übereinstimmung mit den experimentellen Beobachtungen. Darüberhinaus erweist sich dieser Modellierungsansatz als numerisch äußerst effizient. Ein ausführlicher Vergleich des Energieabsorptionsverhaltens zwischen dem Einzellagen- und dem Faserbündel-Modellierungsansatz wird durchgeführt um den Einfluss unterschiedlicher Modellierungs-Längenskalen zu beurteilen.

Schließlich wird ein Modellierungsansatz zur Simulation des Ein- und Durchschlagverhaltens von großen laminierten Verbundwerkstoff-Bauteilen innerhalb einer vernünftigen Rechenzeit vorgestellt. Ein weiterer Schwerpunkt liegt auf der Simulation von Hochenergie-Einschlägen auf glasfasergewebeverstärkten Epoxy Laminaten bis hin zur kompletten Durchlöcherung. Dabei wird der entwickelte Einzellagen-Modellierungsansatz mit einem Einbettungsansatz kombiniert. In einem ersten Schritt wird die Anwendbarkeit des Einzellagen-Ansatzes zur Simulation von Hochenergie-Einschlägen auf Glasfaser/Epoxy Laminate basierend auf Vergleichen mit experimentellen Fallgewicht-Einschlagtests, welche bei Kooperationspartnern durchgeführt werden, überprüft. Darauffolgend werden, als Beispiel einer Anwendung, zwei Konfigurationen eines generischen *fan containment casing* eines Flugzeug-Triebwerks untersucht, welche einem *fan blade out* Lastfall unterzogen werden. Dabei wird eine tiefe Einsicht in das Bauteilverhalten während des *fan blade out* gewonnen.

Chapter 1

Introduction

Laminated composites built from fibre reinforced polymers (FRPs) are widely used within the aerospace and other industries, as their high stiffness to weight and strength to weight ratios are key features for lightweight design. Moreover, these materials exhibit good environmental and fatigue resistance and are easy to form during manufacturing. Considering modern passenger aircrafts as e.g. the Airbus A350 and the Boeing 787, a huge amount of structural components is entirely made up of laminated FRPs. In order to design such components, proper knowledge of the (nonlinear) mechanical behaviour of laminated FRPs under a variety of load cases is required. In this respect, the damage tolerance and the energy absorption behaviour of composite components subjected to impact loads represent important design criteria. Laminated FRP composites exhibit a complex damage and failure behaviour with various modes of failure, such as fibre rupture, matrix cracking, plasticity-like effects and debonding of plies. During impact all of these mechanisms are likely to occur. The present work proposes modelling strategies by means of advanced methods within the framework of the Finite Element Method (FEM) for simulating the impact response of fibre reinforced laminates and components. The presented simulations allow for a detailed assessment of the extent of individual mechanisms and, therefore, give detailed insight into the impact behaviour of laminated FRPs.

1.1 Length scales

Fibre reinforced polymer composites, in general, consist of two different constituents, i.e. the reinforcement (fibres) and the matrix (polymer), where various types of fibre arrangements (i.e. reinforcement styles) are established within engineering applications. Typical reinforcement styles are unidirectionally oriented fibres or interwoven bundles of fibres (i.e. weaves, fabrics). Such planar reinforcements are combined with the matrix material in order to form thin layers (plies). A laminated FRP composite is made up of several plies which are stacked on top of each other.

Within the present work, the hierarchical structure of laminated FRPs is subdivided by the following length scales. The smallest considered length scale in the case of fabric reinforced composites is represented by the topology and the dimensions of the interwoven bundles of fibres. As these bundles of fibres are often referred to as tows, this length scale is denoted the *tow-scale* within the present work. A level higher, individual layers (i.e. plies, laminae) within the laminated composite are considered as homogeneous. This length scale is denoted *ply-scale* or *lamina-scale* within the present work. The largest considered length scale is represented by the dimensions of entire coupon specimens or components and is referred to as *component-scale*.

1.2 General impact behaviour of composites

Impact on laminated composites has been studied extensively in the last decades, where some major topics of research in this area may be found in the comprehensive reviews [1, 2, 31]. More recent reviews on this topic have been conducted in Refs. [14, 42]. The textbook [4] also provides a comprehensive overview on the topic. Considering transverse impact scenarios, the structural response differs depending on the impact velocity, the masses of impactor and target and the material properties. Very short impact durations, in general, lead to responses dominated by stress wave propagation in the thickness direction. Such scenarios are commonly denoted

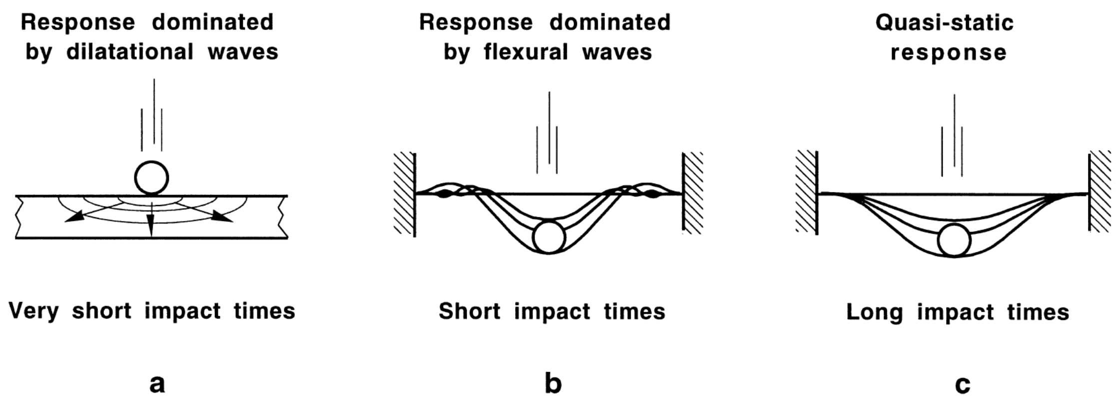

Figure 1.1: Schematic illustration of the different types of impact responses. Taken from Ref. [100]

as high velocity impacts (HVI), cf. Fig. 1.1a. Quasi-static like responses, on the other hand, are observed for very long impact durations, where these situations are often denoted as low velocity impacts (LVI), cf. Fig. 1.1c. In the transition between these two scenarios the response is dominated by flexural waves, cf. Fig. 1.1b.

Several criteria have been proposed to identify the occurring response type, for example the one presented in Refs. [43, 112],

$$v_0 = c\varepsilon_{\mathrm{f}} \quad , \tag{1.1}$$

which gives an estimate on the transition impact velocity, v_0, based on the through-thickness speed of sound of the considered material, c, and the failure strain of the material, ε_{f}. Impact velocities which are significantly lower than the transition velocity are supposed to lead to LVI like responses whereas impact velocities which are significantly higher than the transition velocity are supposed to lead to HVI like responses. Assuming a failure strain of $\varepsilon_{\mathrm{f}} = 1\%$ this criterion gives the transition to stress wave dominated responses at impact velocities above 20 m/s for common epoxy composites.

Another criterion presented in Ref. [100] states that the impact response is governed by the ratio of impactor and target mass. The paper [100] states limiting mass ratios for distinguishing between large (quasi-static like), intermediate and small mass (wave controlled) impact situations.

1.3 Scope of the present work

The aim of the present work is to develop modelling strategies, by means of advanced methods within the framework of the Finite Element Method (FEM), which are capable of predicting the impact behaviour of fabric reinforced laminated composites. Not only the total energy absorption of the laminate, but also the share of energy absorbed by individual mechanisms shall be predicted, where fibre rupture, matrix cracking, delamination and the accumulation of inelastic strains (i.e. plasticity like effects) are considered. Within the present work, mainly high energy impact scenarios with intermediate impact velocities are considered. Hence, a dynamic response dominated by flexural waves, cf. Fig. 1.1, and penetration of the laminate are expected.

In Chapter 2 a literature review on the topic of impact on composite laminates is conducted. The first part focuses on experimental investigations of the impact behaviour of laminated fibre reinforced composites. Observed differences in the damage and failure behaviour of laminates subjected to LVI and HVI are outlined. Moreover, investigations regarding the influence of various factors (e.g. reinforcement architecture, ply stacking sequence, hybridisation, etc.) on the impact behaviour of laminated composites are briefly summarised. The second part discusses the numerical modelling of the damage and failure behaviour of laminated composites subjected to impact loads by means of the FEM. There, a variety of constitutive laws designated for modelling the damage and failure behaviour of laminated composites are briefly summarised. Moreover, modelling strategies proposed in the literature for simulating impact on laminated composites are discussed.

In Chapter 3 a shell element based modelling strategy is developed, which resolves the fabric topology at the tow-level. It is efficient enough to allow for the simulation of the highly dynamic, nonlinear behaviour of fabric reinforced composite coupon specimens under impact loading within reasonable computational resources. The modelling approach is verified based on experimental drop weight impact tests of carbon/epoxy laminates carried out by cooperation partners, where very good agreement between the simulations results and the experimental data is found. Furthermore, the predictions give detailed insight into the impact behaviour of fabric reinforced composites.

In Chapter 4 a ply-level based strategy for modelling and simulating the intermediate velocity/mass impact behaviour of fabric reinforced laminates up to complete perforation is developed. Special attention is directed towards numerical efficiency in order to open up the possibility for simulating impact on structural components much larger than coupon specimens within reasonable computation time. The modelling approach is verified based on experimental drop weight impact tests of carbon/epoxy laminates carried out by cooperation partners, where the predicted damage and failure behaviour is in very close agreement with the experimental observations. Furthermore, the approach is found to be of exceptional numerical efficiency.

A detailed comparison of the predicted energy absorption behaviour between the ply-level and the tow-level modelling approach is conducted in Chapter 5.

Finally, Chapter 6 presents a modelling approach for simulating the impact behaviour of large laminated composite components impacted by large deformable bodies within reasonable computation time and resources. Another focus is set on the simulation of high energy impact on glass fibre fabric reinforced epoxy laminates up to complete perforation. Thereby, the ply-level modelling approach, cf. Chapter 4, is used in combination with an embedding approach. In a first step, the applicability of the ply-level approach to the simulation of high energy impact on glass/epoxy laminates is verified based on a comparison with experimental drop weight impact tests carried out by cooperation partners. Then, to demonstrate an application, two configurations of a generic composite fan containment casing of a jet engine subjected to fan blade out are investigated, where detailed insight into the components' behaviour during the fan blade out event is gained.

Chapter 2

Literature review

2.1 Impact behaviour of composites - Experimental investigations

In the following, experimental studies on the impact behaviour of laminated composites are briefly summarised. These studies include investigations on the damage and failure behaviour of laminated composites based on various material systems under various impact conditions, where the insights of each study into the impact behaviour are outlined.

A review on the LVI behaviour of composite materials is given in Ref. [111]. The typically occurring modes of failure for unidirectionally fibre reinforced laminates are discussed. Moreover, an overview of the influence of the composites constituents (i.e. fibres, matrix) on the impact response is given. For instance, it is stated that E-glass fibres absorb approximately three times the elastic energy of carbon fibres. The effect of strain rate sensitivity is also covered. Finally, a discussion of post-impact residual strength is given.

A comparison of the LVI and HVI behaviour of unidirectionally carbon fibre reinforced epoxy laminates can be found in [30]. The authors state that, in the case of LVI, the elastic energy absorbing capability of the impacted component and, thus, the component's size and shape determines its impact response. Conversely, in the case of HVI, the component's impact response is not governed by its areal size. In general, it is found that HVI is more detrimental to the integrity of a composite structure than LVI when comparing situations with similar impact energy.

In Ref. [125] an experimental investigation regarding the occurring damage within a unidirectionally carbon fibre reinforced epoxy cross-ply laminate subjected to LVI and HVI is conducted. Considering LVI, the laminate shows distributed delaminations and fibre fracture occurs at the laminate's back face due to the bending deformation. In the case of HVI, impact damage is found to be more localised and, at higher impact energies, a shear cone is formed.

The paper [133] investigates HVI damage in unidirectionally carbon fibre reinforced epoxy laminates, where impact velocities in the range from 200 m/s to 1000 m/s are considered. Moreover, the effect of various ply stacking sequences on the extent of damage and delaminations within the laminates is studied. The authors state that laminates with lower bending stiffness exhibit a smaller damaged area than laminates with higher bending stiffness.

A review on the influence of the reinforcement architecture on impact damage mechanisms and the post impact compression behaviour of fibre reinforced polymers is conducted in Ref. [21]. Thereby, unidirectional fibre reinforcement, woven fabrics, multiaxial fabrics, braids and knits are considered and the influence of the reinforcement type on the energy absorption and peak failure load is investigated. It is found that textile fibre reinforcements exhibit an especially beneficial post-impact compressive behaviour compared to unidirectional fibre reinforcement. The same authors conducted an experimental study on the compression after impact strength of non-crimp glass fibre epoxy laminates compared to undirectionally reinforced laminates and woven laminates, cf. [22].

Another experimental study regarding the influence of different reinforcement types on the impact behaviour of E-glass/epoxy laminates is reported in Ref. [123]. The authors compare the LVI damage characteristics of laminates with non-crimp fabric, woven fabric and nonwoven reinforcements, where several layups and laminate thicknesses are studied.

A comparison of impact and delamination failure in woven fabric and unidirectionally fibre reinforced composites is given in [78]. The authors state that woven composites exhibit higher interlaminar fracture toughnesses than unidirectionally reinforced composites. Considering the impact behaviour, the so-called ductility index, i.e. the ratio of energy absorbed after the peak load to the energy absorbed up to the peak load, is evaluated for woven fabric laminates and cross-ply laminates. It is found that the woven fabric laminates exhibit a significantly higher ductility index. Moreover, the compression after impact strength is found to be higher in the case of woven fabric laminates.

Experimental studies of the progression of LVI damage in woven E-glass composites under repeated drop weight impact loading are presented in Ref. [17]. Thereby, plain woven laminates, 3D orthogonally woven monoliths and biaxially reinforced warp knits are considered. It is observed that in the case of a 3D reinforcement the radial extent of damage is greater than for the other reinforcement types. Moreover, the 3D reinforced composite exhibits a greater perforation strength. It is stated that the energy is dissipated over a larger area in the case of this reinforcement type. The authors conducted similar investigations for woven S2-glass composites in Ref. [18], where qualitatively similar observations are made as in the case of woven E-glass composites.

Reference [49] studies the effect of glass fibre hybridisation on the LVI behaviour of woven carbon fibre/epoxy laminates. Different laminate thicknesses and glass fibre contents (up to 21 vol.%) are tested. Impact energies in the range from 30 J to 245 J are considered. It is found that the main deformation and damage mechanisms are independent of the presence of glass fibres. The maximum load during impact is controlled by tensile fracture of the bottom carbon ply and it is observed to be proportional to the square of the laminate thickness. A hybridisation with S2 glass fabric plies leads to increased maximum loads and higher energy absorption (25% increase for 21 vol.% hybridisation). The authors state that these trends are also maintained when the maximum load and the energy absorption are normalised by the areal density of the laminate.

The paper [119] investigates the LVI behaviour of plain woven hybrid glass-carbon/-epoxy laminates. Drop weight impact tests of four different laminate configurations are conducted. A non-hybrid glass/epoxy laminate, a non-hybrid carbon/epoxy laminate and two different hybrid laminates with either carbon skins and a glass core or vice versa are considered. It is observed that the non-hybrid glass/epoxy laminate shows the most resistance to impact while the non-hybrid carbon/epoxy laminate shows the least resistance to impact. The impact resistance of the two hybrid configurations is in between. The authors point out that hybrid laminates are especially prone to delamination due the inherent dissimilarity between plies of different material.

Reference [130] presents an experimental comparison of the LVI response of woven carbon fibre reinforced thermoplastic and thermosetting composites as well as a detailed description of their damage and failure behaviour. It is found that laminates with thermosetting polymer matrices experience larger delaminations than thermoplastic based laminates. The authors state that a tougher matrix, in general, leads to better impact performance.

The damage and failure behaviour of carbon fibre reinforced epoxy laminates subjected to LVI at low temperatures is investigated in Ref. [64]. Laminates with different stacking sequences and reinforcement type (i.e. unidirectional and woven) are tested at temperatures in the range from +20 °C to -150 °C. It is observed that the extent of damage within the laminate increases significantly when it is impacted at lower temperature. Moreover, the threshold energy (i.e. impact energy below which no damage is induced) reduces by up to 50 %. The total energy absorption of the laminate is found to be almost independent of the temperature. The temperature effect on the extent of damage is found to be more pronounced for unidrectionally reinforced laminates than for woven fabric reinforced laminates. The authors state that thermally induced interlaminar stresses contribute to this effect.

The paper [134] investigates the impact velocity effect on the delamination behaviour of woven carbon/epoxy laminates. Therefore, experiments with equienergetic LVI conditions (4 J and 8 J), i.e. different mass and velocity configurations, are conducted where the impact energy is chosen such that delamination is the dominating damage mechanism. With increasing impact velocity, the authors observed that the delaminated area increases significantly while the residual stiffness of the laminate decreases.

In Ref. [8] similar investigations as in Ref. [134] are conducted. The authors study the impactor mass effect on the LVI behaviour of woven carbon/epoxy laminates, where impact energies in the range from 10 J to 110 J are considered. In contrast to Ref. [134], no influence of the impactor mass (and the impact velocity) on the laminate's damage and failure behaviour is observed for the considered range of impact energies.

The energy absorption behaviour of plain woven glass/epoxy laminates subjected to LVI is investigated in Ref. [33]. The aim of this work is to find correlations between the absorbed energy and the occurring failure mechanisms. The experimental results are interpreted based on energy balance considerations and critical energy release rates for fibre breakage and matrix breakage are evaluated.

Reference [124] presents experimental investigations of LVI on low fibre volume glass/polyester laminates. Different degrees of fibre crimp of the woven reinforcement and different laminate thicknesses are considered.

The paper [15] studies the influence of the impactor shape on the energy absorption of long fibre reinforced thermoplastics subjected to intermediate to high velocity impact (40 m/s to 140 m/s). It is observed that the energy dissipation at the ballistic limit is significantly less for conically shaped impactors when compared to flat tipped impactors.

In Ref. [88] the influence of the stacking sequence on the LVI behaviour of unidirectionally fibre reinforced carbon/epoxy laminates is studied. Therefore, one laminate with classical layup and two other laminates with similar in-plane and flexural stiffness but dispersed stacking sequence are considered, where the idea is to maximise the difference in the fibre angle between adjacent plies (i.e. avoid ply clustering). Drop weight impact tests and compression after impact tests are conducted, however, the authors observed no significant differences in terms of impact damage and residual strength between the tested laminates.

The effect of the stacking sequence on the HVI behaviour of unidirectionally carbon fibre reinforced epoxy tubes is investigated in Ref. [131]. Two different layups are considered where significant differences in the ballistic limit and, thus, in the amount of absorbed energy are observed.

The influence of the laminate thickness on the LVI response of carbon fabric reinforced epoxy panels is investigated in [32]. The variations of the threshold force and impact energy for delamination initiation, the maximum force, and the penetration energy with respect to the laminate thickness are considered and corresponding analytical fitting functions are stated. Interestingly, the penetration energy is found to be proportional to the laminate thickness to the power of 1.5.

In Reference [10] experimental investigations of the LVI response of glass fabric reinforced epoxy laminates are presented. A so-called energy profile diagram is used to characterise the impact properties of a laminate with respect to various impact energies. Thereby, the impact energy is compared to the energy absorbed by the laminate where three different types of impact responses can be distinguished. These are non-penetrating impact, penetrating impact and total perforation of the laminate. This technique is also explained in Ref. [5] where experimental investigations of the impact response of multidirectional laminates consisting of unidirectionally glass fibre reinforced epoxy plies are conducted. It is observed that the amount of energy absorbed in the case of total perforation remains approximately constant, even if the impact energy is further increased.

Another, more general, energy profiling approach is proposed in Ref. [109]. The presented approach evaluates the energy absorption of a composite laminate subjected to LVI based on a non-dimensional energy absorption master-curve, which is a function of the absorption coefficient (i.e. ratio of absorbed energy to penetration energy) and the impact intensity coefficient (i.e. ratio of impact energy to penetration energy). Hence, once the penetration energy of a specific laminate is determined (experimentally, analytically or numerically) its energy absorption behaviour can be assessed for all values of impact energies. The proposed approach is validated for different material systems (carbon/epoxy, glass/epoxy) and different reinforcement styles (unidirectional, woven).

2.2 Numerical predictions of the impact behaviour of composites

Although experimental testing gives insight to the effects of impact loading on certain specimens under certain loading conditions, it is very time consuming and expensive to investigate different impact scenarios as well as impact on structural components. Hence, predictions of the damage and failure behaviour are needed for the design of structures subjected to impact. Some analytical and empirical models, such as the ones described in Refs. [3, 42, 89, 102, 109], may be used to gain first predictions of threshold and peak loads. However, in order to reduce conservative assumptions in design and better exploit the potential of composite materials a detailed understanding of the impact behaviour of such structures is necessary. In this regard, numerical simulations by means of the Finite Element Method (FEM), cf. Refs. [16, 135], provide the capability for predicting and investigating the impact characteristics of composite structures.

2.2.1 Constitutive modelling

The prediction of propagating damage and failure in composite laminates requires constitutive theories capable of modelling the inherent failure modes. These may be subdivided into intra-laminar damage and plasticity like effects, occurring within a ply, as well as inter-laminar damage (delamination) arising between adjacent plies. Intra-laminar damage may again be subdivided into fibre fracture, matrix fracture and fibre/matrix debonding. A comprehensive overview of methods for the numerical modelling of damage and failure in composite materials is given in the textbook [28]. In the following, recent developments in the computational modelling of these failure modes are presented.

Intra-laminar damage and plasticity

Considering the modelling of intra-laminar damage, the majority of material models within the literature is based on a ply-level continuum damage mechanics (CDM) approach similar to the one originally proposed in Ref. [80], where propagating damage due to matrix microcracking and fibre/matrix debonding in a unidirectionally fibre reinforced ply is modelled. Therefore, the material stiffness of the ply is degraded according to scalar damage variables describing the extent of the individual failure modes. Additionally to the brittle elasto-damage behaviour, a plasticity model is implemented in Ref. [80] in order to describe the pronounced inelastic behaviour under shear loads observed for fibre reinforced composites.

The general framework of CDM is discussed in Refs. [35, 36]. Damage initiation is usually determined via specific criteria, ranging from simple maximum stress or maximum strain criteria to more complex ones motivated from physical failure mechanisms, cf. the Hashin criterion [68], Puck criterion [107, 108] and the LaRC04 criterion

[106]. These are combined with relations governing the evolution of the individual damage variables, which may be driven by the associated thermodynamic forces, cf. Refs. [80, 85]. One aspect of CDM approaches regarding the FEM implementation evolves from the material stiffness degradation which may lead to strain softening behaviour and, thus, to strain localization in a structure resulting in a strong mesh dependency of FEM results. In order to circumvent this issue, most implementations of such CDM material models utilize a so-called crack band model, cf. Ref. [19].

A huge variety of CDM models for laminated composites has been developed in the last decade, designated to different applications and to the prediction of different failure modes. In Ref. [95] a plane stress constitutive model capturing anisotropic damage in unidirectionally fibre reinforced laminae is presented, where the damage evolution equations have been derived from thermodynamical considerations. The model considers fibre rupture and matrix cracking due to transverse and shear loads via three independent damage variables, where tensile and compressive loading is distinguished.

A more recent thermodynamically based CDM model for unidirectionally fibre reinforced composite laminates is described in Ref. [91], which aims at the prediction of the onset and evolution of intralaminar failure mechanisms. On the basis of a plane stress formulation four damage mechanisms are considered, tensile and compressive fracture in fibre direction and transverse fracture in planes perpendicular and inclined to the laminate mid-plane. The onset of damage is determined based on the LaRC04 criteria, cf. Ref. [106]. The implementation of this model is described in Ref. [92]. The same author also proposed a fully three dimensional formulation of a damage model for unidirectionally fibre reinforced transversely isotropic composite laminates, cf. Ref. [93], which predicts intra-laminar and inter-laminar failure mechanisms in an integrated way, thus, also accounting for the interaction between these mechanisms.

Another anisotropic damage model for UD reinforced composites, adapted from Ref. [95], is presented in Ref. [84]. Special emphasis is put on the FEM appropriate implementation. Accordingly, the crack band model of Ref. [19] is incorporated, as well as a viscous regularization scheme to alleviate convergence difficulties of implicit solvers, which may occur in the strain softening regime. Progressive damage due tensile and compressive fibre and matrix failure is modelled, where the Hashin criterion, cf. Ref. [68], is used to determine damage initiation. The model is formulated in plane stress space and has been permanently implemented in the commercial FEM code Abaqus (Dassault Systemes Simulia Corp., Providence, RI, USA).

The paper [56] presents a plane-stress constitutive model for the simulation of the damage and failure behaviour of unidirectionally fibre reinforced laminae. Distributed matrix cracking and fibre matrix debonding are modelled by stiffness degradation in combination with strain hardening, where a micromechanical approach is used to describe the stiffness change due to distributed cracks within the laminae. Localised brittle damage (i.e. discrete matrix cracks, fibre rupture) is modelled by stiffness degradation in combination with strain softening. Additionally, unrecoverable strain accumulation is accounted for by a multi surface plasticity model which allows to predict plasticity-like behaviour of laminae subjected to shear loads or transverse compressive loads. The model has been implemented in the implicit solver Abaqus/Standard in terms of a UMAT user subroutine.

In Ref. [51] a tri-axial CDM based material model for the simulation of progressive intralaminar degradation of unidirectionally fibre reinforced laminates is presented. Besides tensile and compressive fibre and matrix failure, nonlinear elastic plastic shear behaviour including shear damage are modelled. Furthermore, nonlinear stress-strain behaviour under transverse compression loading is incorporated. The model also features a viscous regularization scheme and has been implemented in the implicit solver Abaqus/Standard via the user-subroutine UMAT. Application examples of the progressive failure model are presented in [52].

Another tri-axial CDM model for unidirectionally fibre reinforced laminates is introduced in Ref. [47]. It considers tensile and compressive fibre and matrix failure, as well as shear failure, where the corresponding damage variables are introduced at the lamina level. Damage onset is predicted by a maximum stress criterion for all failure modes except transverse (matrix) compression. There, a quadratic stress based criterion proposed by Refs. [107, 108] is used. The damage evolution relations are defined as functions of the strains, thus, allowing to control the dissipated energies and ensuring mesh insensitivity of the results by applying a crack band approach. Nonlinear shear behaviour, as well as the accumulation of inelastic strains due to shear loads is also accounted for. The model has been implemented in LS-DYNA for the prediction of LVI damage.

In Ref. [53], a constitutive law specifically developed for the prediction of permanent indentation after LVI on UD reinforced laminates is presented. It is believed that inelastic out-of-plane shear behaviour is responsible for the occurrence of permanent indentation after impact events and, thus, the authors introduce a nonlinear intralaminar shear model. Besides, tensile and compressive fibre and matrix failure are modelled using a common thermodynamically based CDM approach.

A different strategy for modelling damage in unidirectionally fibre reinforced composites is discussed in Ref. [103], where a micro-mechanical approach named matrix-reinforced mixing theory is utilized, which represents a simplification of the serial/parallel mixing theory. Thereby, an isotropic CDM formulation is applied to the matrix, however, fibre damage is not considered. The benefits of this model are stated to be the capability of simultaneously capturing intra-laminar and inter-laminar damage, thus, being computationally less demanding.

The constitutive models discussed so far are all formulated to describe the behaviour of unidirectionally fibre reinforced composites. Besides this type of reinforcement, fabric reinforced composites are frequently applied. A CDM based constitutive law for modelling fabric reinforced composites under plane stress loading is presented in Refs. [74, 76]. It is based on methods developed for UD plies, cf. Ref. [80], and considers tensile and compressive failure in the principal fibre (tow) directions and in-plane shear failure using scalar damage variables. Furthermore, elastic-plastic shear behaviour is incorporated to model inelastic shear effects, where strain hardening is modelled by a power-law. This model has been implemented in the explicit FEM code PAMCRASH where its usage in crash and impact simulations is intended.

A modification of the model [74] has been implemented into Abaqus/Explicit as a built-in VUMAT user subroutine, cf. Ref. [39], where the major differences are in the formulations of the damage activation and evolution functions. In Ref. [39] the damage evolution is based on the corresponding critical energy release rates and incorporates a crack band model to alleviate mesh sensitivity of the results.

Another energy based CDM approach for modelling woven composites is discussed in Ref. [72]. Formulated in plane stress space, five damage variables are used to describe tensile and compressive warp and weft fibre damage and shear damage for each ply. Damage evolution is defined as a function of strain, thus, allowing to obtain mesh size independent results by incorporating a crack band model. Furthermore, strain rate effects under shear loading are accounted for, as well as a permanent damage strain due to loading in the fibre directions and due to shear. The model has been implemented in the explicit FEM code LS-DYNA3D and is intended to be used for impact simulations.

A very recent formulation of a CDM constitutive model for fabric reinforced composites is presented in Ref. [94]. The model considers plane stress states, where tensile and compressive fibre failure in weft and warp directions are modelled and, furthermore, biaxial strengthening behaviour under compressive loads is accounted for. Additionally, isotropic strain hardening plasticity is assumed for the shear stress-strain behaviour. Damage onset is predicted on the basis of an adapted maximum stress criterion. Damage evolution is modelled according to a bi-linear softening law based on the energy release rates and a crack band approach, cf. [19]. This model has been implemented in Abaqus/Explicit via the VUMAT user subroutine.

Delamination

Within the literature, the modelling of delamination in laminated composites is predominantly conducted using so-called cohesive zone (CZ) approaches. In general, CZ models use the framework of damage mechanics in combination with fracture mechanics, where their main advantage lies in the ability to predict both onset and propagation of cracks. Therefore, considering a FEM model, interfaces have to be introduced at locations where crack nucleation and propagation is expected. Hence, the crack path needs to be known a priori. This circumstance is of minor significance when considering delaminations in laminated composites as the crack path follows the interface between adjacent plies. However, when modelling cracks in bulk material the crack path may not be known beforehand. The constitutive behaviour of these CZ interfaces is defined by relating tractions at the interfaces to corresponding displacement jumps. When a specified criterion based on maximum nominal tractions, i.e. interface strengths, is reached the degradation of the interface stiffness is initiated. The degradation and subsequent softening is controlled based on the traction-displacement jump relation, where zero tractions are reached when the critical energy release rate of the interface is met. At this state new crack surfaces are formed.

The predominantly used CZ formulations are based on the work of Dugdale [48], Barenblatt [13] and Hillerborg [70], where in Ref. [70] the CZ approach has already been transferred to a FEM formulation. This model was among the first to allow for capturing growth of existing cracks as well as initiation of new cracks. Some early applications of a CZ formulation applied to predict delamination in laminated composites are presented in Refs. [7, 41]. Here the composite is modelled as a stack of homogeneous layers with CZ interfaces in between, cf. Ref. [81]. The constitutive law of the CZ interface is formulated on the basis of a thermodynamical potential where an elasto-damage behaviour is assumed. Damage progression and softening is modelled as a parabolic relation between the tractions and displacement jumps at the interface. The identification of the model parameters is conducted so that crack growth is predicted when the critical energy release rate is met.

In Refs. [27, 29] a CZ model on the basis of a decohesion element formulation within the FEM framework is presented. The decohesion element is meant to be used between solid finite elements where special focus is set on the prediction of delamination growth under mixed-mode conditions. Therefore, a criterion based on the quadratic interaction of interface tractions is used to determine damage onset in the CZ. Upon damage onset, a linear softening relation is applied where the critical energy release rate under mixed-mode loading is evaluated using a criterion proposed by Benzeggagh and Kenane, cf. Ref. [20]. The built-in cohesive element formulation of the FEM code Abaqus is based on Ref. [27]. It shall be mentioned that the CZ formulation [27, 29] should just be used under constant mixed-mode conditions as the Clausius-Duhem inequality might not be satisfied under variable mode loading.

A thermodynamically consistent damage model for CZ interfaces capable of predicting progressive delamination under variable mode loading is presented in Ref. [127]. Here, the constitutive law is derived from the thermodynamic free (Helmholtz) energy. Damage initiation is determined by a slightly modified quadratic stress interaction criterion to better account for mixed mode conditions. Again, a linear softening relation between tractions and displacement jumps is assumed upon initiation of damage, where the Benzeggagh Kenane criterion is used to control damage progression. The CZ model [127] has been implemented in Abaqus/Standard by means of a user-written element. The CZ formulation [127] has also been implemented in the explicit FEM code Abaqus/Explicit with slight modifications, cf. Ref. [62].

Considering the modelling of laminated composites, a stacking approach using shell elements for discretizing the plies seems beneficial. The interface can then be discretized by cohesive elements with finite non-zero geometrical thickness connecting the nodes on the reference planes of the shell layers. However, in order to achieve kinematic continuity at the position of the interface, the rotational degrees of freedom of the shell element nodes have to be taken into account. These issues are discussed in [44], where a special formulation of cohesive elements for shells, based on [127], is presented.

Considering the discretization of the CZ interface, a necessary condition for obtaining mesh-independent results is that the length of any cohesive damage zone should be large compared to the size of the discretizing elements, cf. Ref. [132], since a minimum number of CZ elements within the cohesive damage zone is necessary to capture the tractions and, thus, the crack propagation correctly. The length of the cohesive damage zone is defined as the distance from the crack tip to the point where the maximum traction is reached. A relation to estimate the cohesive damage zone length based on the material properties is stated in Ref. [132]. This requirement usually results in very fine meshes and increases the computational effort. However, the length of the cohesive damage zone can artificially be increased by lowering the interfacial strength, as stated in Ref. [128], where it is shown that the crack propagation is still properly captured using this strategy when the critical energy release rate is kept unchanged. Additionally, an expression for estimating minimum stiffness values for the CZ interface is given in Ref. [128], which ensures that the contribution of the CZ interface to the overall compliance is small enough.

A further discussion of the effects of the interfacial strengths on the predictions of delamination propagation under pure-mode and mixed-mode loading is given in Ref. [129]. It is shown that, under mixed-mode loading, the computed energy release rate is depending on the ratio between the interfacial strengths, where a relation between these is given to ensure correct predictions. Alternatively, a relation between the interfacial stiffnesses can be imposed too, cf. Ref. [129].

In Ref. [6] a study on the influence of the shape of traction-displacement jump relation of the CZ interface has been conducted, where it has been found out that, for pure-mode loading, there is almost no effect on the solution.

2.2.2 Modelling impact on laminated composites

As impact problems, in general, represent dynamic events, numerical simulations are almost exclusively conducted using explicit time integration schemes where in most cases the FEM framework is applied. The damage and failure behaviour of laminated composites is most commonly predicted using so-called meso-models, cf. [81]. Thereby, the laminate is considered as a stack of homogeneous orthotropic layers with inter-laminar interfaces in between, where these two basic constituents are assigned individual constitutive laws as described in Section 2.2.1. The differences in the proposed models in the literature are typically represented by variations in the constitutive models ranging from different failure modes considered, over the use of plane stress or fully tri-axial formulations, to the consideration of different reinforcement types (i.e. unidirectionally reinforced plies vs. fabric reinforced plies). Moreover, different levels in the modelling detail (i.e. the number of plies and interfaces modelled) and geometrical discretisations at different length scales are dealt with. Additionally, the impact scenario itself (i.e. LVI or HVI) induces further requirements to the modelling strategy as the structural response may differ substantially, cf. Chapter 1 and Section 2.1. In the following, an overview of various modelling strategies proposed in the literature is given. The references are sorted by the length scale of the models' geometrical discretisations, where the intended use and special model features are outlined.

Sublaminate-scale models

In [77] a modelling strategy for predicting impact damage in fabric reinforced composites is presented. Here, the laminate is considered as a stack of shell elements, where several sub-laminates are represented by individual layers of shell elements. These shell-layers are connected via a traction-displacement based interface contact formulation in order to capture delamination between sub-laminates. The intra-ply behaviour is modelled using the constitutive law presented in [74]. Simulations of impact of a steel sphere on a quadratic plate, consisting of 16 plies, are conducted where impact velocities in the range of 2 m/s to 6 m/s and resulting impact energies from about 60 J to 400 J are considered. The results, obtained using the explicit FEM code PAMCRASH, are compared to equivalent experiments. Furthermore, the influence of the consideration of delamination on the impact response is investigated by comparing results of a model consisting of a stack of 4 sublaminates (and 3 interfaces) with those of a model where just a single shell layer is used to discretize the laminate and delamination is not modelled. A significant difference in the results has been found, thus, highlighting the importance of modelling delamination in impact scenarios. A similar modelling strategy has been applied to model impact on cylindrical glass fabric reinforced composite shell structures, cf. [75], where impact velocities of about 100 m/s and impact energies of about 700 J are considered. Accompanying experiments have been conducted and compared to the numerical predictions. Significant differences in the failure modes regarding impact on the convex or concave sides of the shell structure have been reported, especially regarding the extent of delaminations.

In [73] a fabric reinforced laminate is modelled as a stack of two sublaminates represented by continuum shell elements. The constitutive behaviour of the sublaminates is modelled using an energy based CDM constitutive law formulated in plane stress space, which has been developed by the same authors, cf. [72]. The interface between the sublaminates is modelled by interface elements in combination with a cohesive zone approach. Simulations of 5 J, 9 J and 15 J impacts in a so-called CRAG impact test setup are conducted using the explicit FEM code DYNA3D. The results are compared to experimental test results.

The work presented in [11] is dedicated to the simulation of impact induced delamination in graphite/epoxy cross-ply laminates. The laminate is discretised at the sublaminate-scale, where each sublaminate consists of three plies with equal fibre orientation. These sublaminates are represented by two continuum elements over their thickness. Delamination is modelled by a cohesive zone approach and is just considered at interfaces where a change in the fibre orientations of adjacent sublaminates occurs. The model assumes quarter symmetry with respect to the location of impact. Considering ply damage mechanisms, just matrix cracking along one symmetry plane is modelled by use of an additional cohesive zone. Simulations of drop weight impact tests in the range from 1 J to 7 J are conducted using Abaqus/Explicit, where a good correlation of projected delamination areas, compared to equivalent experiments, is found.

Reference [63] proposes a strategy for simulating low velocity impact (20 J to 40 J) and compression after impact subsequently. A multidirectional laminate consisting of unidirectionally fibre reinforced carbon/epoxy plies is modelled such that sublaminates containing plies with equal fibre orientation are discretised by a single continuum element in thickness direction. Intralaminar damage is modelled using the constitutive law described in [91, 92]. Cohesive zone elements are inserted between sublaminates with different fibre orientations in order to account for delamination in those interfaces, where the cohesive zone approach of Ref. [62] is applied. The authors consider friction between the impactor and the laminate, as well as between delaminated plies. A drawback of the model presented in [63] is the huge computational effort. The computations for a laminate of typical coupon specimen dimensions take between 12 and 15 days on a cluster system with 24 CPUs.

Another sublaminate-scale model for simulating LVI on multidirectional laminates consisting of unidirectionally fibre reinforced carbon/epoxy plies is presented in [25], where two adjacent plies with equal orientation are discretised by a single continuum element in thickness direction. The interfaces between these sublaminates are modelled using a cohesive zone approach. The speciality of the modelling strategy in Ref. [25] is represented by the way of modelling matrix cracks within the sublaminates. Therefore, the finite element mesh of individual sublaminates is divided into strips with a width of a single continuum element. These strips are connected via zero-thickness interface elements, which are used to represent matrix cracking within the sublaminate. This technique requires each sublaminate's mesh to be aligned with its fibre direction and, hence, results in a very complex meshing procedure. Moreover, this method implies a certain amount of mesh sensitivity as the maximum number of matrix cracks within a sublaminate is determined by the element size.

The continuation of the work of Ref. [25] is presented in Ref. [26], which aims at the prediction of permanent indentation after LVI (25 J) on a multidirectional laminate consisting of unidirectionally fibre reinforced carbon/epoxy plies. The approach for modelling matrix cracks is extended by the capability to account for permanent strains and a CDM approach is used to account for fibre damage and failure. Simulations are conducted using Abaqus/Explicit and good agreement with experimental results is found. However, the predictive character of the model is limited as parameters for describing permanent indentation need to be calibrated based on impact experiments. In Ref. [71] the work is further continued and, additionally, fibre compressive damage and failure is modelled.

The paper [103] proposes a micro-mechanically based approach to predict low velocity impact damage in multidirectional laminates consisting of unidirectionally carbon fibre reinforced epoxy plies, cf. Section 2.2.1 where the concept of the so-called matrix reinforced mixing theory is explained briefly. The constitutive model is applied to simulate LVI (6 J to 70 J) on a multidirectional 40-ply laminate, where the discretisation is conducted such that several plies are represented by a single layer of continuum elements. The authors state that the discretisation at sublaminate scale is chosen in order to reduce the computational effort. Moreover, just a quarter of the laminate is modelled and symmetry boundary conditions are applied. The simulation results are shown to be in agreement with experimental test data.

Ply-scale models

Reference [53] aims at simulating permanent indentation after LVI (5 J). A multidirectional laminate consisting of unidirectionally reinforced carbon/epoxy plies is modelled at the ply-scale, where each ply is discretised by a single continuum element in thickness direction and every interface is modelled by a cohesive zone approach. Permanent indentation is simulated by modelling nonlinear out-of-plane shear damage within the plies, cf. Section 2.2.1. Interestingly, the simulations are conducted using an implicit FEM solver (Abaqus/Standard).

The paper [120] proposes another ply-scale modelling strategy to simulate LVI (7 J to 15 J) on unidirectionally reinforced cross-ply carbon/epoxy laminates. Thereby, each ply is discretised by two continuum elements in thickness direction and each interface is modelled by a cohesive zone approach. Friction between the impactor and the laminate, as well as between delaminated plies is considered. The ply constitutive model also incorporates nonlinear out-of-plane shear behaviour and, therefore, predictions of permanent indentation after LVI are possible. Simulations of drop weight impact tests are conducted using Abaqus/Explicit and comparisons to experimental results show good correlations. The continuation of the work of Ref. [120] is presented in Ref. [121]. There, the modelling of fibre splitting and transverse matrix cracking is addressed by introducing cohesive zones within individual plies, similarly to the modelling approach presented in Ref. [25]. A certain degree of mesh sensitivity seems to be implied, as the maximum number of cohesive zones within a ply is determined by the element size of the ply's mesh.

A numerical investigation of the effect of various ply stacking sequences on the LVI behaviour (9 J to 30 J) of a multidirectional laminate consisting of unidirectionally reinforced carbon/epoxy plies is conducted in Ref. [87]. Thereby, each ply is discretised by a single continuum element in thickness direction and each interface is modelled by a cohesive zone approach. Intralaminar damage is modelled by the constitutive law [91, 92], which has been applied in an extended formulation in order to describe tri-axial stress states. The applied cohesive zone approach is based on Ref. [63]. The simulations are conducted using Abaqus/Explicit and the results are compared to corresponding experiments, which are published in Ref. [88]. Considering the computational effort, the authors state that the simulation of a drop weight impact test on a laminate with typical coupon specimen dimensions (i.e. 150 mm×100 mm) takes 4-5 days on a cluster system with 32 CPUs.

In Reference [55] the importance of modelling intra-ply damage regarding the predicted delamination pattern is assessed. The authors utilise a ply-scale discretisation where a single layer of continuum elements is used for each ply. The ply constitutive model is based on [51, 52]. Delamination is modelled using a cohesive zone approach and is just considered in interfaces between plies with different fibre orientations. Simulations of LVI (1 J to 8 J) on a multidirectional carbon/epoxy laminate are conducted using Abaqus/Explicit. Special emphasis is put on the prediction of the through-thickness distribution of delaminations, where good agreement to experimental results is found. Moreover, it is observed that the predicted size and shape of delaminations significantly differs if intra-ply damage is not modelled.

The authors of Ref. [55] also propose a modelling strategy to simulate LVI (1 J to 9 J) on composite sandwich panels, which is presented in Ref. [54]. Thereby, the facesheets, consisting of unidirectionally fibre reinforced carbon/epoxy plies in a multidirectional layup, are modelled in the same way as described in Ref. [55]. The constitutive behaviour of the foam core is modelled using the crushable foam plasticity model which is readily available within Abaqus/Explicit. The material input for the foam plasticity model is gained from uniaxial transverse compression tests at intermediate strain rates. The authors report good agreement between their predictions and experimentally obtained data, where special attention is directed towards the investigation of the size and shape of delaminations in individual interfaces within the facesheets.

The paper [104] proposes a modelling approach to simulate HVI (60 m/s to 500 m/s, up to 7 J) on a multidirectional laminate consisting of unidirectionally reinforced carbon/epoxy plies using the explicit FEM solver LS-DYNA. Each ply of the laminate is discretised by a single layer of continuum elements. Ply damage is modelled based on [37]. The interfaces between plies are modelled using a cohesive zone approach. The main focus of the work [104] lies in the prediction of the ballistic limit of the laminate and the residual velocity of the projectile for various impact velocities. The simulation results are validated with experiments and further investigations regarding the influence of the projectile geometry on the impact behaviour of the laminate are conducted.

In Reference [90] simulations of ballistic impact on carbon fabric reinforced epoxy laminates are conducted using Abaqus/Explicit. The laminate is discretised using continuum elements (two per ply thickness). Intra- and inter-ply damage and failure are modelled within a single constitutive law and, hence no additional interface elements are needed. This strategy implies that delamination is not modelled at the position of the interface between plies but within the plies. Normal and oblique impact with various impact velocities are studied and good agreement with gas-gun experiments is found in terms of damaged area and the projectile's residual velocity.

Reference [45] presents simulations of ballistic impact on E-glass/polypropylene plain weave laminates. The authors assume quarter symmetry of the impact problem and discretise each ply of the laminate using a single layer of continuum elements. Intra- and inter-ply damage and failure is modelled within a single constitutive law and no interface elements are introduced. Hence, as mentioned in the context of Ref. [90], delamination is not modelled at the position of the actual interface. The proposed model accounts for strain rate sensitive behaviour of the glass fibre reinforced laminate. Moreover, the elastic-plastic behaviour of the steel projectile is modelled. The simulations are conducted using LS-DYNA, where the ballistic limit, as well as the energy absorption of the laminate are investigated and comparisons to experimental data (gas-gun) are given.

The paper [110] addresses the challenge of mesh-regularisation in the context of LVI simulations in combination with CDM approaches. The authors propose a tri-axial constitutive law for modelling progressive damage and failure of multidirectional laminates, consisting of unidirectionally fibre reinforced carbon/epoxy plies, which are subjected to LVI. Mesh regularisation for the fibre damage modes is conducted using a classical crack band formulation originally proposed by [19]. Considering matrix damage, the authors propose a novel mesh regularisation strategy which allows to account for several matrix cracks within an element. This is realised by scaling the critical energy release rate corresponding to intralaminar matrix cracking by the number of matrix cracks per element at crack saturation. Therefore, a so-called intralaminar crack saturation density parameter is introduced, which is determined inversely based on experimental impact tests. Delamination is also accounted for within the proposed constitutive law, where the distinction between matrix damage and delamination is conducted using the failure criteria [105] which determine a fracture plane based on a given stress state. A drawback of this approach is that delamination is modelled at the ply mid-planes rather than at the interfaces. LVI impact simulation results (37 J and 75 J) are presented and compared to equivalent experimental results. It is shown that the novel mesh regularisation for intralaminar matrix damage allows for coarser discretisations and, thus, helps in reducing computational cost of LVI simulations.

Models considering fabric topology

Reference [66] presents a modelling strategy for simulating ballistic impact on non impregnated textile fabrics (i.e. dry fabrics). Thereby, a single layer of a plain woven textile fabric is modelled at the length scale of individual yarns, which are discretised by shell elements. Hence, the fabric topology is explicitly accounted for by the geometrical discretisation. The explicit FEM solver RADIOSS is used to conduct simulations of a ballistic impact on a single layer of a plain woven aramid fibre fabric. The predicted residual velocity is compared to experimental data reported in the literature. Moreover, the simulation results are compared to additional simulations where the fabric is modelled as a homogenous orthotropic material and the differences to the yarn-scale modelling approach are discussed. The paper [65] proposes a strategy to combine the yarn-scale modelling approach [66] with a homogenised model of a textile fabric in terms of a multiscale representation. Various configurations are studied with different partitioning between the yarn-scale and the homogenised discretisation are studied, where the aim of this strategy is to reduce the computational effort.

Another yarn-scale modelling approach for simulating impact on dry fabrics is proposed in Ref. [99]. Thereby, a single layer of a textile fabric is discretised with varying level of modelling resolution depending on the distance to the impact zone. A continuum element discretisation of individual yarns is chosen at the region closest to the impact zone, followed by an intermediate region where individual yarns are discretised by shell elements. Regions remote from the impact zone are modelled as homogeneous orthotropic material. The authors emphasize the necessity of matching the acoustic impedance between the homogenised region and the yarn-level region in order to avoid the reflection of stress waves at the domain transition boundary. Simulations of LVI (non-penetrating) and HVI (penetrating) on a single layer of a plain woven aramid fibre fabric are conducted using the explicit FEM solver LS-DYNA. Several configurations regarding the size and shape of the domains with different discretisations are studied and the results, as well as the computational cost of the configurations are compared.

The paper [101] presents a modelling strategy for fabric reinforced laminates (i.e. impregnated fabrics), which accounts for the interwoven topology of a 5-harness satin weave in a simplified way. Thereby, the fabric topology is approximated by a combination of truss and shell elements. The uniaxial tensile and compressive behaviour of individual tows (i.e. bundles of impregnated fibres) is represented by the truss elements. The shell elements model the membrane behaviour of the matrix and the bending and transverse shear behaviour of the homogenised ply. The effect of the interwoven topology is modelled by assigning different failure strains to the rods depending on their location with respect to the weaving pattern. The interfaces between adjacent plies are modelled using a cohesive zone approach. Simulation results of LVI on a two-ply carbon/epoxy laminate are presented and good correlation with experiments is found. Additionally, simulations of an oblique impact (90 m/s) on a foam core sandwich panel with 3-ply facesheets are compared to experimental data obtained by a gas-gun impact test, where again good correlation is achieved. The simulations are conducted using the explicit FEM solver RADIOSS.

Multi-scale models

The modelling approaches presented in [65, 99] combine discretisations at yarn-level and ply-level in order to model the mechanical behaviour of a single layer of a textile fabric. In the following, multi-scale approaches directed towards the simulation of the impact behaviour of laminates and components are briefly summarised.

Reference [50] proposes a model for simulating LVI on a stiffened composite panel. The authors apply an embedding approach, where a ply-scale discretisation is used at the impact zone (one continuum element per ply in thickness direction) while the rest of the component is discretised at the laminate scale using continuum shell elements. Within the ply-scale domain, intra-ply damage and failure is modelled based on the constitutive law [47] with slight modifications. The interface between plies is modelled using the cohesive zone approach [29]. Within the laminate scale domain linear elastic material behaviour is modelled. The simulations are conducted using Abaqus/Explicit, where the computation on a cluster system with 8 CPUs took 4 days. The predictions are in good agreement with experimental results. Moreover, the model is also capable to predict the permanent indentation after impact.

A novel embedding approach for combining geometrical discretisations at different length scales is presented in Ref. [60]. The so-called mesh superposition technique uses transition regions instead of sudden transitions between differently discretised regions. Within the transition region, the meshes of the differently discretised regions are superposed and the corresponding stiffness and mass matrices are scaled in order to satisfy the conservation of energy principle. This way, stress disturbances at domain transition regions are eliminated and, hence, the size of the detailed discretised domain can be reduced. The mesh superposition technique is applied to simulate LVI (3 J) on a unidirectionally carbon fibre reinforced epoxy cross-ply laminate in a drop weight impact test setup. The simulations are conducted using Abaqus/Explicit. Model configurations using a sudden transition technique are compared to those using the mesh superposition technique and the required minimum dimensions of the detailed discretised domain are evaluated for both techniques. Additionally, a co-simulation technique is applied such that implicit time integration is used for the embedding domain whereas explicit time integration is used in the detailed discretised region where material nonlinearities are expected. Based on the presented application example both the mesh superposition technique and the co-simulation technique, contribute to reducing the computational effort. The paper [61] presents another application example of the mesh superposition technique [60]. There, simulations of LVI (12 J) on a composite sandwich rotor blade are presented.

In Reference [96] an adaptive multiscale modelling strategy for modelling HVI on composite panels is presented. The general idea is to switch between different constitutive laws during the simulation. Initially, a linear elastic orthotropic material response is modelled at the ply-scale, where the effective material properties are evaluated based on the rule of mixtures. Once a modified Hashin-Rotem criterion, cf. [69], is satisfied, the so-called generalised method of cells is used to model the material response. Thereby, while conducting a FEM simulation at the macroscopic length scale, the microstructure of the composite is considered at each integration point using analytical micro-mechanical considerations. At the micro-scale, nonlinear material behaviour of the composite's constituents, i.e. the fibres and the matrix, is modelled. The modelling approach is validated based on simulations of HVI (200 m/s to 500 m/s) on a unidirectionally carbon fibre reinforced epoxy panel with multidirectional layup, where the predicted projectile's residual velocity is compared to the experimentally determined one.

Chapter 3

Tow-scale modelling approach

3.1 Introduction

The simulation of impact on fibre reinforced composite laminates has been studied extensively within the literature, cf. e.g. Refs. [55, 63, 87, 120, 121]. These papers focus on the simulation of drop weight impact tests on multidirectional laminates consisting of unidirectionally (UD) fibre reinforced plies with impact energies up to 30 J. The simulations feature explicit time integration schemes to predict the dynamic impact response. All of the models use sublaminate-level or ply-level based modelling approaches, where the laminate is discretised by three dimensional continuum elements. The interfaces are modelled by cohesive zone elements (CZEs). Specific continuum damage mechanics (CDM) constitutive models are applied to model damage and failure within the UD plies.

Many applications, however, feature fabric reinforced laminates. One way for modelling woven composites is to consider the ply as homogeneous orthotropic material, similar to the approach typically applied for UD composites. In Refs. [75, 77] such a CDM constitutive model for the simulation of impact in fabric reinforced composites is presented. The laminate is modelled as a stack of sub-laminates represented by individual layers of shell elements. The interfaces between the sub-laminates are modelled by a traction-displacement based contact formulation. Another energy based CDM approach for modelling impact on woven composites at the ply level is presented in Ref. [73].

The homogeneous representation of the woven plies, however, neglects effects arising from the fabric topology as e.g. fluctuations of the stress and strain fields. These fabric topology induced effects, consequently, influence the damage and failure behaviour of an impact loaded laminate. The models proposed in Refs. [65, 99] discretise individual bundles of fibres in order to simulate the high velocity impact behaviour of a single layer of dry fabric. Some concepts for modelling the topology of woven plies at the level of individual tows are presented in Refs. [12, 86]. As 3D continuum elements are used for the discretisation, the complexity of these models restricts the range of application to the static analysis of periodic unit cells. A shell element based approach for modelling periodic unit cells of textile composites at tow-level is proposed in Refs. [58, 59]. This approach proves to be of exceptional computational efficiency while providing accurate results. Another approach for modelling the topology of the fabric reinforcement is presented in the paper [101]. There, the interwoven topology of a 5 harness satin weave is simplified by an approximation with rod and shell elements to simulate low to medium velocity impact.

To the author's knowledge, however, there are no numerical investigations of the impact response of fabric reinforced laminates which account for the fabric topology in a detailed way. Moreover, numerical predictions on the effect of the weaving pattern on the impact behaviour and the associated energy absorption of a fabric reinforced laminate have not yet been reported within the open literature.

This chapter presents a shell element based modelling strategy which resolves the fabric topology in a detailed way and is efficient enough to allow for the simulation of the highly dynamic, nonlinear behaviour of woven composite coupon specimens under impact loading within reasonable computational resources. Thereby, the topology of the laminate is modelled at the tow-level for a sub-domain in the proximity of the impact zone, which is embedded in a region with a homogenised representation of the laminate. The modelling approach is exemplified by numerical simulations of a rectangular laminated composite plate with quasi-isotropic layup in a drop weight impact test setup. Results from accompanying experiments are used to verify the numerical model. Furthermore, the effect of different weaving styles on the energy absorption of the laminate is investigated based on the present model's predictions. The simulations are realised using the explicit FEM code Abaqus/Explicit v6.14 (Dassault Systemes Simulia Corp., Providence, RI, USA).

3.2 Modelling approach

Fabric reinforced laminates exhibit complex topologies leading to inherent fluctuations in the stress and strain fields. Within this chapter, the fabric topology is resolved by discretising individual tows within a laminate. This way, the influence of the fabric topology on the damage and failure behaviour of laminated fabric composites is accounted for.

3.2.1 Discretisation of the fabric topology

A fabric reinforced laminate consists of several layers comprising two main constituents, i.e. resin impregnated bundles of fibres (tows) and unreinforced resin zones (matrix pockets). Within the present chapter, a shell element based modelling strategy is utilised to discretise the fabric topology, which represents an extension of the approach presented in [58]. Thereby, the tows as well as the matrix pockets are discretised by individual layers of shell elements, where the following geometrical idealisations of the fabric topology are applied. The weaving pattern is assumed to be perfectly periodic, the tow undulation path is modelled piecewise linear and the tow cross-section is assumed to be rectangular and uniform along the undulation path. A schematic illustration of the idealised geometry is given in Fig. 3.1 (left), where a section of a woven fabric reinforcement, as modelled by the present approach, is

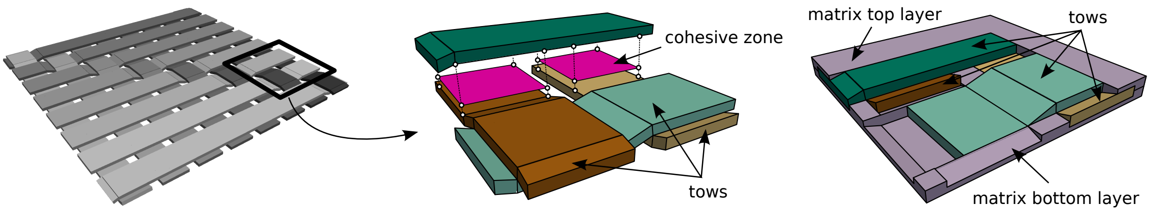

Figure 3.1: Left: Schematic illustration of a section of an eight harness satin fabric as modelled by the present approach (showing tows only). Middle: Coupling of individual tows via CZEs at tow-tow crossings. Right: Cutaway view of a single ply.

depicted. First, the modelling of a single ply is discussed. Considering the shell representation of the tows, the corresponding reference planes are located at the tow mid-planes. The matrix pockets are modelled by two shell layers with the corresponding reference planes located at the top and bottom of the ply where the shell thickness is varied according to the local geometry, cf. Fig. 3.1 (right). As the shell layers representing the tows and matrix pockets are not connected directly, appropriate coupling conditions have to be utilised. The interface between overlapping tows (i.e. at tow-tow crossings) is modelled by CZEs, as illustrated by the shaded areas in Fig. 3.1 (middle). This way, the shell layers representing individual tows are properly connected to each other and, provided that appropriate constitutive laws are applied, debonding of individual tows can be modelled. The top and bottom matrix shell layers are coupled to the tows using surface based constraints. Thereby, the nodes on the slave surface (matrix layers) are constrained to have the same motion as the closest point on the master surface (tows), taking into account the local shell thickness as well as the shell kinematics, cf. Ref. [40].

The extension to a laminate comprising several plies is straightforward. Therefore, zero thickness CZEs are introduced between surfaces of adjacent plies where surface based constraints are used to couple the CZEs to the corresponding ply surfaces, cf. Fig. 3.2. This way, arbitrary stacking sequences can be modelled and, provided that appropriate constitutive laws are applied, delamination between plies can be accounted for.

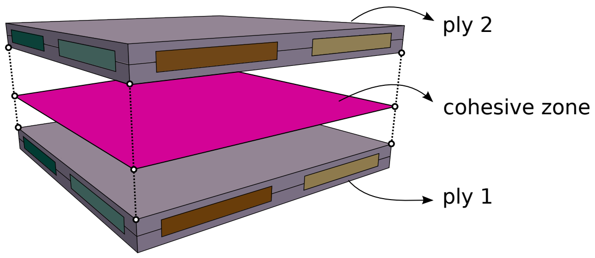

Figure 3.2: Schematic illustration of the composition of a laminate comprising several plies.

Due to the geometrical idealisations of the fabric topology, the modelled tow volume fraction is smaller than the tow volume fraction in a real fabric reinforced ply, where nesting and other irregularities are compacting the topology. This circumstance has to be taken into account when the mechanical response of some real fabric ply shall be predicted, as the overall fibre volume fraction of the model needs to match the real fibre volume fraction.

One aspect of the explicit FEM solver Abaqus/Explicit is that every element within the computational domain has to be assigned some mass density. Hence, also the interfaces represented by CZEs need to be assigned some mass density and, therefore, part of the nominal mass of the tows and matrix pockets is attributed to the interfaces while ensuring the correct representation of the laminate mass. As Abaqus/Explicit uses lumped mass matrices, the nodal masses remain unchanged and the dynamic behaviour of the laminate is retained, regardless of the actual mass distribution.

It shall be noted that the pre-processing step for the generation of such a FEM model is fully scripted so that arbitrary weaving patterns and laminate stacking sequences can be generated in an automated way.

3.2.2 Constituents' constitutive modelling

The tows are treated as homogeneous orthotropic material where an energy based CDM approach is utilised to account for tensile and compressive damage along the tow direction, as well as along the transverse direction of the tows. Furthermore, plastic deformation due to shear is accounted for. The described behaviour is modelled using a built-in VUMAT user subroutine, which is readily available within the FEM package Abaqus/Explicit v6.14, cf. Ref. [39]. A summary of this material model is given in Appendix B of the present work.

The mechanical behaviour of the matrix pockets is modelled as isotropic elasto-plastic with isotropic strain hardening, where associated flow is assumed. The linear Drucker-Prager plasticity model available within Abaqus/Explicit v6.14 is applied, cf. [40]. In order to account for damage and failure within the matrix pockets, additionally, ductile damage behaviour is assigned.

The constitutive response of the ply-ply and tow-tow interfaces is modelled using the Abaqus built-in traction-separation based constitutive model for CZEs, cf. Ref. [40]. The normal and shear traction components are assumed to be uncoupled within the elastic range. Damage initiation is predicted using a quadratic nominal stress criterion. Damage progression is driven according to the corresponding critical energy release rate of the interface, where a linear softening relation based on an effective displacement is assumed. Mixed-mode conditions are accounted for using the criterion proposed by Benzeggagh and Kenane, cf. Ref. [20].

The stiffness degradation associated with the damage models used within the tows, matrix pockets and interfaces can lead to excessive element distortions and further numerical difficulties. In order to overcome these issues, element deletion is utilised, cf. Ref. [40]. Thereby, a shell element of a tow is deleted when both damage variables, i.e. damage along the tow and damage transverse to the tow, reach a value of 0.99. A shell element of the matrix pockets is deleted when the corresponding damage variable reaches a value of 1.0. Finally, CZEs belonging to the ply-ply or tow-tow interfaces are deleted when the corresponding damage variable reaches a value of 1.0.

It shall be noted that all necessary material parameters can be determined from coupon experiments which are independent of any experimental impact test. Hence, no inverse calibration needs to be conducted and the predictive capability of the model is ensured. Moreover, all but one of these experimental setups are standardised. Only the determination of the intra-ply critical energy release rates is still subject to research, where an overview of proposed methods is given in Appendix A.

3.2.3 Multiscale embedding approach

The tow-level modelling of the fabric topology, as described above, necessitates the use of a shell element based discretisation in order to get FEM models with a reasonably low number of degrees of freedom (DOFs). However, simulations of whole coupon specimens entirely discretised using such a tow-level modelling approach are still very demanding in terms of computational resources. Considering the case of transverse impact, the domain where material nonlinearities are encountered is limited to the region in the proximity of the impact zone. Therefore, it is justified to limit the domain with tow-level discretisation of the fabric topology to this region and use some less detailed (i.e. homogenised) representation for regions remote from the impact zone. This way, the number of DOFs is decreased considerably while maintaining a sufficiently high resolution to capture the nonlinear mechanisms within the fabric reinforced plies.

Within the present chapter, the tow-level domain is surrounded by a single layer of shell elements with layered section definition representing the plies of the laminated composite as homogeneous orthotropic elastic material, as illustrated in Fig. 3.3. The elastic properties of the plies within the surrounding (embedding) domain are chosen to be identical to the homogenised properties of the plies within the tow-level domain in order to yield the corresponding mechanical behaviour. These are obtained using the numerical homogenisation approach presented in Ref. [58] in combination with symmetry boundary conditions in the out-of-plane direction to account for the effect of adjacent plies. The size of the tow-level domain is determined by the spatial extent

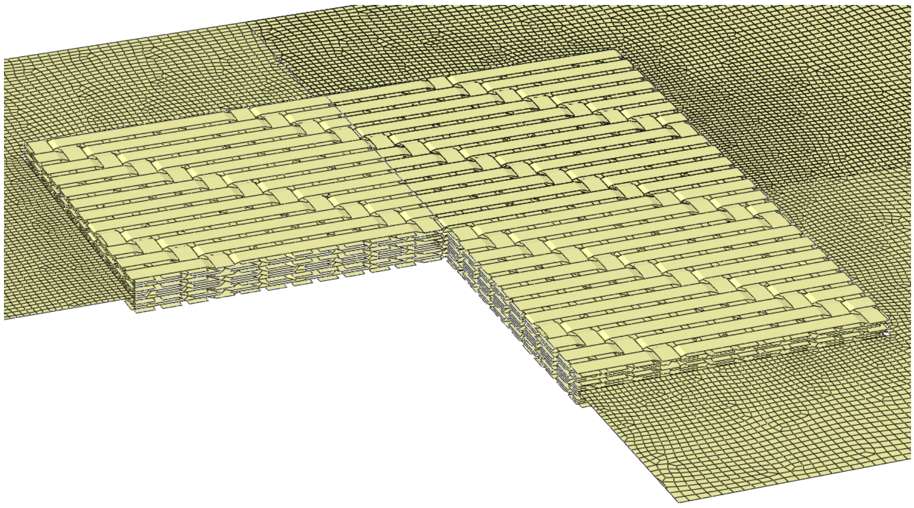

Figure 3.3: Embedding of a patch with discretised topology of a fabric reinforced laminate (matrix pockets are not shown) in a homogenised shell region.

of the arising material nonlinearities as they shall be contained entirely within the tow-level domain.

The edges at the transition between the two domains are coupled according to shell kinematics, so that spatial offsets in thickness direction are taken into account appropriately. Therefore, so-called edge surface based tie constraints are used, cf. Ref. [40]. Note that the edge surfaces which are going to be coupled are not required to be perfectly aligned. In the case of non-aligned edge surfaces, a rigid connection is modelled within the corresponding offset distance.

Within a small region at the transition between the tow-level domain and the embedding domain, elastic behaviour of tows and matrix pockets is modelled in order to alleviate damage accumulation due to coupling interferences. The composition described within this section will be referred to as multiscale embedding approach (MEA) in the following.

3.2.4 Contact modelling

As contact between an impactor and a target is an inherent part of any impact problem, an appropriate contact modelling is particularly important in order to make conclusive numerical predictions of the impact behaviour. Within this chapter, all contact constraints are enforced using the general contact algorithm of Abaqus/Explicit, which utilises a penalty algorithm to compute the contact forces, cf. [40]. The associated penalty stiffnesses are chosen such that the work done by the contact forces is small compared to any of the other energy contributions. Within the present simulations the contact work is kept smaller than a tenth of any other energy contribution. This way, proper contact definitions are ensured.

The CZEs at the interfaces between adjacent plies and between overlapping tows also model the contact behaviour between the plies and tows. In regions of delaminations, however, CZEs are deleted and, thus, are no longer available to model inter-ply and inter-tow contact. Therefore, additional contact definitions between every tow and matrix layer are applied in order to prevent inter- and intra-ply penetrations. These additional contact definitions are just active in regions of delaminations, which is ensured by scaling the thicknesses of tow and matrix layers used within the contact calculation by a factor of 0.95. It shall be noted that frictionless behaviour is assumed for inter- and intra ply contact.

3.3 Experimental setup

The carbon fibre reinforced epoxy prepreg material Cycom 5276-1/T650-35-3K-8HS supplied by Cytec Industries Inc. (Wrexham, GB) is used for the fabrication of the laminate plates. The laminates consist of eight carbon fabric reinforced epoxy plies with an eight harness satin weaving style in a quasi-isotropic layup ($[0/45/0/45]_s$). All laminate plates are autoclave-cured at 177°C under 6 bar pressure for 2.5 hours resulting in a laminate thickness of 3.4 mm. Rectangular test specimens, 150 mm in length and 100 mm in width, are cut from the cured laminate plates using a water jet cutting plant. It has to be noted that the zero degree fibre direction is parallel to the longer edge of the specimens. The fabrication of the laminates has been conducted at FACC AG (Ried im Innkreis, Austria).

All Impact tests are performed at room temperature on a CEAST 9350 Drop Tower Impact System (Instron, High Wycombe, GB) at the Polymer Competence Centre Leoben (PCCL) GmbH (Leoben, Austria). The total mass of the drop weight is 2 kg, which is composed of the mass from the sled of the drop tower test system and additionally added ballast. The test device is equipped with an anti-rebound mechanism in order to prevent multiple strikes. The rectangular specimens are supported on the bottom side by a steel frame with an inner cut out of 125 mm×75 mm, while the top side of the investigated specimens is pressed down via four spherical pads of 12.2 mm diameter at the corners of a 100 mm×87.5 mm rectangle, cf. Fig 4.2. All test specimens used in this study are subjected to a central impact by a hemispherical impactor of 20 mm diameter with an impact energy of 400 J. The applied impact velocity of 20 m/s is monitored by a pair of photoelectric diodes and the impact force is measured with a load cell ($F_{\mathrm{max}} = 36\,\mathrm{kN}$), which is located just above the semi-spherical impactor. The energy absorbed by each test specimen is calculated based on the recorded force versus time curves.

3.4 Application example - verification

The described MEA is exemplified by the numerical simulation of a rectangular laminated composite plate with quasi-isotropic layup in a drop weight impact test setup, as described in Section 3.3. Moreover, the example of the drop weight impact test is used to verify the MEA. An exploded view of the modelled drop tower test setup is shown in Fig. 3.4.

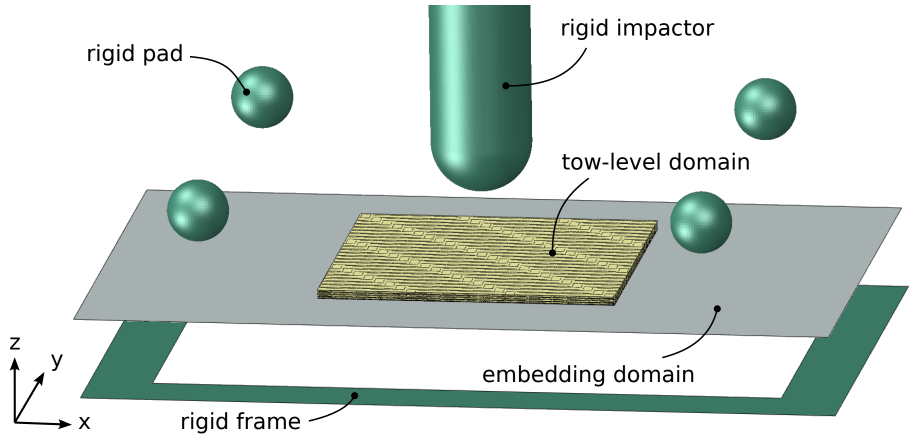

Figure 3.4: Exploded view of the modelled drop tower test setup.

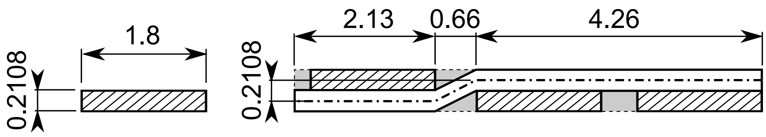

Figure 3.5: Idealised topology of the woven fabric reinforcement with dimensions in mm.

3.4.1 Geometric modelling and boundary conditions

The presented MEA is utilised to model the laminate consisting of eight fabric plies with eight harness satin weaving style, cf. Section 3.3. A section of the modelled (idealised) fabric topology and the corresponding dimensions are shown in Fig. 3.5. The quasi-isotropic $[0/45/0/45]_s$ laminate layup with respect to the fabric topology is modelled such that all $0\,^\circ$ plies and all $45\,^\circ$ plies are stacked in-phase, respectively. The tow-level domain with a size of $59\,\text{mm}\times59\,\text{mm}$ is placed at the centre of the plate where the tows as well as the matrix pockets are discretised using linearly interpolated, fully integrated 4-noded, Mindlin-Reissner type shell elements with an average element edge length of $0.3\,\text{mm}$. For the given fabric topology, cf. Fig. 3.5, this yields 6 elements along the width of a tow. The thickness integration of the shell elements is conducted using the Simpson rule where five section points through the thickness are modelled. The interfaces (ply-ply and tow-tow) are discretised using 8-noded, brick shaped CZEs. The ply-ply interface features an in-plane element dimension of 0.24 mm×0.24 mm, whereas the tow-tow interface features an in-plane element dimension of 0.3 mm×0.3 mm.

The embedding domain is discretised by a single layer of linearly interpolated, fully integrated 4-noded shell elements with layered section definition, where each section corresponds to an individual ply of the laminate and features five section points for the thickness integration using the Simpson rule. The average element edge length varies from 0.5 mm at the transition to the tow-level domain to 1 mm at the outer regions.

The mounting of the laminate is modelled by four spherical rigid pads of 12.2 mm diameter at the corners of a 100 mm×87.5 mm rectangle on top of the laminate and a rigid frame with an inner cut-out of 125 mm×75 mm at the bottom side of the laminate, cf. Fig. 3.4. The movement of the pads and the frame is fixed in all degrees of freedom. Contact is defined between the top surface of the laminate and the pads, as well as between the bottom surface of the laminate and the top surface of the frame, where Coulomb friction with a friction coefficient of 0.3 is modelled.

The impactor is modelled as a hemispherical rigid body and its movement is fixed for every degree of freedom except the translational movement along the z-direction, cf. Fig. 3.4. The total mass of 2 kg of the impacting part is modelled by assigning two regions of different mass density to the impactor. The region which comes into contact with the laminate features the mass density of steel whereas the top region of the impactor is assigned a higher mass density in order to reach the total mass. An initial velocity of 20 m/s is assigned to the impactor, resulting in an impact energy of 400 J. Frictionless contact is defined between the impactor and the top surfaces of every tow and every matrix layer.

3.4.2 Material properties

The mass densities assigned to the tows, the matrix pockets and the interfaces are listed in Tab. 3.1. The mass density of the tows in regions where no CZEs are attached

Table 3.1: Mass densities assigned to tows, matrix pockets and interfaces. See the text for an explanation.

ρ_{tow}	$\rho_{\text{tow}}^{\text{int}}$	ρ_{mat}	$\rho_{\text{mat}}^{\text{int}}$	$\rho_{\text{CZE}}^{\text{ply}}$	$\rho_{\text{CZE}}^{\text{tow}}$
1685 kg/m^3	1545 kg/m^3	1200 kg/m^3	800 kg/m^3	0.0448 kg/m^2	0.0592 kg/m^2

Table 3.2: Material properties defining the constitutive response of the tows. The subscript 1 denotes the direction along the undulation path of the tows whereas the subscript 2 denotes the direction perpendicular to the undulation path. Details are given in [39] and Appendix B.

elastic	E_1	E_2	ν_{12}	G_{12}	
constants	142.177 GPa	13.82 GPa	0.23	6.252 GPa	
nominal	X_{1+}	X_{1-}	X_{2+}	X_{2-}	S_{12}
strengths	2116.32 MPa	1610.27 MPa	83.183 MPa	333.38 MPa	159 MPa
crit. energy	$\mathscr{G}_{\text{Ic}}^{1+}$	$\mathscr{G}_{\text{Ic}}^{1-}$	$\mathscr{G}_{\text{Ic}}^{2+}$	$\mathscr{G}_{\text{Ic}}^{2-}$	
release rates	123.29 N/mm	107.5 N/mm	0.2746 N/mm	1.0434 N/mm	
shear	β_{12}	$d_{12}^{\max}$	$\tilde{\sigma}_{\text{y0}}$	C	p
behaviour	0.18634	1.0	55 MPa	669.94 MPa	0.823

is ρ_{tow} and $\rho_{\text{tow}}^{\text{int}}$ is the mass density of the tows where CZEs are attached. The mass density of the matrix pockets in regions where no CZEs are attached (i.e. at the top and bottom side of the laminate) is denoted by ρ_{mat} and the mass density of matrix pockets with CZEs attached is $\rho_{\text{mat}}^{\text{int}}$. Further, $\rho_{\text{CZE}}^{\text{ply}}$ is the mass density assigned to the CZEs at the interfaces between adjacent plies and $\rho_{\text{CZE}}^{\text{tow}}$ is the mass density assigned to the CZEs at the interfaces between tows. It shall be noted that $\rho_{\text{CZE}}^{\text{ply}}$ and $\rho_{\text{CZE}}^{\text{tow}}$ are defined in terms of mass per unit area.

The material properties defining the constitutive behaviour of the tows are listed in Tab. 3.2. Details can be found in [39] and Appendix B. The elastic properties and the nominal strengths of the tows are estimated from datasheets for UD carbon/epoxy plies and the critical energy release rates are estimated from [92]. Thereby, the tow material properties are determined by scaling the UD-ply properties such that an overall modelled fibre volume fraction of 0.7 is reached, cf. [38, 57] and Section 3.2.1.

Table 3.3: Material properties assigned to the matrix pockets. See the text for an explanation.

E_M	ν_M	σ_y0	friction angle	$\bar{\varepsilon}_\mathrm{f}^\mathrm{pl}$	$\mathscr{G}_\mathrm{f}$
3520 MPa	0.37	55 MPa	25°	0.0778	0.5 N/mm
σ_yi	73.55 MPa	91.78 MPa	108.27 MPa	110.7 MPa	136.9 MPa
$\bar{\varepsilon}_i^\mathrm{pl}$	0.0128	0.0294	0.0461	0.0487	0.0778

Table 3.4: Material properties of the homogenised plies within the embedding domain. The subscripts 1 and 2 indicate the tow directions.

ρ_lam	E_1	E_2	ν_{12}	G_{12}
1560 kg/m^3	57.281 GPa	57.281 GPa	0.045	4.206 GPa

The material properties assigned to the matrix pockets are given in Tab. 3.3. The elastic properties are taken from a corresponding material datasheet and the properties describing the plastic behaviour are assumed based on the typical behaviour of epoxy resins. The initial yield stress is indicated by σ_y0 and the pressure dependency is given by the friction angle. The hardening behaviour is defined by pairs of uniaxial tensile yield stresses, $\sigma_{\mathrm{y}i}$, and corresponding tensile plastic strains, $\bar{\varepsilon}_i^\mathrm{pl}$. The ductile damage behaviour is defined by the equivalent plastic strain at the beginning of damage, $\bar{\varepsilon}_f^\mathrm{pl}$, and the associated energy release rate, $\mathscr{G}_\mathrm{f}$. The properties of the homogenised plies within the embedding domain are listed in Tab. 3.4.

The parameters defining the constitutive response of the interfaces between adjacent plies are listed in Tab. 3.5. The nominal strengths for pure mode II and mode III

Table 3.5: Ply-ply interface properties describing the initial stiffness of the interface, as well as damage initiation and propagation.

	Mode I	Mode II	Mode III
init. stiffness	10^6 N/mm^3	10^6 N/mm^3	10^6 N/mm^3
interlam. strength	60 MPa	79.289 MPa	79.289 MPa
crit. energy rel. rate	0.9 N/mm	2.0 N/mm	2.0 N/mm

Table 3.6: Tow-tow interface properties describing the initial stiffness of the interface, as well as damage initiation and propagation.

	Mode I	Mode II	Mode III
init. stiffness	10^6 N/mm^3	10^6 N/mm^3	10^6 N/mm^3
interlam. strength	82.37 MPa	108.86 MPa	108.86 MPa
crit. energy rel. rate	1.24 N/mm	2.75 N/mm	2.75 N/mm

loading of the interface are taken from a corresponding material data sheet. The nominal strength for mode I loading is assumed. The critical energy release rates are estimated from values published in Ref. [67]. The parameters defining the constitutive response of the interfaces between overlapping tows are listed in Tab. 3.6. They are estimated based on the ply interface properties, cf. Tab.3.5. Due to the geometrical idealisations of the fabric topology, cf. Section 3.2.1, the total modelled tow-tow interface area is smaller than in a real fabric reinforced ply. Therefore the properties of the tow-tow interfaces are scaled such that they correspond to an overall fibre volume fraction of 0.7.

3.4.3 Results and discussion

In the following, the predictions by the MEA model are presented and compared to results from corresponding experiments. Details regarding the experimental setup are described in Section 3.3. Figure 3.6 shows the predicted and the experimentally observed failure pattern at the back face of the laminate after the 400 J impact. Total perforation occurs in both simulation and experiment. The intra-ply cracks depicted in Fig. 3.6 (left) arise due to propagating damage within individual tows, as well as within matrix pockets. The predicted cross shaped cracks in the bottom ply correspond very well to the experimentally observed failure pattern. Also, some small cracks between tows within the unreinforced resin zones are predicted. Such small cracks are also visible in the tested plate, cf. the bottom part of Fig. 3.6 (right). As can be seen, the predicted failure pattern is in very close agreement to the one

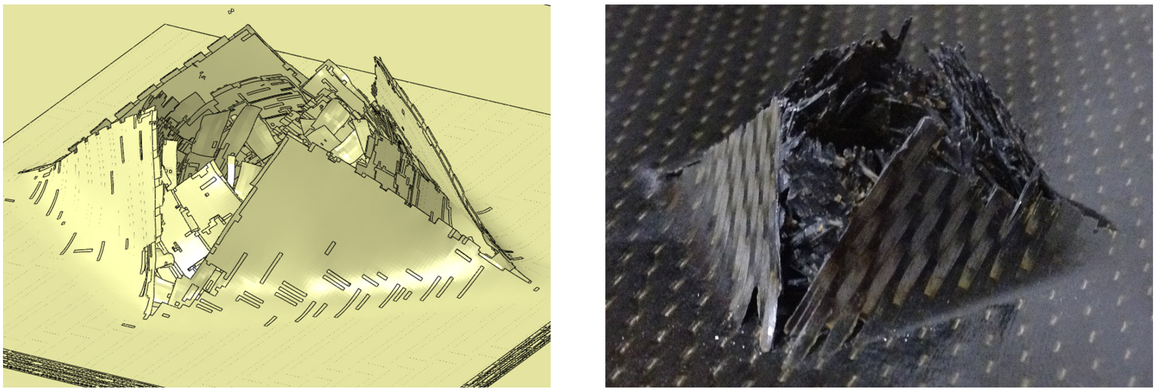

Figure 3.6: Failure pattern at the back face of the laminated plate after 400 J impact. Left: Predicted impact response. Right: Experimentally observed response. The images are depicted at the same length scale.

observed experimentally indicating that the intra-ply damage and failure mechanisms are modelled appropriately within the proposed model.

The predicted delamination pattern within the ply-ply interfaces at the end of the impact event is shown in Fig. 3.7 (left). The shadings indicate an overlay of the delamination areas of all seven interfaces. The darker the shadings are, the more interfaces are delaminated at a specific location of the laminate. Figure 3.7 (right) shows the front face of the experimentally tested plate. The white lines indicate the projected delamination area as determined by a ultrasonic scan, which is also represented by the black solid lines in Fig. 3.7 (left). As can be seen, the predicted shape and size of the projected delamination area is in very close accordance with the experimentally determined one. Hence, as far as the comparisons in Figs. 3.6 and 3.7 show, the spatial distribution of intra- and inter-ply damage is predicted very well by the MEA model.

Now, the quantitative predictive capabilities of the MEA are assessed. Figure 3.8 (left) shows a comparison of the predicted and experimentally evaluated amount of energy absorbed by the laminate during the impact event. The predicted energy absorption is evaluated as the reduction of the kinetic energy of the impactor whereas the measured energy absorption is evaluated from the recorded force–time signal. As

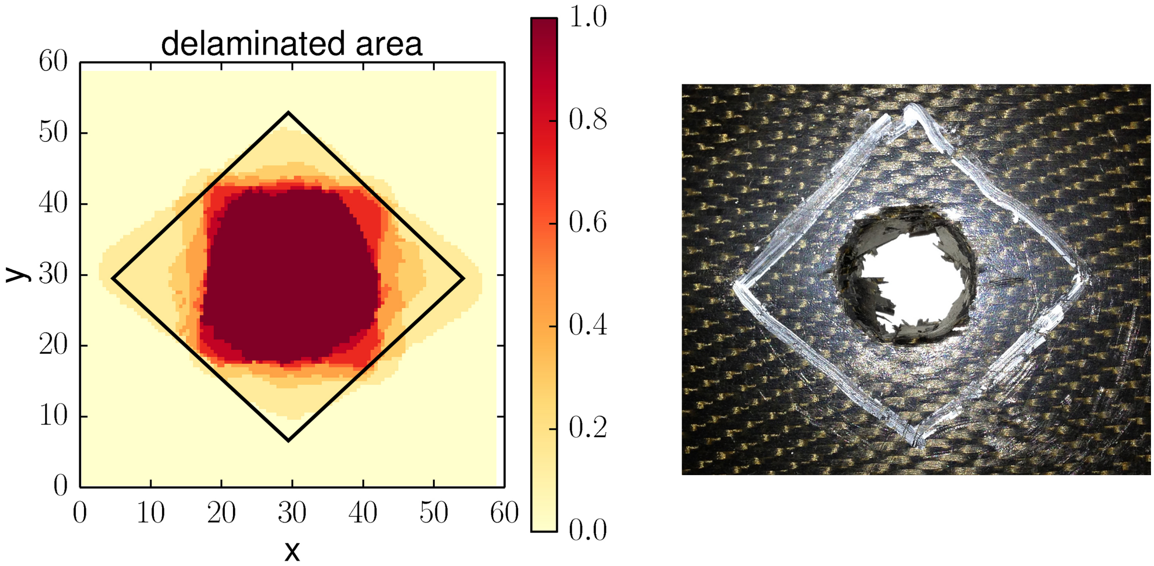

Figure 3.7: Left: Overlay of predicted delamination areas. A value of 0.0 indicates that no delamination is predicted, whereas 1.0 corresponds to delamination at every interface. The impactor hits the plate at $x = 29.5$mm and $y = 29.5$mm with respect to the depicted coordinates. Right: Projected delamination area according to a ultrasonic scan of the impacted plate. The images are depicted at the same length scale.

can be seen, the prediction matches not only the total amount of absorbed energy of the laminate but also the progression of energy absorption with respect to time very closely. Considering Fig. 3.8 (right), the predicted and measured total force acting on the impactor during the impact event are compared. Very close agreement is found at every instant of time throughout the impact event and the time of occurrence of the peak force, as well as its magnitude is well predicted. Note that the oscillations of the measured force-time signal are partly caused by slight elastic deformations of the impactor and that the sudden stop of the measured force-time signal at about 0.74ms is due to the activation of the anti-rebound mechanism of the drop tower test system. These effects are not modelled within the present simulation. From the comparisons presented above it is concluded that the MEA model is able to predict the qualitative and quantitative impact behaviour of a fabric reinforced laminate to a high degree of precision. Some more detailed evaluations of the simulation results, which exceed usual experimental evaluation capabilities, are discussed in Section 3.5.

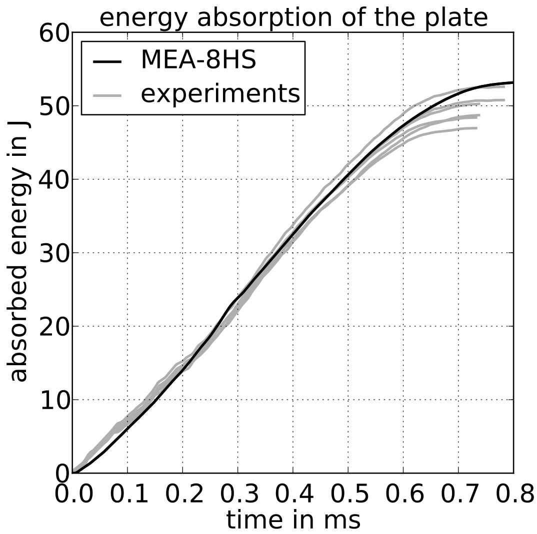

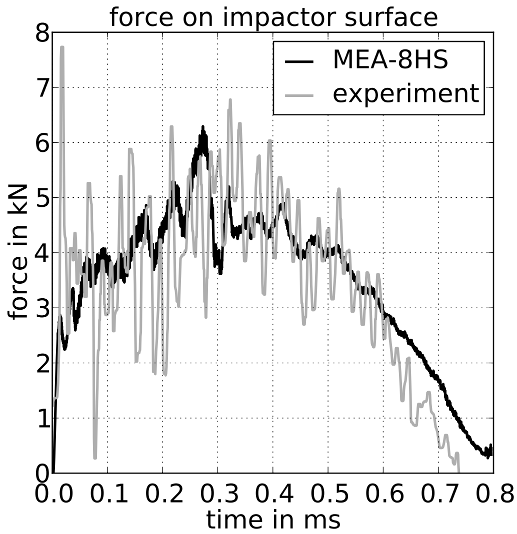

Figure 3.8: Left: Comparison of the predicted and experimentally obtained energy absorbed by the laminate with respect to time. Right: Comparison of predicted and experimentally measured total force acting on the impactor with respect to time. At the time $t = 0$ms first contact between the impactor and the plate is observed.

Next, the computational effort is considered. The MEA model features approximately 12.5 million degrees of freedom and the computations are conducted using a distributed memory cluster system of four standard PC workstations with, in total, 16CPUs at 3.3GHz. In this configuration, the computation of the laminate's impact response for a time span of 0.8 ms takes about 2.4 days.

3.5 Effect of weaving pattern

In the following, the effect of different weaving patterns on the energy absorption behaviour is investigated based on the example of a laminate in a drop weight impact test setup, as discussed in Section 3.4. Further, some detailed evaluations of the simulation results, exceeding usual experimental evaluation capabilities, are discussed.

Figure 3.9 shows the three weaving patterns which are going to be investigated, an eight harness satin, a 2/2 twill weave and a plain weave. As can be seen, the degree

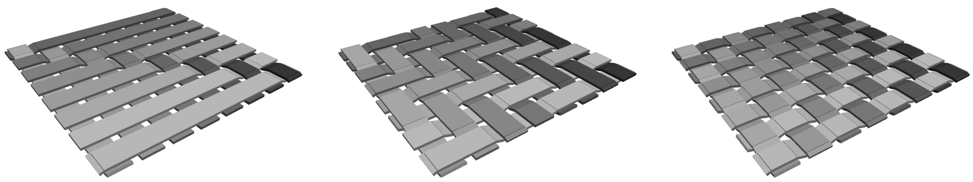

Figure 3.9: Weaving patterns considered for comparison. Left: Eight harness satin. Middle: 2/2 twill. Right: Plain.

Table 3.7: Homogenised elastic properties of plies with different reinforcement weaving style. The subscripts 1 and 2 indicate the tow directions.

	$E_1 = E_2$	ν_{12}	G_{12}
8HS	57.281 GPa	0.045	4.206 GPa
2/2 twill	56.589 GPa	0.045	4.186 GPa
plain	55.249 GPa	0.045	4.146 GPa

of tow undulation varies depending on the weaving style. The MEA is utilised in order to study the effect of these weaving patterns (i.e. the effect of different degrees of tow undulation) on the impact behaviour and the energy absorption behaviour of fabric reinforced laminates, where the FEM modelling and simulation strategy is the same as presented in Section 3.4. Thereby, the micro-geometry of the fabric, i.e. the tow cross-section and the distance between the tows, is kept identical and just the tow undulation is varied. The quasi-isotropic $[0/45/0/45]_s$ laminate layup with respect to the fabric topology is modelled such that all $0\,^\circ$ plies and all $45\,^\circ$ plies are stacked in-phase, respectively, cf. Section 3.4. The material properties of the tows, the matrix pockets and the interfaces are identical for all considered configurations and correspond to the values in Tabs. 3.2, 3.3, 3.5 and 3.6. Due to the different degree of tow undulation, the homogenised properties of the corresponding plies are slightly different, as can be seen in Tab. 3.7.

Figure 3.10 (left) shows a comparison of the total energy absorbed by laminates with different reinforcement weaving pattern. The solid line correponds to the laminate with eight harness satin fabric reinforcement from Section 3.4, the dashed line represents the laminate with the 2/2 twill weaving pattern and the dotted line represents

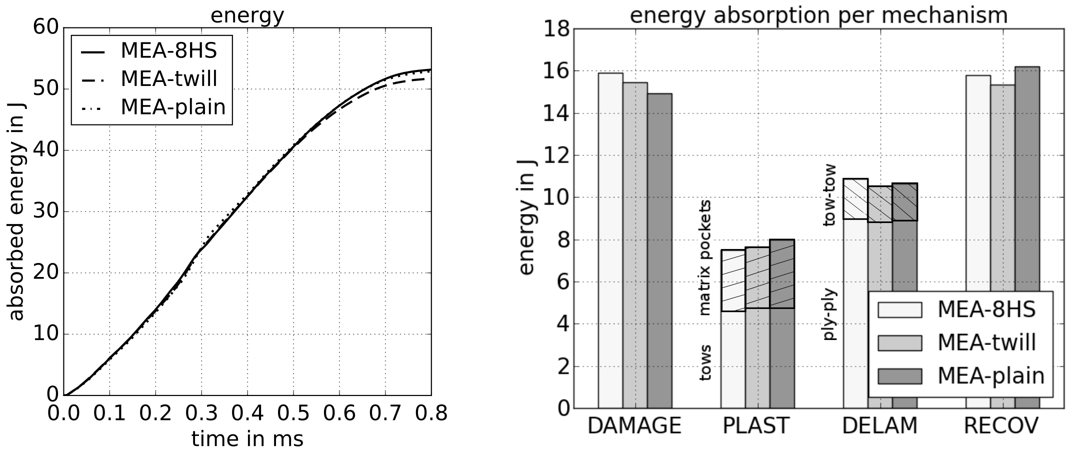

Figure 3.10: Comparison of the effect of different weaving patterns on the impact behaviour. Left: Predicted total energy absorption of the laminate. Right: Predicted energy absorption of individual mechanisms at the end of the impact event.

the laminate with the plain weaving pattern. The progression of energy absorption is almost identical for all configurations. Considering the scatter in the experimental data, cf. 3.8 (left), the differences in the predicted total energy absorption of laminates with different reinforcement weaving pattern are very small.

Figure 3.10 (right) shows the contributions of individual mechanisms to the total amount of energy absorbed by the laminate. The bars with index "DAMAGE" identify the amount of energy absorbed by ply fracture, where the major part is represented by tow fracture. The bars with index "PLAST" correspond to the energy absorbed due to plastic deformation within the tows and the matrix pockets. The bars with index "DELAM" represent the energy absorbed by ply-ply and tow-tow delamination. The bars "RECOV" identify the recoverable part of the absorbed energy being the sum of the plate's kinetic energy and the elastic strain energy stored within the plate. They correspond to the elastic oscillation of the plate. As can be seen, there is no significant difference in the energy absorption of individual mechanisms with respect to the different reinforcement weaving styles. The highest contributions to the absorbed energy are predicted to arise from ply fracture and from the elastic

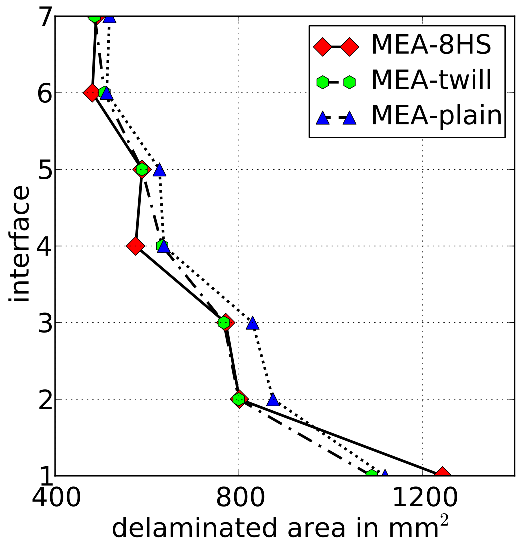

Figure 3.11: Prediction of delaminated areas within individual interfaces of the laminate after impact. Interface number seven is the one closest to the impacted surface.

oscillation of the laminate. The energy dissipated due to ply-ply delaminations is roughly 9 J and the energy dissipated due to tow-tow delamination is about 2 J. The energy dissipated due to plastic deformations is roughly 8 J and, thus, also represents a significant contribution. Interestingly, roughly one third of the total plastic dissipated energy is associated with plastic deformations within the matrix pockets. Note that the modelled volume fraction of the matrix pockets is slightly higher than the one in a real fabric reinforced laminate due to the applied geometrical idealisations, cf. Section 3.2.1. Concluding from Fig. 3.10 (right) it can be stated that all mechanisms represent a significant part of the total energy absorption. However, the degree of tow undulation does not seem to have a significant effect on the extent of any of the mechanisms.

Figure 3.11 shows the delaminated areas within each interface, as predicted by the MEA model. A trend with delamination areas becoming larger towards the back face of the laminate is recognisable. The delaminated area within the interface closest to the back face of the laminate is significantly larger than the one within the other interfaces. This corresponds to the failure pattern shown in Fig. 3.6, where the ply at the back face exhibits a long cross-shaped crack. It can be seen that there is almost no difference in the delaminated areas with respect to the different reinforcement weaving styles. Hence, the conclusions from Fig. 3.10 (right) are affirmed.

3.6 Summary

A multiscale modelling approach (MEA) for simulating impact damage in fabric reinforced composite laminates is developed. Thereby, the topology of a multi-layered fabric reinforced laminate is modelled at tow-level for a sub-domain embedded in a shell layer with a homogenised representation of the laminate. Within the tow-level domain, individual tows as well as unreinforced resin zones are entirely modelled using shell elements, which are coupled appropriately. The interfaces between adjacent plies, as well as the interfaces between tows, are modelled using cohesive zone elements. Material nonlinearities such as damage and plasticity like behaviour of tows, inelastic behaviour of unreinforced resin zones up to fracture and delamination of plies and tows are accounted for.

As an example, a numerical simulation of a laminated plate consisting of eight carbon fabric plies with eight harness satin weaving style in a drop tower test setup is conducted using the explicit Finite Element code Abaqus/Explicit v6.14. The spatial distribution of intra- and inter-ply damage is predicted and the total amount of energy absorbed by the plate, as well as the contributions of individual mechanisms are evaluated. Comparisons to results from equivalent experiments show very good agreement. Insights into the impact behaviour of fabric reinforced laminates are gained at a high level of detail, exceeding usual experimental evaluation capabilities. The presented MEA offers the possibility to investigate the effect of the fabric topology on the impact behaviour of woven laminates, as different weaving styles can be modelled in a fully automated way. Furthermore, the damage and failure behaviour of hybrid fabric plies composed of tows made from different materials can be modelled.

3.7 Publications

The work presented in this chapter resulted in the publications [114, 117].

Chapter 4

Ply-scale modelling approach

4.1 Introduction

Within this chapter, a strategy for modelling and simulating the intermediate velocity/mass impact behaviour of fabric reinforced laminates up to complete perforation is developed. Special attention is directed towards numerical efficiency in order to open up the possibility for simulating impact on structural components much larger than coupon specimens within reasonable computation time. Therefore, a ply-level based discretisation in combination with shell elements is proposed. As an example of the proposed modelling strategy, numerical predictions of a rectangular laminated composite plate with quasi-isotropic layup in a drop weight impact test setup are presented. The acquired simulation results are verified with accompanying experiments. Moreover, simulations with different mesh sizes are conducted in order to investigate possible improvements regarding numerical efficiency and the accompanied trade-off in accuracy. The simulations are realised using the explicit FEM code Abaqus/Explicit v6.14 (Dassault Systemes Simulia Corp., Providence, RI, USA).

4.2 Modelling approach

Impact on laminated composites, in general, is a highly dynamic loading scenario involving nonlinear material behaviour. An overview of occurring damage and failure modes within FRP laminates for different impact scenarios is given in [2, 42]. The acting mechanisms can be categorised by their location of occurrence into intra-laminar and inter-laminar mechanisms. The intra-laminar failure mechanisms include matrix cracking, fibre rupture and plasticity like effects whereas inter-laminar failure denotes the debonding of adjacent plies, i.e. delamination. Each of these mechanisms contributes to the overall response of the laminate and their interaction results in penetration or even perforation of the laminate, depending on the actual impact scenario. Hence, meaningful predictions require a mechanism based modelling approach. This encompasses the modelling and simulation of propagating damage and failure of several mechanisms using suitable constitutive theories applied at appropriate geometrical length scales.

The proposed modelling strategy provides the ability to predict the overall energy absorption of a laminate subjected to transverse impact as well as the energy contributions of individual mechanisms. Furthermore, the approach is suitable to simulate complete perforation of the laminate. The modelling strategy is realised within the framework of the FEM, whereby an explicit time integration scheme is applied in order to simulate the highly nonlinear dynamic impact response of the laminate.

4.2.1 Geometrical modelling

Within this chapter, laminated composites consisting of several layers of fabric plies are considered. The smallest length scale to be resolved within the geometrical modelling is chosen to be the ply-level. Thereby, the laminate is modelled as a stack of various homogeneous orthotropic layers connected via inter-laminar interfaces, cf. [81]. The mid-plane of each ply is discretised by an individual layer of shell elements

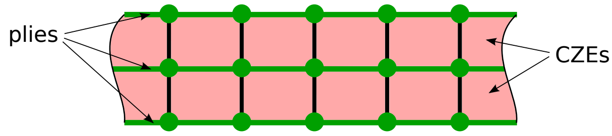

Figure 4.1: Schematic illustration of the stacked shell approach (SSA). The plies are represented by the shell layers at the plies' mid-planes where the corresponding nodes are marked as dots. The CZEs are illustrated as shaded areas confined by black lines.

whereas the interfaces are represented by hexahedral elements in combination with a cohesive zone approach. These cohesive zone elements (CZE) share the nodes of the adjacent shell layers located at the corresponding plies' mid-planes. Hence, the in-plane dimensions of the CZEs are identical to the dimensions of the corresponding shell elements and their geometrical thickness corresponds to the normal distance between adjacent shell layers. It shall be noted that despite their finite geometrical thickness, the CZEs model the mechanical behaviour of a zero-thickness interface since a traction-separation based constitutive law is applied.

The total mass of the laminate is distributed between the plies and the interfaces, since the explicit FEM code Abaqus/Explicit demands that every element within the computational domain is assigned some mass density. As Abaqus/Explicit uses lumped mass matrices, the nodal masses remain unchanged and the dynamic behaviour of the laminate is retained, regardless of the actual mass distribution between plies and interfaces. This arrangement is called stacked shell approach (SSA) in the following and is schematically depicted in Fig. 4.1.

Major benefits in terms of computational efficiency of the proposed SSA arise from the use of shell elements for modelling the intra-ply behaviour of the composite. This way, the required amount of degrees of freedom is reduced significantly compared to an equivalent model discretised by three dimensional continuum elements, cf. [58]. Linearly interpolated continuum elements, as usually applied in explicit FEM codes, require aspect ratios close to one and considerably small element dimensions in order to alleviate the effect of shear locking which typically occurs during bending deformations. In the context of Fig. 4.1, moreover, each ply should be discretised by two or more continuum elements in thickness direction in order to describe the possibly nonlinear stress distribution over ply thickness. In this respect, a shell element based discretisation allows for larger element dimensions due to its kinematic assumptions and, furthermore, the discretisation in the thickness direction of the plies is not necessary.

A further advantage of the use of a shell element based discretisation arises from the definition of the smallest stable time increment of the explicit time integration scheme. In general, it is dependent on the material properties and the smallest element dimension of the mesh. Considering a mesh composed of continuum elements, the smallest element dimension is governed by the usually small ply thicknesses of the laminate. However, when using shell elements the smallest element dimension is governed by the in-plane element dimensions which, typically, are significantly larger than the ply thicknesses. Hence, larger stable time increments arise resulting in shorter computation times.

A limitation of the shell formulation lies in the fact that damage and failure within the shell layers representing individual plies results from in-plane stress and strain components only. However, the out-of-plane stress state is resolved within the CZEs at the interfaces between adjacent plies. The latter representation of the out-of-plane stress state is shown to be quite reliable, cf. [126]. This way, delamination due to transverse shear and out-of-plane tension is accounted for, provided appropriate constitutive theories are applied.

Hence, impact scenarios where bending effects are dominating the overall response and ply damage and failure occurs due to in-plane stresses and strains are fully covered by the SSA, as well as scenarios where delaminations occur. Scenarios where ply failure occurs due to transverse crushing of the laminate, as typically observed for high velocity impact, are beyond the scope of the SSA.

4.2.2 Constitutive modelling

The constitutive behaviour is described using individual constitutive laws for plies and interfaces. The fabric reinforced plies are modelled as homogeneous orthotropic material in combination with an energy based continuum damage mechanics approach to account for tensile and compressive fibre damage. Furthermore, plastic deformation and damage under in-plane shear loading are modelled in order to capture the matrix dominated shear response of the ply. As the stiffness degradation associated with the continuum damage mechanics approach may lead to excessive element distortions and other related numerical difficulties, element deletion is utilised during the simulation. Thereby, a shell element is deleted when one of the damage variables describing tensile or compressive damage along fibre directions reaches a value of 0.99 at one integration point but all associated section points. The described constitutive model is readily available within the FEM package Abaqus/Explicit as a built-in VUMAT user subroutine (ABQ_PLY_FABRIC), cf. [39]. A summary of this material model is given in Appendix B.

The interface constitutive response is modelled using the Abaqus built-in traction-separation based constitutive model for CZEs, cf. [40]. Within the elastic range the normal and shear traction components are assumed to be uncoupled. Damage initiation is predicted according to a quadratic nominal stress criterion. Damage evolution is modelled based on the critical energy release rate of the interface in combination with a linear softening relation. Mixed-mode conditions are accounted for using the criterion proposed by Benzeggagh and Kenane, cf. [20], where a constant mode mix upon damage initiation is assumed. Once the damage variable reaches a value of 1.0 at all integration points of a CZE, it is considered fully damaged and, therefore, deleted. For further details on the constitutive model and the corresponding equations, the reader is referred to the Abaqus manual [40].

It shall be noted that all necessary material parameters can be determined from coupon experiments which are independent of any experimental impact test. Hence, no inverse calibration needs to be conducted and the predictive capability of the model is ensured. Moreover, all but one of these experimental setups are standardised. Only the determination of the intra-ply critical energy release rates is still subject to research, where an overview of proposed methods is given in Appendix A.

4.2.3 Contact modelling

Considering impact problems, the loads are applied by an impactor contacting the specimen. Hence, contact modelling is essential for the prediction of the impact response. The contact constraints within the simulation are enforced using the general contact algorithm of Abaqus/Explicit, which utilises a penalty algorithm to compute contact forces. The adequacy of the associated penalty stiffnesses is evaluated based on the work done by the contact forces. This contact work shall be small compared to other energy contributions in the model, which can be controlled by variation of the penalty stiffnesses. Within the present simulations, the penalty stiffnesses are chosen such that the contact work is smaller than a tenth of the energy contribution of any other mechanism. This way, proper contact definitions are ensured.

In the SSA, the CZEs at the interfaces also model the contact behaviour between the plies. In regions of delaminations, however, CZEs are deleted and, thus, no longer available to maintain inter-ply contact. Therefore, additional contact definitions between individual plies are applied. These additional contact definitions are just active in regions of delaminations, which is ensured by scaling the ply thickness used within the contact calculation by a factor of 0.9.

4.3 Application example - verification

The described modelling approach (SSA) is exemplified by simulating the response of a rectangular laminated composite plate in a drop weight impact test setup, as

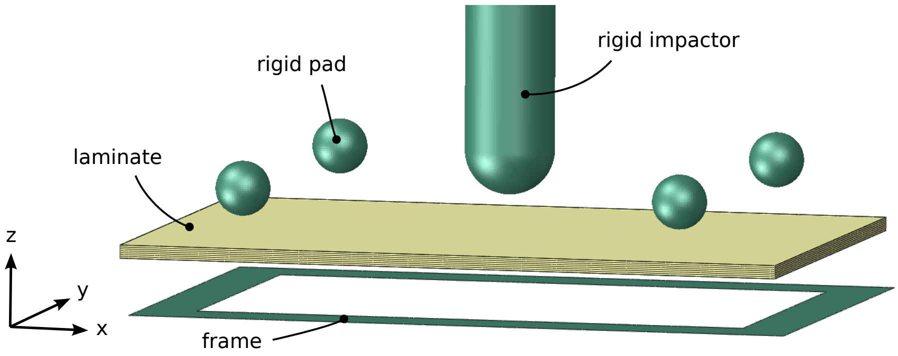

Figure 4.2: Exploded view of the modelled drop tower test setup.

described in Section 3.3. A schematic illustration of the modelled experimental setup is shown in Fig. 4.2.

4.3.1 Geometrical discretisation

The laminate consisting of eight carbon fabric/epoxy plies in a quasi-isotropic layup ($[0/45/0/45]_s$) is modelled applying the SSA described above, where a nominal ply thickness of 0.4216 mm is assigned. In the baseline configuration, the plies are discretised by a regular mesh of four-noded linearly interpolated, fully integrated, Mindlin-Reissner type shell elements (four integration points) with an element dimension of 0.5 mm×0.5 mm. The thickness integration of the shell elements is conducted using the Simpson rule, where five section points are assigned through the thickness. The interfaces are discretised by 8-noded, brick shaped CZEs. Based on this configuration, models with coarser mesh sizes of 1 mm and 1.5 mm element edge length, respectively, are created in order to investigate possible improvements regarding numerical efficiency and the accompanied trade-off in accuracy.

Additionally, the applicability of the presented modelling approach to larger components subjected to impact is investigated by combining the SSA with an embedding approach. Thereby, a region with dimensions of 80 mm×60 mm, located at the centre of the laminate, is modelled using the SSA whereas the rest of the laminate is modelled by a single layer of shell elements with layered section definition. The dimensions of the SSA domain are chosen such that the arising material nonlinearities are contained entirely within this domain. Within the SSA domain, a regular mesh with an element dimension of 1 mm×1 mm is chosen. The edges at the transition between the SSA domain and the surrounding shell layer are coupled according to shell kinematics.

4.3.2 Boundary conditions

The mounting of the laminated plate is modelled using contact boundary conditions. Therefore, the spherical pads as well as the frame are discretised as rigid bodies and their movement is fixed in all degrees of freedom. The impactor is also modelled as a rigid body and is composed of a cylinder with a hemispherical end. Its movement is fixed for every degree of freedom except the translational movement along the z-direction, cf. Fig. 4.2. The total mass of 2 kg of the impacting part is modelled by assigning two regions of different mass density to the impactor. The region which comes into contact with the laminate features the mass density of steel whereas the top region of the impactor is assigned a higher mass density in order to reach the total mass. The initial velocity of the impactor is set to 20 m/s resulting in an impact energy of 400 J. The load introduction to the laminate is modelled by defining contact between the impactor and the top surfaces of each ply. The contact definitions between delaminated plies are discussed in Section 4.2.3. It shall be noted, that frictionless behaviour is assumed for every contact definition.

4.3.3 Material properties

The nominal mass density of the laminate is 1560 kg/m^3. The resulting laminate mass is distributed between the plies and interfaces, cf. Section 4.2.1, where the mass density assigned to the top and bottom plies is 1040 kg/m^3 and the mass density assigned to the inner plies is 520 kg/m^3. The interfaces feature a mass per unit area of 0.438464 kg/m^2.

Table 4.1: Material properties describing the elastic behaviour, the damage and failure behaviour along the fibre directions (1,2) as well as shear damage and plasticity behaviour of the carbon fabric/epoxy ply. Details are given in [39] and Appendix B.

elastic	E_1=E_2=56.813 GPa	G_{12}=4.2058 GPa	ν_{12}=0.047
strengths	X_1^+=X_2^+=802.11 MPa	X_1^-=X_2^-=707.88 MPa	S_{12}=115.8 MPa
crit. energy	$\mathscr{G}_{\mathrm{Ic}}^{1+}$=$\mathscr{G}_{\mathrm{Ic}}^{2+}$=44.9 N/mm	$\mathscr{G}_{\mathrm{Ic}}^{1-}$=$\mathscr{G}_{\mathrm{Ic}}^{2-}$=39.15 N/mm	
shear dam.	β_{12}=0.18634	$d_{12}^{\max}$=1.0	
shear plast.	$\tilde{\sigma}_{\mathrm{y0}}$=55 MPa	C=669.94 MPa	p=0.823

Table 4.2: Interface properties describing the initial stiffness of the interface, as well as damage initiation and propagation.

	Mode I	Mode II	Mode III
initial stiffness	10^6 N/mm^3	10^6 N/mm^3	10^6 N/mm^3
interlaminar strength	60 MPa	79.289 MPa	79.289 MPa
crit. energy	0.9 N/mm	2.0 N/mm	2.0 N/mm

The material properties defining the constitutive behaviour of the carbon fabric reinforced epoxy plies are given in Tab. 4.1. The elastic constants, as well as the nominal strengths are taken from corresponding material data sheets. The critical energy release rates are estimated from values determined for unidirectional (UD) fibre reinforced carbon/epoxy laminates in [92] by taking half of the value determined for UD laminates. The parameters defining the plastic, as well as the damage behaviour of a ply under shear loading are evaluated from available test data of UD reinforced carbon/epoxy laminates collected at the Polymer Competence Center Leoben (Leoben, Austria).

The material parameters defining the constitutive response of the interface (CZEs) are listed in Tab. 4.2. The initial stiffness is chosen such that a quasi-rigid connection between the plies is ensured within the elastic regime. The nominal strengths for pure mode II and mode III loading of the interface are taken from a corresponding material data sheet. The nominal strength for mode I loading is estimated. The critical energy release rates are estimated from values published in [67].

It shall be noted that all material parameters presented above represent quasi-statically obtained values. The assumption of rate-independent material behaviour of carbon/epoxy laminates is supported to some extent by the literature review given in [79], where investigations on the strain rate sensitivity of carbon fibres and unidirectionally reinforced carbon/epoxy laminates are summarised.

4.3.4 Results and Discussion

The simulation results, together with the data gained in the accompanying experiments, cf. Section 3.3, are presented in the following. Note that no inverse model calibration has been applied. The simulations represent genuine predictions with all material parameters originating from sources which are independent from the presented drop tower experiment. In the first part, the predictions corresponding to the baseline configuration are considered and compared to the experimental data.

Figure 4.3 shows a comparison of the predicted and experimentally obtained failure pattern at the back face of the laminated plate after the 400 J impact. The depicted cracks in Fig. 4.3 (left) arise due to propagating damage in the individual plies. Total perforation of the laminate is observed in the simulation as well as in the experiments. The predicted failure pattern is very similar to the experimental one indicating an appropriate representation of intra-ply damage mechanisms within the model.

The model's predictions regarding inter-ply failure are assessed by comparing the numerically predicted and experimentally observed interface damage. Figure 4.4 (left) shows an overlay of the predicted delamination areas of all seven interfaces of the laminate after the impact. The darkness of the shadings indicates the number of delaminated interfaces at a specific location of the laminate. At the darkest regions, every interface is delaminated whereas the lightest regions indicate that no delamination has occurred. The projected delamination area of the experimentally tested

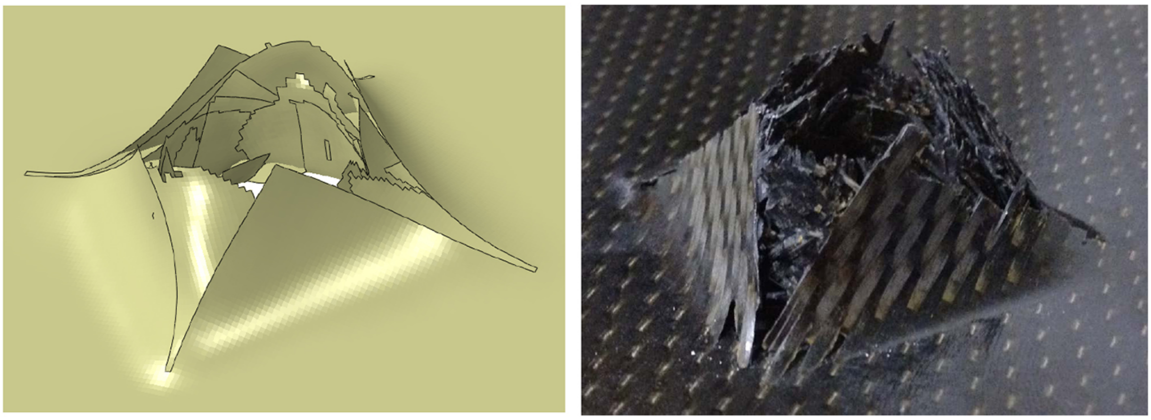

Figure 4.3: Failure pattern at the back face of the laminated plate after 400 J impact. The predicted impact response is shown on the left, the experimentally observed response on the right. The images are depicted at the same length scale.

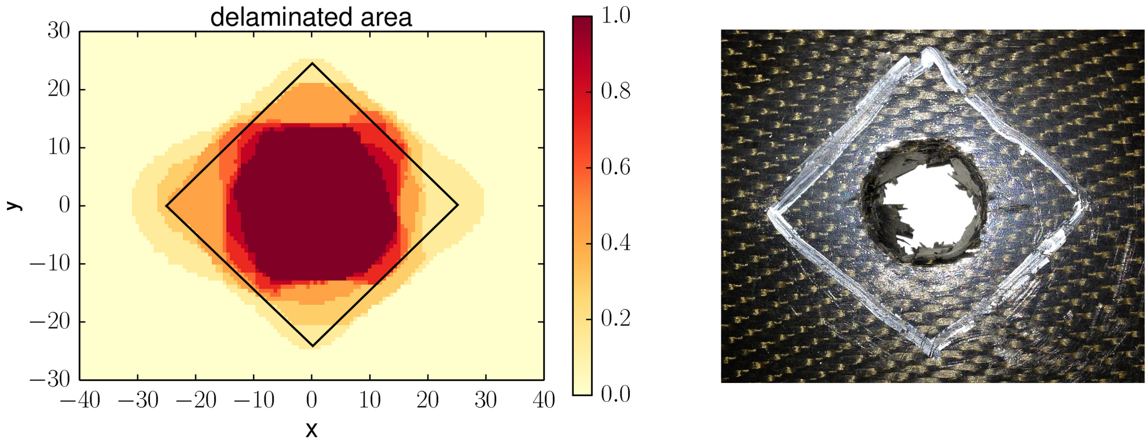

Figure 4.4: Left: Overlay of predicted delamination areas. The coordinates are given in mm where the plate is impacted at the origin. Right: Projected delamination area according to an ultrasonic scan of the impacted plate. The length scales of the images are identical.

plate, determined by an ultrasonic scan, is indicated by the white lines in Fig. 4.4 (right) as well as by the black lines in Fig. 4.4 (left). As can be seen, the predicted shape and extent of delaminations agree well with the experimental results. From Figs. 4.3 and 4.4, it is concluded that the model is able to predict the spatial distribution of intra- and inter-ply damage resolving the corresponding mechanisms.

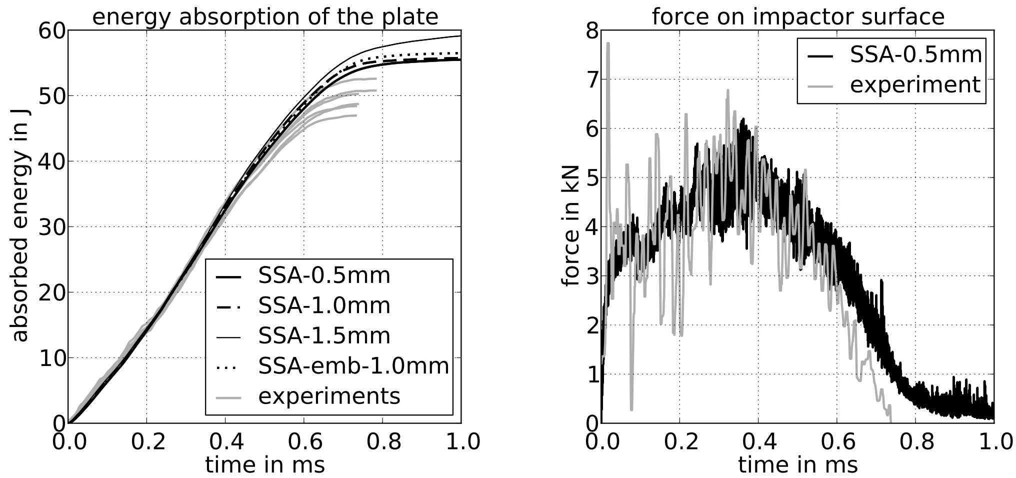

Figure 4.5: Comparison of the total predicted and experimentally measured energy absorption of the laminate (left) and the total force acting on the impactor (right) with respect to time. At the time $t = 0$ms first contact between the impactor and the plate is observed.

The left plot in Fig. 4.5 shows a comparison of the energy absorbed by the plate with respect to time. For the simulations the predicted energy absorption is evaluated as the reduction of the kinetic energy of the impactor during the impact event. The energy absorption of the tested laminates is determined with respect to the recorded force-time response of the impactor. The black solid line indicates the energy absorption predicted by the baseline model (*SSA-0.5mm*) and the grey solid lines represent the experimentally determined energy absorptions. The dashed and the dotted black lines correspond to the coarse mesh configuration (*SSA-1mm*) and the embedding model (*SSA-emb-1mm*), respectively. As can be seen, there is almost no deviation between the baseline model, the *SSA-1mm* and the *SSA-emb-1mm* configurations. The progression of the predicted and measured absorbed energy matches closely with the predicted values being slightly higher at the end of the impact event. The energy absorption predicted by the coarsest mesh model with 1.5mm element edge length (*SSA-1.5mm*) is indicated by the thin black line in Fig. 4.5 (left). The visible deviation in the total absorbed energy compared to the baseline model indicates that the mesh is too coarse. Furthermore, it is observed that results of coarse mesh models, obtained using domain-level parallelisation, are more sensitive to round-off differences caused by domain decomposition, cf. [40]. For these reasons, the *SSA-1.5mm* configuration is no longer considered in the following.

Figure 4.5 (right) shows a comparison of the total force acting on the impactor surface with respect to time. The black solid line represents the results of the baseline model configuration whereas the grey solid line indicates the measured signal. The other model configurations, *SSA-1mm* and *SSA-emb-1mm*, are not shown as no differences are recognisable in the oscillating force-time response. The predicted force–time response agrees very well with the measured signal throughout the entire impact event. The magnitude of the peak force, as well as its time of occurrence are in very close agreement. Starting at about 0.6 ms, the predicted force is slightly higher than the measured one, corresponding to the slight overprediction in the absorbed energy. Note that the sudden stop of the measured force–time signal at about 0.74 ms is due to the activation of the anti-rebound mechanism of the drop tower test system, which is not modelled within the simulation.

Taking uncertainties in the material parameters into account, cf. Section 4.3.3, the presented modelling approach provides outstanding predictions of the qualitative and the quantitative impact behaviour of a laminated plate. It is concluded that the model configurations *SSA-0.5mm*, *SSA-1mm* and *SSA-emb-1mm* are applicable to the present problem.

In the following, the results of these model configurations are investigated in more detail. Figure 4.6 (left) shows the contributions of individual mechanisms to the total energy absorbed by the laminate, as predicted by the three models. The bars with index "DAMAGE" identify the amount of energy absorbed by ply damage, the bars with index "PLAST" are the energy absorbed due to plastic deformation within the plies and the bars with index "DELAM" represent the energy absorbed by delamination between plies. The bars with the index "RECOV" represent the recoverable part of the absorbed energy being the sum of the plate's kinetic energy and the elastic strain energy stored within the plate. It corresponds to the vibration

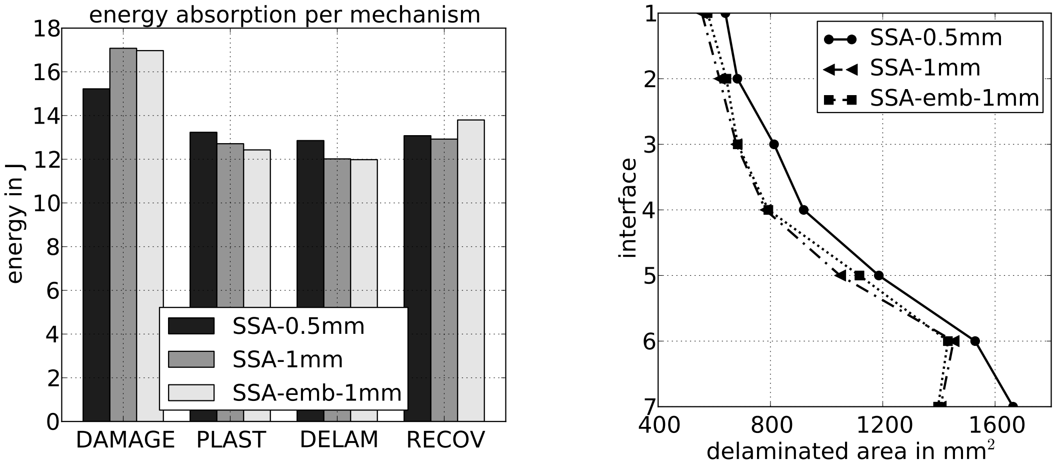

Figure 4.6: Left: Predicted energy absorption of individual mechanisms at the end of the impact event (explanation is given in the text). Right: Predicted delaminated area per interface. Interface number one is the one closest to the impact surface of the laminate.

state of the plate. The models *SSA-1mm* and *SSA-emb-1mm* dissipate some 2 J more energy due to ply damage, whereas they predict a bit less energy spent for delamination and ply plasticity. The recoverable part of the absorbed energy shows very slight differences between the three models.

Considering the assumption of frictionless contact, accompanying simulations have shown that the amount of energy dissipated due to Coulomb friction between delaminated plies is considerably small compared to the contributions of the other mechanisms. Applying a friction coefficient of 0.3 results in about 4 J of energy dissipated due to this friction. Moreover, the simulations show that Coulomb friction between delaminated plies, as well as Coulomb friction between the impactor and the laminate, does not have a significant influence on the amount of energy absorbed by ply damage, delamination, plasticity and elastic deformation. It shall be noted that there is a considerable uncertainty regarding friction coefficients describing friction between delaminated plies, as well as between carbon/epoxy laminates and steel, and their dependency on the normal force and sliding velocity. From that point of view, the assumption of frictionless contact seems justified.

Table 4.3: Comparison of computational demands for three different model configurations. The stated computation time refers to the simulation of 1ms of real time.

	SSA-0.5mm	*SSA-1mm*	*SSA-emb-1mm*
DOFs	3,643,476	1,471,476	1,040,082
comput. time	5h 01min	1h 08min	1h 01min

Figure 4.6 (right) shows a comparison of the delaminated areas per interface for each of the models. All models predict smaller areas of delamination at the interfaces close to the impact surface of the laminate and larger areas of delamination at interfaces at the backside of the laminate. The models *SSA-1mm* and *SSA-emb-1mm* predict slightly smaller delaminated areas throughout the thickness of the laminate, as indicated in Fig. 4.6 (left).

Finally, the computational efficiency of the presented modelling approach is considered. Table 4.3 lists a comparison of computation time versus number of degrees of freedom (DOFs) for the models *SSA-0.5mm*, *SSA-1mm* and *SSA-emb-1mm*. The computations are conducted using a cluster system of a four standard PC workstations with, in total, 16CPUs at 3.3GHz. The models *SSA-1mm* and *SSA-emb-1mm* provide a very good compromise between numerical efficiency and accuracy with a computation time of approximately one hour for the simulation of one millisecond of real time. The computation time for the embedding model, *SSA-emb-1mm*, is roughly the same although it has a lower number of DOFs. This circumstance seems reasonable as the extent of material nonlinearities, which in general drives the computational effort, is almost identical in both models.

The outstanding numerical efficiency of the SSA, together with its applicability in combination with an embedding approach paves the way for impact simulations at component level with conventional computer hardware. Considering the dimensions of the modelled laminate and its number of plies, component level simulations are possible with reasonable computational effort. Having in mind the model's high level of detail (i.e. every ply and interface modelled), the results are even more encouraging.

4.4 Summary

A shell element based modelling approach for simulating impact on fabric reinforced laminates by means of the Finite Element Method is presented. The approach utilises a ply-level based discretisation where every ply and every interface of the laminate is (explicitly) modelled. The damage and failure behaviour of the plies is modelled using an orthotropic energy based continuum damage mechanics approach. The interfaces between the individual plies are modelled by cohesive zone elements in combination with a traction-separation based constitutive law.

Numerical predictions of a rectangular laminated composite plate with quasi-isotropic layup in a drop tower test setup are conducted. The predictions are based on material parameters partly from corresponding material data sheets and partly estimated from the literature. Thus, no inverse model calibration is applied. The acquired simulation results are verified with accompanying experiments. The predicted damage and failure behaviour, as well as the spatial distribution of intra- and inter-ply mechanisms is in very close agreement to the experimental observations and the predicted amount of absorbed energy agrees very well with the experimentally determined values.

The approach shows exceptional numerical efficiency while maintaining a high level of predicted details. In the case of modelling impact on large components, a patch modelled using the SSA can be embedded at the region of impact while some less detailed representation is used at remote regions of the component. This way, further improvements in computational efficiency are achieved and simulations of the impact response of complex FRP laminates at component level are possible with reasonable computational effort.

4.5 Publications

The work presented in this chapter resulted in the publications [116, 118].

Chapter 5

Ply-scale vs. tow-scale modelling

In the following, the effect of the length scale of the geometrical discretisation on the predicted energy absorption of a fabric reinforced laminate is investigated. Thereby, the proposed ply-level modelling approach (SSA), cf. Section 4.2, is opposed to the proposed tow-level modelling approach (MEA), cf. Section 3.2. The investigations are based on the simulation results for the presented drop weight impact test setup, cf. Sections 4.3 and 3.4.

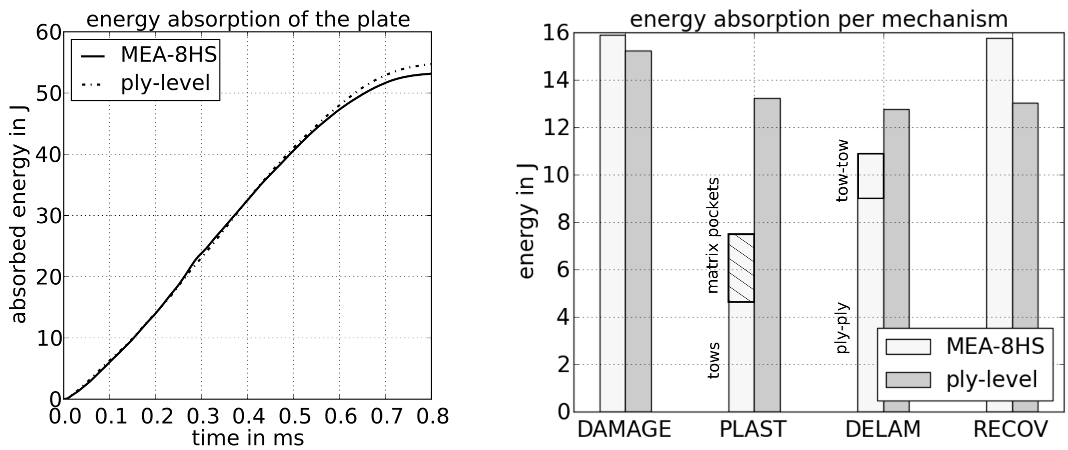

Figure 5.1: Comparison of the effect of the length scale of the geometrical discretisation on the predicted energy absorption behaviour. Left: Predicted total energy absorption of the laminate. Right: Predicted energy absorption of individual mechanisms at the end of the impact event.

Figure 5.1 (left) shows a comparison of the total absorbed energy. The ply-level simulation is indicated by the black solid line and the tow-level simulation (MEA) is represented by the dotted line. As can be seen, the progression of energy absorption is almost identical for both models up to 0.5 ms after the impactor hit the laminate. Afterwards, the ply-level model predicts a slightly higher energy absorption. Considering the experimental scatter, cf. Fig. 4.5 (left), the differences in the total energy absorption are not significant and, thus, Fig. 5.1 (left) indicates that the length scale of the geometrical discretisation does not influence the predicted overall energy absorption of a fabric reinforced laminate subjected to impact.

Considering the energy absorption of individual mechanisms, cf. Fig. 5.1 (right), significant differences with respect to the energy dissipated due to plastic deformations (bars with index "PLAST") are observed. The predicted plastic dissipation by the tow-level model is approximately half of the amount which is predicted by the ply-level model. The tow-level model predicts the amount of energy dissipated due to plastic deformations within a ply based on the plastic deformations within the matrix pockets and the tows. The ply-level model considers a fabric ply as a homogeneous material and, therefore resolves the plastic dissipation in a homogenised way. The fluctuations in the stress and strain fields (i.e. stress concentrations) arising due to the fabric topology are not resolved within the ply-level model which, in turn, influences the accumulation of plastic strains. Fig. 5.2 illustrates the distribution of the in-plane shear stress component within the tows and the matrix pockets of a tow-level patch subjected to in-plane shear. The stress concentrations in regions of tow-crossings, as well as in unreinforced resin zones are clearly visible.

Considering the energy dissipated due to delaminations, cf. the bars "DELAM" in Fig. 5.1 (right), there is just a slight difference in the overall dissipated energy. However, within the tow-level model delaminations are also occurring between individual tows whereas this mechanism is not accounted for in the ply-level model. Hence, when comparing just the ply-ply delamination behaviour differences between the models become more apparent. Fig. 5.3 shows a comparison of the delaminated area per

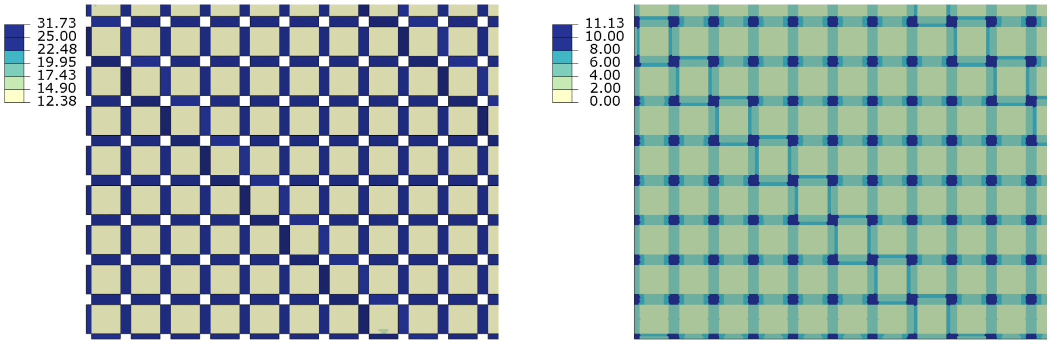

Figure 5.2: Fluctuations in the field of the in-plane shear stress component (in MPa) within a tow-level patch (eight harness satin) subjected to in-plane shear. Left: Tows. Right: Matrix pockets.

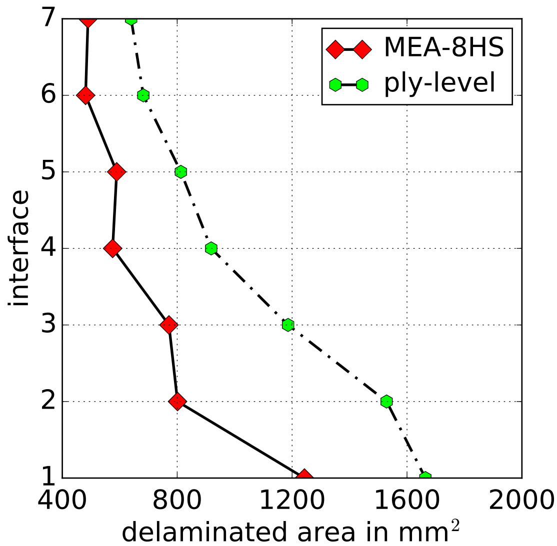

Figure 5.3: Comparison of predicted delaminated area per interface. Interface number one is the one closest to the impact surface of the laminate.

interface between the tow-level model (MEA-8HS) and the ply-level model. It can be seen that the ply-level model predicts larger delaminated areas in every interface. The through-thickness distribution predicted by the ply-level model follows the same trend as predicted by the tow-level model, where the differences get slightly larger towards interfaces at the backside of the laminate. One cause of these differences is, obviously, represented by the tow-level model's capability to account for tow-tow delamination. Another reason is represented by the effect of the fabric topology,

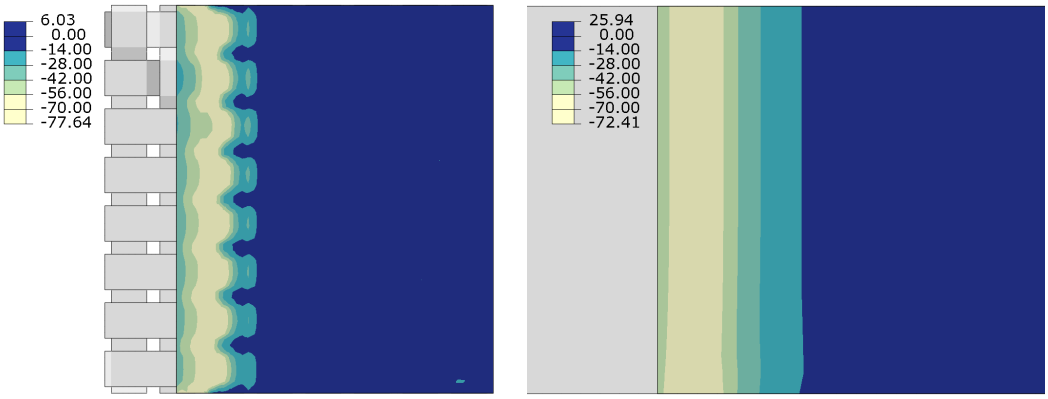

Figure 5.4: Fluctuations in the field of the transverse shear stress component (in MPa) within the middle interface of a laminate in a 3-point bending end notched flexure test. Left: Tow-level model. Right: Ply-level model.

i.e. the fluctuations in the stress and strain fields within the fabric plies, on the interface tractions. Figure 5.4 shows a comparison of the predicted transverse shear stress component distribution within the middle interface of a laminate in a 3-point bending end notched flexure test, cf. [34]. It can be seen that the distribution of the transverse shear stress component is markedly influenced depending on whether the fabric plies are modelled at the tow-level or at the ply-level. As the onset of delamination is predicted by a traction based criterion, the effect of the length scale of the geometrical discretisation of the plies on the distribution of the interface tractions obviously influences the predicted delamination behaviour.

The energy absorbed due to ply damage is represented by the bars "DAMAGE" in Fig. 5.1 (right). Considering the tow-level model, this part of dissipated energy encompasses fibre damage and matrix damage within the tows, as well as matrix damage within the matrix pockets. In the ply-level model, these failure modes are modelled in a homogenised way, i.e. as ply damage. As can be seen, the predicted amount of energy dissipated due to ply damage is almost equal for both models indicating that there is no significant influence of the modelling length scale.

The difference in the recoverable energy, cf. the bars "RECOV" in Fig. 5.1, originates from a different amount of predicted kinetic energy within the laminate, which is higher in the case of the tow-level model. A reason might be that the laminate can be split up into more individual parts (e.g. individual tows may be separated from each other) in the case of the tow-level model and, thus, the damaged laminate exhibits more motion after impact.

Concluding, it is stated that the overall energy absorption of a fabric reinforced laminate subjected to impact is very well predicted by both, the ply-level model and the tow-level model. Considering the energy absorption of individual mechanisms, some differences between the models, especially with respect to the plastic dissipation, are recognisable. Considering the numerical effort, the computation of the impact response of a laminated composite plate in a drop weight impact test setup takes several days in the case of the tow-level model while it takes several hours in the case of the ply-level model. Taking into account the computational efficiency of the ply-level modelling approach and the resulting possibility of simulating the impact behaviour of entire components, the ply-level modelling approach represents a very good compromise between modelling detail and computational effort.

Chapter 6

Structural application

6.1 Introduction

The simulation of impact on FRP laminates is a highly active field of research. FEM simulations of experimental impact tests on unidirectionally carbon fibre reinforced laminates are extensively reported in the literature, e.g. [55, 63, 87, 104, 120]. Considerably less literature is available on numerical investigations of the impact behaviour of glass fibre reinforced laminates, cf. [45, 97]. In the studies [45, 55, 63, 87, 97, 104, 120] coupon specimens are modelled at the length scale of individual plies using three dimensional continuum elements in combination with tri-axial constitutive laws. A major drawback of these models is the quite long computation time even for models of small specimens. This is mainly caused by the large number of degrees of freedom associated with the continuum element discretisation, as very small element dimensions are required due to the small ply thicknesses of typical FRP laminates. In the case of explicit time integration schemes small element dimensions, in addition, decrease the stable time increment. Hence, from the perspective of computational effort such modelling approaches are hardly applicable to simulate the impact response of entire components.

In Ref. [118] a shell element based modelling strategy is applied for simulating the impact response of a FRP laminate in a drop weight impact test setup. The modelling approach shows exceptional computational efficiency while maintaining a high level of predicted details regarding the laminate's damage and failure behaviour and, therefore, features key qualities for modelling impact at component-level. Another step towards component-level impact simulations is presented in Ref. [50], where low velocity impact on a stiffened composite panel is modelled using an embedding approach. Thereby, a ply-level discretisation with continuum elements is used to model a rather small domain at the impact zone, whereas the rest of the panel is modelled in less detail. The very recent paper [61] uses a multiscale superposition technique, cf. [60], to simulate a low velocity impact of a small spherical projectile on a composite sandwich structure. As for Ref. [50], material nonlinearities are just accounted for in a rather small domain in the proximity of the impact zone. The Refs. [50, 61] demonstrate the applicability of embedding techniques to cover the gap in length scales between typical component dimensions and the length scales where damage and failure mechanisms arise. However, the area where the presented models are capable to simulate impact damage, i.e. where material nonlinearities are accounted for, is of the same size as typical coupon specimen dimensions. In aeronautics, there are impact scenarios where components are hit by large bodies, e.g. fan blade out of a jet engine. In such cases, the area of the component which is affected by the impact is considerably larger than typical coupon specimen dimensions. Yet, the author does not know of any modelling approach capable of simulating impact of large bodies on large composite structures up to complete perforation while resolving damage and failure mechanisms in a natural way. Moreover, the prediction of the impact behaviour of glass fibre reinforced laminates has rarely been studied within recent years and the author is not aware of any numerical study dealing with the simulation of high energy impacts on glass fabric reinforced laminates or components.

The present chapter proposes a modelling approach for simulating the impact behaviour of large laminated composite components impacted by large deformable bodies within reasonable computation time and resources. Further attention in this chapter is directed towards the simulation of high energy impact on glass fabric reinforced epoxy laminates up to complete perforation. Advanced methods within the framework of the FEM are applied, where an efficient shell element based modelling strategy in combination with a multiscale embedding approach allows the computational effort to be kept within reasonable bounds. Within a highly resolved subsection of the component, placed at the region where impact and associated material nonlinearities are expected, damage and failure mechanisms are modelled naturally at the length scale of individual plies and interfaces. Regions remote from the impact zone, where no material nonlinearities are expected, are modelled by a common laminate approach. The described modelling approach is used to simulate high energy impact on glass fabric reinforced epoxy components. In a first step, its applicability is verified based on experimental drop weight impact tests. The corresponding material data is obtained from the literature and, thus, no inverse model calibration is applied. Then, to demonstrate an application, two configurations of a generic composite fan containment casing of a jet engine subjected to fan blade out are investigated. The simulations are conducted using the explicit FEM solver Abaqus/Explicit v6.14 (Dassault Systemes Simulia Corp., Providence, RI, USA). Detailed insight into the components' behaviour during the fan blade out event is gained. Eventually, conclusions drawn from such predictions contribute to improvements in the design of impact loaded composite components and help in reducing the experimental effort associated with their design.

6.2 Modelling approach

The present chapter considers the modelling of the nonlinear mechanical behaviour of laminated composite components consisting of several layers of fabric plies. Damage and failure mechanisms arise at small length scales within individual plies and interfaces. In order to account for these mechanisms in a natural way, the geometrical modelling needs to take place at these length scales. Typical component dimensions are orders of magnitude larger and, hence, a wide range of length scales has to be considered when modelling entire components. Therefore, it is appropriate to adapt the length scale of the component's local geometrical discretisation based on the local requirements. Regions where damage and failure is expected to occur are resolved down to the ply-scale, whereas the other regions are modelled at the component-scale. This results in a multiscale description of the component and represents the basis for a numerically efficient model.

6.2.1 Modelling – ply scale

The ply-scale model is intended to describe the material nonlinearities occurring within a fabric reinforced laminate during impact. One objective of the present chapter is to open up the possibility to simulate impact damage within large areas of a component within reasonable computation time and resources. Therefore, the ply-scale modelling approach itself needs to be numerically efficient. In Chapter 4, cf. also Ref. [118], a shell element based ply-scale approach for modelling impact on carbon fabric reinforced laminates is proposed. Thereby, the laminate is modelled as a stack of homogeneous orthotropic plies discretised by individual layers of shell elements. The interfaces between individual plies are modelled using cohesive zone elements (CZEs). This arrangement is called stacked shell approach (SSA) in the following and is schematically depicted in Fig. 6.1.

Individual constitutive laws for plies and interfaces are used to account for the constituents' nonlinear mechanical behaviour. Mechanisms associated with intra-ply damage and failure are accounted for within the shell layers, which model the fabric reinforced plies as homogeneous orthotropic material in combination with an energy based continuum damage mechanics approach to model tensile and compressive damage along the yarn directions. Furthermore, plastic deformation and damage under shear loading are modelled in order to capture the matrix dominated shear re-

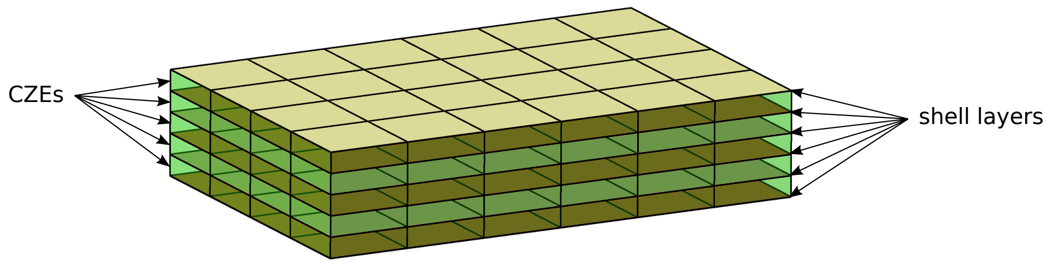

Figure 6.1: Schematic of the stacked shell approach (SSA). The plies are represented by the shell layers at the plies' mid-planes. The CZEs are illustrated as shaded areas between adjacent shell layers.

sponse of the ply. This constitutive model is readily available within the FEM package Abaqus/Explicit as a built-in VUMAT user subroutine (ABQ_PLY_FABRIC), cf. [39]. A summary of this material model is also given in Appendix B. Inter-ply failure, i.e. debonding of plies, is accounted for within the cohesive zone elements which model the interfaces between plies using an uncoupled traction-separation based constitutive law, cf. [29, 40]. Damage initiation is predicted according to the quadratic interaction of interface tractions and damage evolution is modelled based on the critical energy release rates of the interface in combination with a linear softening relation. The interaction of energy release rates under mixed-mode conditions is accounted for using the Benzeggagh-Kenane criterion, cf. [20]. It shall be noted that all material parameters needed to describe the nonlinear material behaviour of plies and interfaces are determinable via independent coupon tests without the need of any inverse model calibration. For more details regarding the ply-scale modelling using the SSA, the reader is referred to Chapter 4 and Ref. [118], respectively.

The described SSA shows exceptional numerical efficiency while giving very good predictions of the qualitative and quantitative impact behaviour of a carbon fabric reinforced coupon specimen in a drop weight impact test setup, cf. Chapter 4 and Ref. [118], respectively. Within the present chapter, the SSA is applied to simulate the damage and failure behaviour within a sub-domain of a glass fabric reinforced component subjected to high energy impact at moderate velocity. In general, glass fibre reinforced epoxy composites exhibit strain rate dependent mechanical behaviour. However, there is no straight consensus on the degree of strain rate sensitivity of the individual mechanical properties within the open literature, cf. the literature review conducted in Ref. [122] where the findings of many experimental investigations are summarised. In the author's point of view the consideration of strain rate sensitive material behaviour will not lead to more accurate predictions due to the uncertainty in the determination of the strain rate sensitive material parameters. Furthermore, the number of material parameters needed to define the constitutive response shall be kept to a reasonably low number, as models get less usable the more complex the material input gets. Therefore, strain rate independent constitutive behaviour of plies and interfaces is modelled within the present chapter. The applicability of the assumption of strain rate independent constitutive behaviour is going to be assessed in Section 6.3.

6.2.2 Modelling – component scale

The component-scale model is intended to represent the mechanical behaviour within regions of the component where no material nonlinearities occur. The laminate is modelled by a single layer of shell elements where the laminate layup is accounted for by a layered shell section definition, cf. [40]. Each ply is considered as homogeneous linear elastic orthotropic material. Debonding of plies is not possible.

The ply-scale model and the component-scale model are combined using an embedding approach to form a model of the entire component. The position where the ply-scale model is embedded into the component-scale model is determined by the position where the impactor hits the component, as material nonlinearities are expected to occur within the proximity of the impact zone. The size and shape of the ply-scale domain needs to be chosen such that all occurring material nonlinearities are contained and decayed towards the domain transition boundary. As the spa-

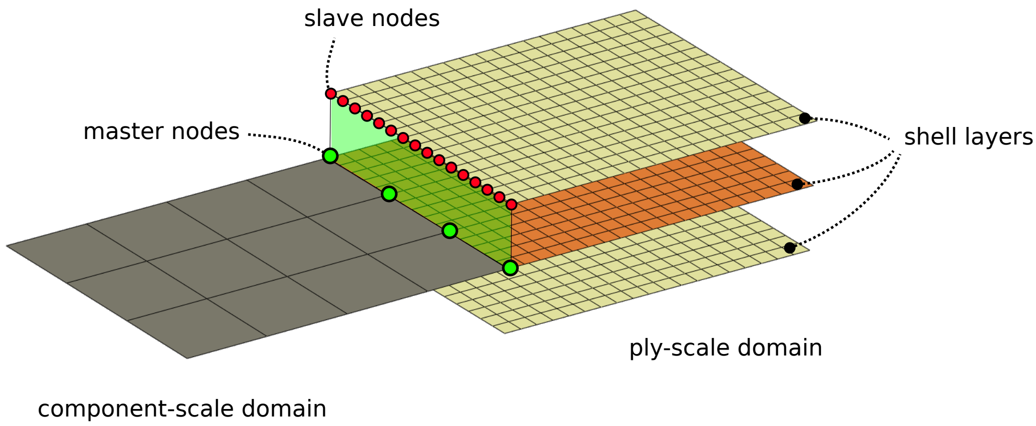

Figure 6.2: Schematic of the coupling between a shell layer of the ply-scale domain (slave nodes) and the shell representation of the component-scale domain (master nodes). See the text for a detailed explanation.

tial extent of the occurring material nonlinearities is usually not known a priori, the ply-scale domain size and shape may be determined iteratively based on preceding simulations.

The ply-scale and the component-scale domain are connected by so-called edge surface based tie constraints, cf. [40]. This constraint is based on a node to surface formulation where the motion of each node on the slave surface is constrained to the motion of the corresponding point on the master surface. The surfaces which are going to be coupled are represented by the edges at the transition between the two domains, cf. Fig. 6.2. The master surface is formed by the edge of the shell layer representing the component-scale domain. The edges of the individual shell layers of the ply-scale domain form the slave surfaces. Note that although these edges are illustrated by lines they represent surfaces and the displacements and rotations of each point on these edge surfaces are evaluated based on shell kinematics. In Fig. 6.2 the coupling between a single shell layer of the ply-scale domain and the shell layer of the component-scale domain is illustrated, where the coupling procedure works as follows. First the position of the slave node is projected onto the master surface in order to evaluate which nodes on the master surface form the constraint. The slave node is then constrained to have the same displacement and rotation as the corresponding point on the master surface. The displacement and rotation at this point are computed based on the element interpolation function and kinematics of the corresponding element on the master surface. Within the present chapter, the edge surfaces which are going to be coupled are perfectly aligned. In the general case of non-aligned edge surfaces, a rigid connection is modelled within the corresponding offset distance.

In contrast to other multiscale embedding approaches, e.g. [50] and [60], the embedding in the present chapter is realised by a pure shell to shell coupling. This multiscale shell to shell coupling is particularly beneficial as the underlying element kinematics are identical for both domains. Moreover, the overall kinematics are identical in both domains for membrane and bending stress states without transverse shear contributions. Therefore, no coupling interferences as e.g. stress concentrations at the domain transition region are expected for such stress states. However, slight interferences may occur for stress states with significant transverse shear contributions, as well as due to significant differences in the in-plane element dimensions between the domains. As the present chapter concentrates on impact scenarios where bending effects are dominating the overall response, coupling interferences should, therefore, be negligible. Nevertheless, to avoid any premature damage and failure possibly arising due to coupling interferences, the shell layers of the ply-scale domain are assigned linear elastic material behaviour within a small region at the domain transition boundary.

The described two-scale shell modelling approach provides a numerically efficient framework for the simulation of the impact response of large composite components. It allows to model damage and failure mechanisms sufficiently detailed within large areas while the computational effort is kept within reasonable bounds.

Another aspect when considering impact on large components concerns the size and the mechanical behaviour of the impactor. The assumption of a rigid impactor, typically taken when simulating the impact response of coupon specimens, cf. [63, 120], may no longer hold true in the case of impact of large bodies on entire components.

Elastic and non-elastic deformations of the impactor contribute to the overall energy absorption during the impact event and, thus, influence the component's impact response. The present chapter considers impactors made from metallic materials. The impactors' constitutive behaviour is modelled as elastic-plastic using a J2 plasticity model. Isotropic strain hardening and rate dependent yield stresses are included. Furthermore, material failure within the impactor is accounted for by a ductile damage approach, cf. [40].

6.3 Verification

In the following, the applicability of the ply-scale modelling approach (SSA) to the simulation of high energy impact on glass fabric reinforced laminates shall be investigated. Particularly, the assumption of strain rate independent constitutive behaviour of plies and interfaces shall be assessed regarding its influence on the predicted energy absorption of the laminate. To this end, a drop weight impact test setup is modelled using the SSA and the simulation results are compared to experimentally measured data.

The E-glass fabric reinforced epoxy prepreg material Hexcel M21/37%/7581/G, supplied by Hexcel Composites (Dagneux, France), is used to fabricate laminated plates. The fabrication is conducted at FACC AG (Ried im Innkreis, Austria). The laminate consists of 14 plies in a $[0/45/0/45/0/45/0]_S$ layup and is autoclave cured under standard conditions recommended by the supplier. The resulting laminate thickness is approximately 3.5 mm. Rectangular test specimens with dimensions of 150 mm times 100 mm are cut out using a water jet cutting plant, where the zero degree fibre direction is parallel to the longer edge of the specimens. Drop weight impact tests are performed on a CEAST 9350 Drop Tower Impact System (Instron, High Wycombe, GB) at the PCCL GmbH (Leoben, Austria), where the test setup and conditions are identical to the ones described in Section 3.3. The total drop weight is 2 kg and an impact velocity of 20 m/s is applied resulting in a total impact energy of 400 J.

Table 6.1: Material parameters of the glass fabric/epoxy plies. The subscript 1 and 2 denote the weft and warp directions, respectively. Details are given in [39] and Appendix B.

elastic	E_1	E_2	ν_{12}	G_{12}	
constants	24 GPa	24 GPa	0.10825	4.8 GPa	
nominal	X_{1+}	X_{1-}	X_{2+}	X_{2-}	S_{12}
strengths	410 MPa	660 MPa	395 MPa	490 MPa	94 MPa
crit. energy	$\mathscr{G}_{\mathrm{Ic}}^{1+}$	$\mathscr{G}_{\mathrm{Ic}}^{1-}$	$\mathscr{G}_{\mathrm{Ic}}^{2+}$	$\mathscr{G}_{\mathrm{Ic}}^{2-}$	
release rate	65 N/mm	65 N/mm	65 N/mm	65 N/mm	
shear	α_{12}	$d_{12}^{\max}$	$\tilde{\sigma}_{\mathrm{y0}}$	C	p
behaviour	0.18634	1.0	55.0 MPa	669.94 MPa	0.823

The described test setup is modelled using the SSA, where a nominal ply thickness of 0.254 mm and a nominal mass density of 2100 kg/m^3 are assigned. The plies are discretised by a regular mesh of 4-noded, fully integrated, linearly interpolated, Mindlin-Reissner type shell elements with an element dimension of 1 mm$\times$1 mm. The thickness integration of the shell elements is conducted using the Simpson rule with 5 section points over the shell thickness. The interfaces are discretised by 8-noded, brick shaped CZEs, which share the nodes of the corresponding shell layers. The boundary conditions of the test setup are modelled in the same way as described in Section 4.3, cf. also Fig. 4.2 where the modelled test setup is illustrated. Note that the impactor is considered rigid within the drop weight impact test model described in the present section.

The material parameters of the glass fabric/epoxy plies are listed in Tab. 6.1. The elastic constants and nominal strengths are taken from a corresponding material data sheet. The critical energy release rates are estimated from Ref. [33]. The plastic behaviour under in-plane shear is assumed based on the typical behaviour of fibre reinforced epoxy laminates. The properties of the interface are listed in Tab. 6.2. The initial stiffness is chosen so that a quasi-rigid connection between the plies is ensured before the emergence of delaminations. The mode II and mode III strengths are taken from a corresponding material data sheet, whereas the mode I strength is

Table 6.2: Parameters describing the initial stiffness of the interface, as well as damage initiation and propagation.

	Mode I	Mode II	Mode III
initial stiffnesses	10^6 N/mm^3	10^6 N/mm^3	10^6 N/mm^3
interlaminar strengths	35.07 MPa	68 MPa	68 MPa
crit. energy release rates	1.21 N/mm	4.55 N/mm	4.55 N/mm

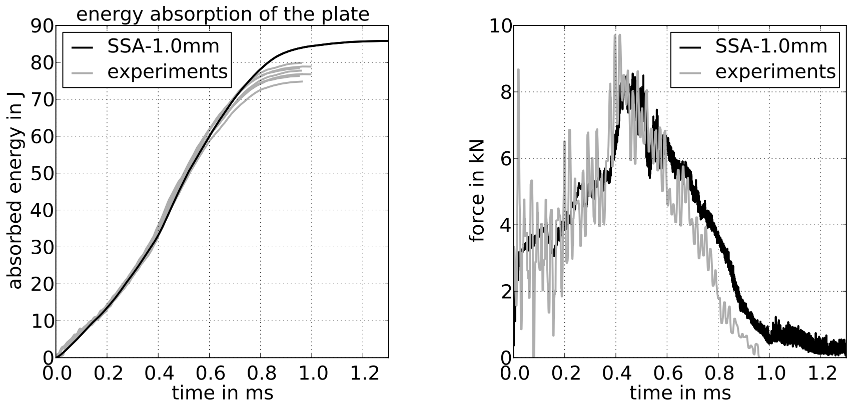

Figure 6.3: Comparison of the total predicted and experimentally measured energy absorption of the laminate (left) and the total force acting on the impactor (right) with respect to time. At the time $t = 0$ms first contact between the impactor and the plate is observed.

evaluated based on the mode II strength according to Ref. [129]. The critical energy release rates are taken from Ref. [46]. As the material parameters characterising the nonlinear mechanical behaviour are based on literature sources and datasheets the results of this verification example are also used to confirm the composed material input.

In Fig. 6.3 (left) a comparison of the total energy absorbed by the laminate with respect to time is shown. The black solid line corresponds to the predicted energy absorption, evaluated based on the reduction of the impactor's kinetic energy, and the grey solid lines represent the experimentally determined energy absorption, determined based on the measured force-time response. As can be seen the whole trend of the predicted energy absorption with respect to time, as well as the total predicted amount of energy absorbed by the plate match very closely with the experimentally determined values and just a slight overprediction towards the end is observed.

A comparison of the total force acting on the impactor with respect to time is shown in Fig. 6.3 (right). Again, the black solid line corresponds to the predicted force-time response and the grey solid line represents the experimentally measured force-time signal. There is a very close agreement of the predicted and measured force-time responses throughout the entire impact event.

The good agreement between the simulations and the experimental results throughout the entire progression of the impact event suggests that rate dependent material behaviour cannot be very distinct for the investigated impact scenario. Therefore, it is concluded that the SSA, in combination with the composed material input, cf. Tabs. 6.1 and 6.2, is applicable to simulate the impact response and, in particular, the energy absorption behaviour of a glass fabric reinforced epoxy laminate impacted at velocities up to 20 m/s. In order to assess the applicability of the present modelling approach to scenarios with even higher impact velocities, of course, further investigations are required as rate dependency may get more distinct in those scenarios. Some preliminary simulations of high velocity oblique impact on glass fabric reinforced laminates in a gas-gun test setup are presented in Appendix C. Once corresponding experimental data is available, these simulations may be used for a further verification of the SSA.

6.4 Application Example

As an example, a generic model of a composite fan containment casing of a jet engine is studied using the presented approach, cf. Fig. 6.4, and its behaviour during a fan blade out event is investigated based on the simulation results. The containment casing is of cylindrical shape with an inner diameter of 834 mm and a width of 358 mm. The edge at the front side of the casing (+z direction) is fully clamped, whereas a free edge is modelled at the back side. The casing is made up of the same glass fabric reinforced epoxy prepreg material as described in Section 6.3, cf. Tabs. 6.1 and 6.2. Two configurations are considered, one featuring 60 plies ($[(0_2/45_2/0_2)_5]_S$) and one featuring 100 plies ($[(0_2/45_2/0_2/45_2/0_2)_5]_S$), where the zero degree fibre direction is parallel to the casing's circumferential direction. A subsection of 93° in circumferential direction is modelled in high detail using the SSA (ply-scale domain). The SSA is applied such that each shell layer represents two adjacent plies with equal orientation. The entire casing is discretised by linearly interpolated, fully integrated four-noded Mindlin-Reissner type shell elements. The thickness integration is conducted using the Simpson rule, where 5 section points over the ply thickness are used. The component-scale domain features an average element edge length of 5 mm. Within the ply-scale domain, the discretisation is identical to the one in the verification example, cf. Section 6.3. The interfaces between individual shell layers within the ply-scale domain are discretised by 8-noded, brick shaped CZEs.

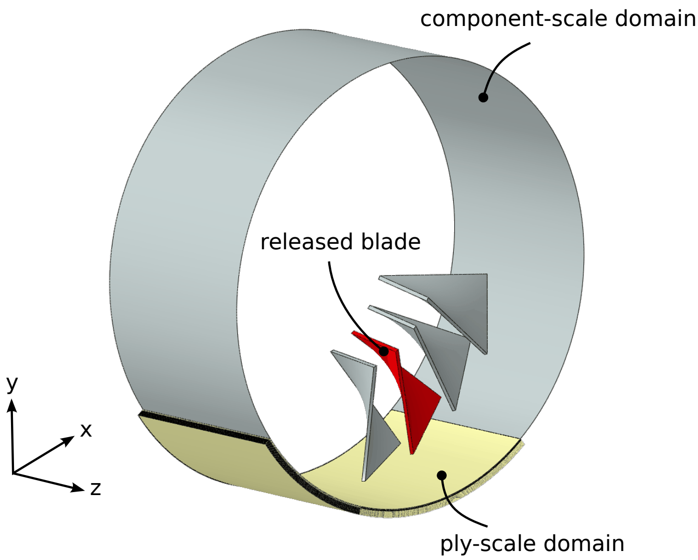

Figure 6.4: Generic model of a jet engine fan blade containment casing. The subsection where impact and associated material nonlinearities are expected is modelled in high detail using a stacked shell approach (ply-scale domain).

Table 6.3: Material properties defining the rate dependent, isotropic strain hardening J2 plasticity model assigned to the fan blades (Ti-6Al-4V). Taken from [98]. See the text for an explanation.

E	ν	$\bar{\varepsilon}_{\mathrm{f}}^{\mathrm{pl}}$	$\mathscr{G}_{\mathrm{f}}$
114 GPa	0.342	0.28	8.0 N/mm
E_{P}	$\sigma_{\mathrm{y}}(\dot{\varepsilon} = 0.001\mathrm{s}^{-1})$	$\sigma_{\mathrm{y}}(\dot{\varepsilon} = 2000\mathrm{s}^{-1})$	$\sigma_{\mathrm{y}}(\dot{\varepsilon} = 6000\mathrm{s}^{-1})$
1.4 GPa	1012.0 MPa	1325.0 MPa	1387.4 MPa

Four titanium fan blades (Ti-6Al-4V) with generic geometry are modelled. Each blade features a length of 212 mm, an average width of 149 mm, and a thickness of 7 mm where the blade's cross-section is twisted along its length direction. With a density of 4390 kg/m^3 of the titanium alloy, cf. [98], the mass of a single blade yields 0.8 kg. The blades are rotating in negative z-direction with an initial rotational velocity of 10,000 rpm. This results in an initial kinetic energy of 42 kJ for each blade. The released blade, cf. Fig. 6.4, is just assigned the initial rotational velocity and its motion is unconstrained from the beginning of the simulation. The other blades are modelled to be driven at constant rotational velocity throughout the fan blade out event. The blades are discretised by 8-noded, fully integrated, linearly interpolated three dimensional continuum elements. The released blade features an average element edge length of 1 mm while the other blades feature an average element edge length of 2 mm. All blades are modelled as elastic-plastic with isotropic strain hardening, rate dependent yield and ductile damage. The material parameters characterising the mechanical behaviour of the blade's titanium alloy (Ti-6Al-4V) are taken from [98] and are listed in Tab. 6.3. E and ν denote the Young's modulus and the Poisson ratio. The uniaxial yield stresses at different strain rates are denoted by $\sigma_{\mathrm{y}}(\dot{\varepsilon})$. E_{P} represents the plastic modulus, which is independent of the strain rate. Ductile damage is initiated at the equivalent plastic strain $\bar{\varepsilon}_{\mathrm{f}}^{\mathrm{pl}}$ and damage evolution is based on the critical energy release rate $\mathscr{G}_{\mathrm{f}}$.

The contact constraints within the simulation are enforced using the general contact algorithm of Abaqus/Explicit, which utilises a penalty algorithm to compute contact forces. Contact is defined between the blades and the individual shell layers within the ply-scale domain. As the trailing blades may collide with the released blade during the fan blade out event, contact between individual blades themselves is modelled. Additionally, contact between each of the shell layers within the ply-scale domain is modelled in order to prevent inter-ply penetration in regions of delamination, cf. Section 4.2. It shall be noted that frictionless behaviour is assumed for every contact definition.

6.4.1 Results and Discussion

In the following, the results obtained for the fan blade out simulations are discussed. Figure 6.5 shows the deformation states of the two investigated configurations (60 plies vs. 100 plies) of the composite containment casing at 1.2 ms after the blade release. The ply-scale domain is depicted in yellow colour and the released blade is highlighted in red colour. As can be seen, the 60-ply casing undergoes severe

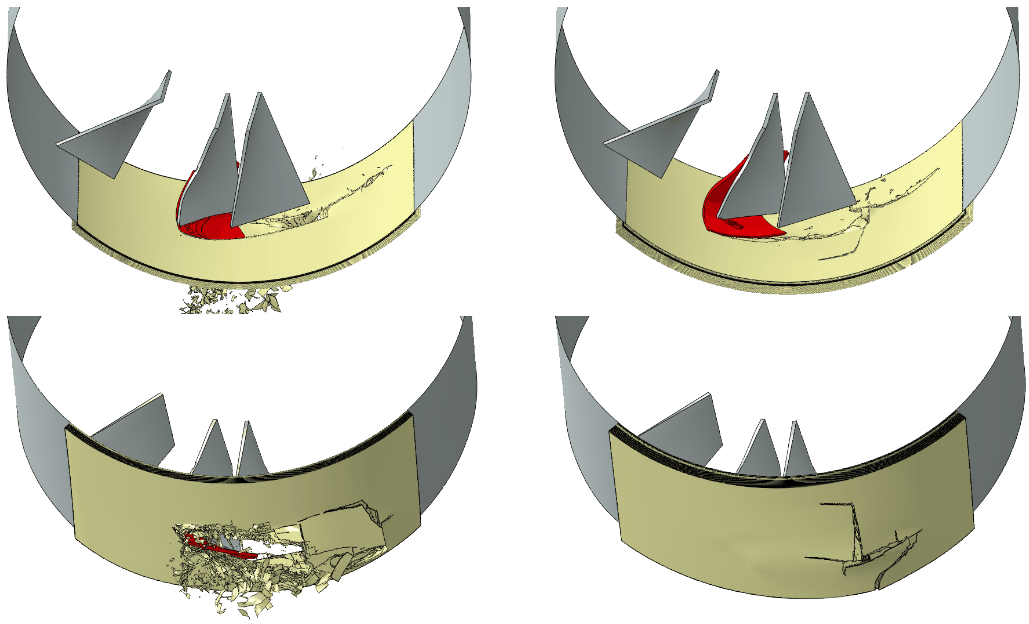

Figure 6.5: Inside (top) and outside (bottom) view of deformed shape of the containment casing at 1.2 ms after blade release. The released blade is highlighted. Left: 60-ply configuration. Right: 100-ply configuration.

Figure 6.6: Cut-view along the xy plane of the 100-ply casing at 1.2 ms after blade release. The cutting plane is positioned at the region where the blade tip hits the laminate.

damage and the laminate is totally perforated within a large area, cf. Fig. 6.5 (left). The released blade first penetrates the laminate in radial direction and then cuts it through the entire thickness along the circumferential direction. This cutting process is additionally driven by the trailing blade which pushes the released blade along the circumference of the casing once they come into contact. The large perforation of the laminate in the 60-ply configuration shown in Fig. 6.5 (left) already suggests that the blade cannot be contained. The 100-ply casing exhibits significantly less damage compared to the 60-ply casing and there is no perforation occurring, cf. Fig. 6.5 (right). Here, the outer tip of the released blade starts to bend rather than to penetrate the laminate, although ply cracks are arising due to the impact of the blade tip. Note that the crack on the outside of the laminate stops to propagate after the blade tip has bent, cf. Fig. 6.5 (bottom right).

So far, the extent of laminate damage is just investigated from viewing its surfaces. In order to evaluate the severity of damage within the 100-ply casing, more information on the through-thickness distribution of cracks is necessary. Figure 6.6 shows a cut-view along the xy plane of the 100-ply laminate at 1.2 ms after the blade release. The position of the cutting plane with respect to the casing's width direction (z-direction) is chosen such that the it lies within the region where the blade tip hits the laminate. At the position of the first impact of the blade tip a crack starting from the inner surface propagates almost through the entire thickness of the lami-

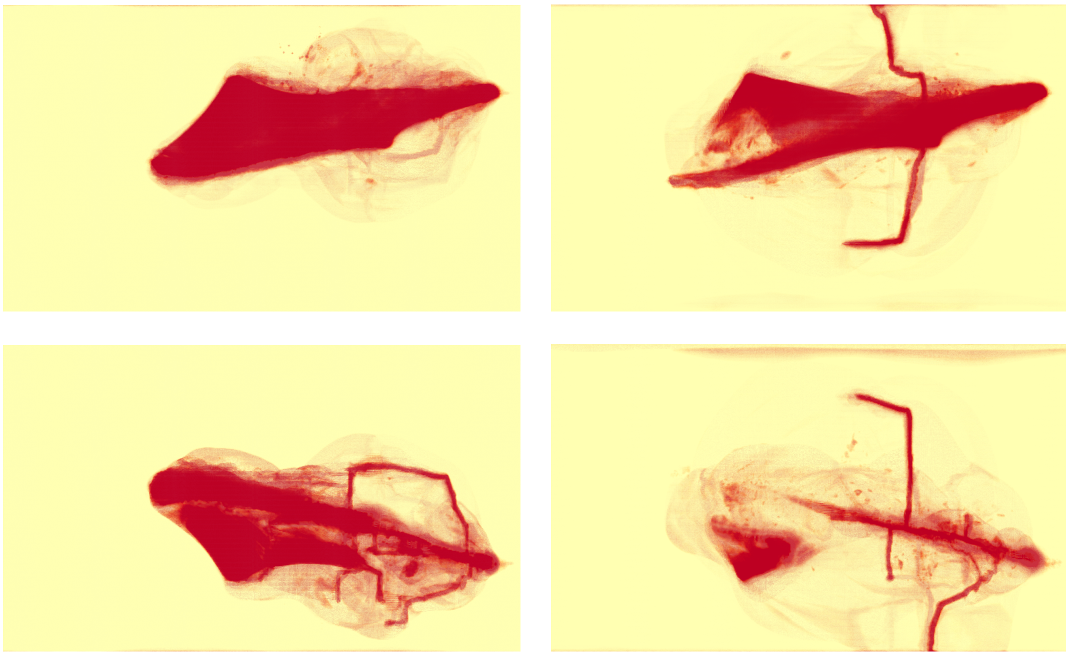

Figure 6.7: Translucent projected view of delaminated areas within the containment casing at 1.2 ms after blade release. View from the inner surface (top) and outer surface (bottom). The blade movement is from right to left. Left: 60-ply configuration. Right: 100-ply configuration.

nate. Large areas of delaminations are evolving from this crack and split the casing into several sub-laminates. Note that the kink within the laminate left of the cracks and delaminations marks the current position of the released blade. The spatial extent of delaminations within both casing configurations is shown in Fig. 6.7, where delaminated areas are visualised in a projected translucent view from the inner and outer surfaces. Note that the blade movement is towards the left in Fig. 6.7. It can be seen that delaminations mostly spread along the circumferential direction and hardly propagate towards the front and back edges of the casing. A major difference between the two casing configurations lies in the distribution of delaminated areas per interface. Within the 60-ply casing large areas of delaminations are emerging in almost every interface whereas in the case of the 100-ply casing just several interfaces show large areas of delamination and the laminate is split into several sub-laminates, cf. Fig. 6.6. Moreover, within the 100-ply casing the delaminated areas are significantly smaller in interfaces close to the outer surface, cf. Fig. 6.7 (bottom).

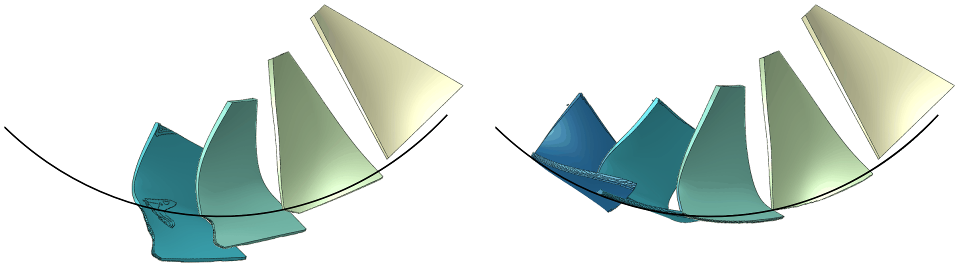

Figure 6.8: Time series of the position of the released blade in steps of 0.4 ms (clockwise rotation). The circular black line represents the inner surface of the undeformed casing. Left: 60-ply configuration. Right: 100-ply configuration.

The spatial extent of the crack along the thickness direction of the 100-ply laminate, cf. Fig. 6.6, is also visible in Fig. 6.7 as delaminations emerge from this crack. The crack shape corresponds to the damage pattern in Fig. 6.5 (right). From Figs. 6.5, 6.6 and 6.7 it is concluded that the structural integrity of the 100-ply casing is retained to a certain degree, whereas the 60-ply casing loses its structural integrity within a large subdomain.

In the following, the motion of the released blade is discussed in more detail. Figure 6.8 shows a time series of the position of the released blade in steps of 0.4 ms. The blade moves in clockwise direction and the inner surface of the undeformed casing is represented by a black solid line. The released blade hits the inner surface of the containment casing with a radial velocity component of approximately 60 m/s at about 0.2 ms after its release. The blade's trailing tip hits the casing slightly before the leading tip comes into contact with the laminate. As can be seen in Fig. 6.8, the motion of the released blade is almost identical for both casing configurations up to 0.4 ms after blade release (second blade position). At this stage, the blade is already in contact with the laminate but no significant penetration occurs yet, although the laminate undergoes elastic deformations. From this point on a different behaviour of the released blade, as well as of the laminate, is observed for the two configurations. In the case of the 60-ply casing, the released blade totally perforates the laminate and the radial outwards motion cannot be stopped. Once the blade has pushed through

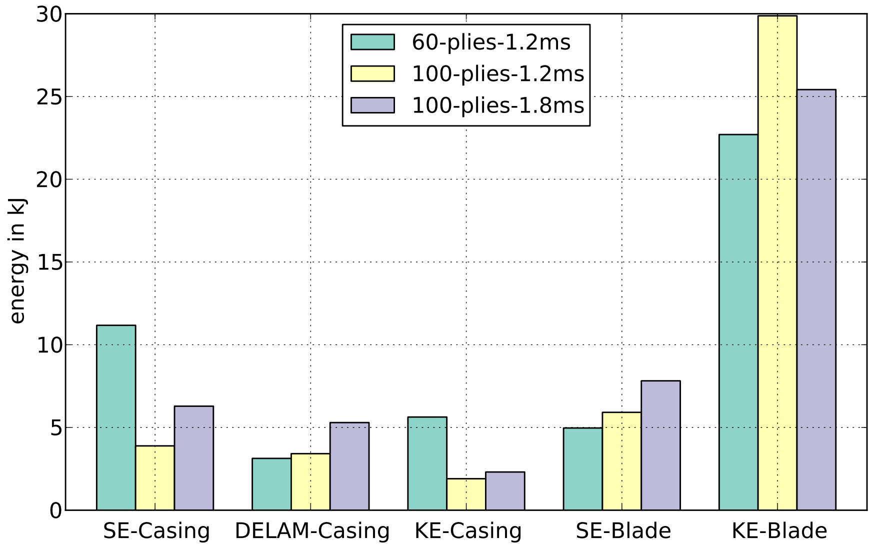

Figure 6.9: Predicted allocation of energy absorption during the fan blade out event. The initial kinetic energy of a single blade is 42 kJ.

the laminate its leading edge cuts the casing along the circumferential direction, cf. last blade position in Fig. 6.8 (left). Considering the 100-ply configuration, the tip of the released blade starts to bend rather than to penetrate the laminate and the blade undergoes significant deformations subsequently. After the blade's tip has bent, the entire blade tilts and the region of contact passes over to the blade's back (downstream) surface, cf. last blade position in Fig. 6.8 (right). The blade's radial outwards motion is stopped in this case and it is concluded that the blade is contained within the 100-ply casing.

Next, the energy absorption behaviour is investigated. Figure 6.9 illustrates the allocation of energy absorption to different mechanisms within the containment casing and the released blade. The two casing configurations are compared at 1.2 ms after blade release and, additionally, the state of the 100-ply casing at 1.8 ms is shown. The bars with index "SE-Casing" represent the total strain energy within the casing and contain the elastically stored energy as well as the energy contributions dissipated due to damage and plasticity within the plies. The energy dissipated due to debonding of plies (delamination) is represented by the bars with index "DELAM-Casing". The bars with index "KE-Casing" represent the kinetic energy of the casing. The total strain energy of the released blade is denoted by "SE-Blade" and sums up the elastically stored energy and the dissipated energy due to plasticity and ductile damage. The kinetic energy of the released blade is denoted by "KE-Blade". Note that the initial kinetic energy of the released blade is 42 kJ. Additional energy is introduced to the released blade due to the collision with the trailing blades. Comparing the energy allocation of the two casing configurations at 1.2 ms after blade release, it can be seen that the 60-ply casing has absorbed more energy at this state and, thus, reduced the kinetic energy of the released blade by a larger amount. Especially the total strain energy is significantly higher within the 60-ply laminate suggesting a greater extent of ply damage in this case. The amount of energy dissipated due to delaminations is equal for both configurations at this state. Considering the difference in the number of interfaces between the two configurations, the relative amount of delaminations is significantly higher within the 60-ply casing. The higher amount of ply and interface damage within the 60-ply laminate is also reflected by the higher amount of kinetic energy, as the casing gets more compliant with increasing damage.

Considering the energy allocation within the released blade, it is observed that a significant amount of energy is absorbed by the blade itself, cf. the bar "SE-Blade" in Fig. 6.9, where the energy dissipated due to plastic deformations within the blade represents the major part. Hence, the consideration of the blade's mechanical behaviour is especially important in this case and the assumption of rigid behaviour would lead to unphysical results.

As the 60-ply casing is already totally perforated at 1.2 ms after blade release, the energy allocation of this configuration is not considered for later stages during the fan blade out event. Considering the state of the 100-ply casing at 1.8 ms after blade release, the energy absorption of the casing has further increased but the overall amount is still less than the one for the 60-ply casing at 1.2 ms, cf. Fig. 6.9. Hence, the process of energy absorption is slower in the case of the 100-ply configuration and, thus, the energy absorption is distributed over a larger area. The distribution of energy absorption represents a key aspect for the casing to withstanding the blade impact, as the local energy absorption capability of the laminate is limited.

Finally, the computational effort is considered. The computations are conducted on a distributed memory cluster consisting of fourteen standard PC workstations with, in total, 44 CPUs at 3.3 GHz. The 60-ply casing model features approximately 45 million degrees of freedom (DOFs) and the computation of the casing response for a time span of 1 ms takes 1.6 days. The 100-ply casing model features about 75 million DOFs and the simulation of 1 ms takes 4.4 days. Taking into account the huge model sizes, this represents an exceptional computational performance and clearly demonstrates that the simulation of impact on entire composite components is possible within reasonable time and resources.

6.5 Summary

A modelling approach for simulating the mechanical behaviour of large composite components impacted by large deformable bodies, by means of advanced methods within the framework of the Finite Element Method, is presented. Thereby, an efficient shell element based modelling strategy in combination with a multiscale embedding approach allows the computational effort to be kept within reasonable bounds. Within a highly resolved subsection of the component, placed in the proximity of the impact zone, damage and failure mechanisms are modelled naturally at the length scale of individual plies and interfaces. Regions remote from the impact zone are modelled by a common laminate approach.

The described modelling approach is used to simulate high energy impact on glass fabric reinforced epoxy components. In a first step, its applicability is verified based on experimental drop weight impact tests. The corresponding material data is obtained from the literature and no inverse model calibration is applied. To demonstrate an application, two configurations of a generic composite fan containment casing of a jet engine subjected to fan blade out are investigated. Detailed insight into the components' behaviour and the emergence and propagation of individual damage and failure mechanisms, and their contributions to the overall energy absorption, throughout the fan blade out event is gained. The simulation results allow for conclusions whether the released blade is contained within the casing. It is found that a key aspect for the casing to withstand the blade impact is represented by its ability to distribute the energy absorption over a large area. Moreover, it is shown that the energy absorption of the blade itself represents a significant part of the overall energy absorption. It is concluded that the proposed modelling approach is capable to simulate the impact response of large composite components within reasonable computation time and resources. Eventually, conclusions drawn from such predictions contribute to improvements in the design of impact loaded composite components and help in reducing the experimental effort associated with their design.

6.6 Publications

The work presented in this chapter resulted in the publications [113, 115].

Chapter 7

Summary

Within the present work, modelling strategies are developed which aim at simulating the impact behaviour of fabric reinforced laminated composites by means of advanced methods within the framework of the Finite Element Method. Not only the total energy absorption of the laminate, but also the share of energy absorbed by individual mechanisms is predicted, where fibre rupture, matrix cracking, delamination and the accumulation of inelastic strains are considered. The application of this work is mainly directed towards high energy impact scenarios with intermediate impact velocities. Hence, the dynamic impact response and penetration of the laminate are modelled. Modelling strategies at different geometrical length scales are developed which on the one hand, aim at gaining a detailed insight into the impact behaviour of fabric reinforced laminates and on the other hand, aim at simulating the impact behaviour of entire composite components.

A shell element based modelling strategy, which resolves the fabric topology at the level of individual tows (i.e. impregnated bundles of fibres) is developed. Thereby, effects arising from the fabric topology, as e.g. fluctuations of the stress and strain fields, are accounted for in a natural way. The modelling approach is verified based on experimental drop weight impact tests of carbon/epoxy laminates carried out by cooperation partners. Very good agreement between the simulation results and the experimental data is found. The predictions give detailed insight into the impact behaviour of fabric reinforced composites and, furthermore, the effect of different weaving styles on the impact energy absorption of individual mechanisms is assessed.

Also, a ply-level based strategy for modelling and simulating the intermediate velocity/mass impact behaviour of fabric reinforced laminates up to complete perforation is developed. Special attention is directed towards numerical efficiency in order to open the possibility for simulating impact on structural components much larger than coupon specimens within reasonable computation time. The modelling approach is verified based on experimental drop weight impact tests of carbon/epoxy laminates carried out by cooperation partners. The predicted damage and failure behaviour is in very close agreement with the experimental observations. Furthermore, the approach is found to be of exceptional numerical efficiency. A detailed comparison of the predicted energy absorption behaviour between the ply-level and the tow-level modelling approach is conducted and the effect of different modelling length scales is evaluated.

Finally, a modelling approach for simulating the impact behaviour of large laminated composite components impacted by large deformable bodies within reasonable computation time and resources is presented. Another focus is set on the simulation of high energy impact on glass fabric reinforced epoxy laminates up to complete perforation. Thereby, the developed ply-level modelling approach is used in combination with an embedding approach. In a first step, the applicability of the ply-level approach to the simulation of high energy impact on glass/epoxy laminates is verified based on a comparison with experimental drop weight impact tests carried out by cooperation partners. Then, to demonstrate an application, two configurations of a generic composite fan containment casing of a jet engine subjected to fan blade out are investigated, where detailed insight into the components' behaviour during the fan blade out event is gained. Eventually, conclusions drawn from such predictions contribute to improvements in the design of impact loaded composite components and help in reducing the experimental effort associated with their design.

Appendix A

Intralaminar fracture toughness testing

A.1 Introduction

Composite laminates exhibit a complex damage and failure behaviour with different modes of failure. These can be summarized as delamination, tensile and compressive intra-ply fracture as well as plasticity like effects. Their individual extent is depending on the loading conditions, the lay-up and the fibre/matrix system. Furthermore, intra-ply fracture may be subdivided into fibre fracture, matrix fracture and fibre/matrix debonding. A quantitative measure describing the resistance to fracture is represented by the critical energy release rate, G_c, which may exhibit different values depending on the crack opening mode. In the case of orthotropic materials, the value of the critical energy release rate may also depend on the crack propagation direction.

The prediction of propagating damage and failure in composite laminates requires appropriate constitutive laws capable of modelling these inherent failure modes, where the critical energy release rates are used to define the fracture behaviour. Thus, knowledge of the critical energy release rates of the considered material is required for quantitative predictions of the fracture behaviour. This chapter discusses methods for the experimental determination of the critical mode I tensile energy release rate associated with intra-ply cracks perpendicular to the fibre direction (i.e. fibre fracture), $G_{\mathrm{Ic}}^{\mathrm{f}}$, with special regard to woven composite laminates.. In the literature $G_{\mathrm{Ic}}^{\mathrm{f}}$ is also denoted as critical mode I intralaminar tensile energy release rate.

A.2 Best practice according to literature

In literature, several configurations of test setups and specimen designs for the determination of the critical mode I intralaminar tensile energy release rate of unidirectionally (UD) fibre reinforced and fabric reinforced composite laminates have been investigated, as reported in the review [83]. Among the described configurations, compact tension (CT) and extended compact tension (ECT) specimens seem to be best suited for isolating the desired failure mode, where the use of CT specimens dominates within the literature.

Besides the test configuration, the method of data reduction, i.e. how the measured quantities (crosshead displacement, force and crack length) are related to the critical energy release rate, is of great importance. Some standards have been developed for determining the critical energy release rate of isotropic materials, e.g. [9], however their data reduction schemes are not appropriate due to the orthotropic nature of the composite specimens, cf. [105]. A comparison of different methods of data reduction applied to laminated carbon/epoxy CT specimens is given in [82], where the so-called modified compliance calibration (MCC) method has been found to be best suited in terms of reproducibility of results and simplicity. This method will be briefly explained in section A.2.2.

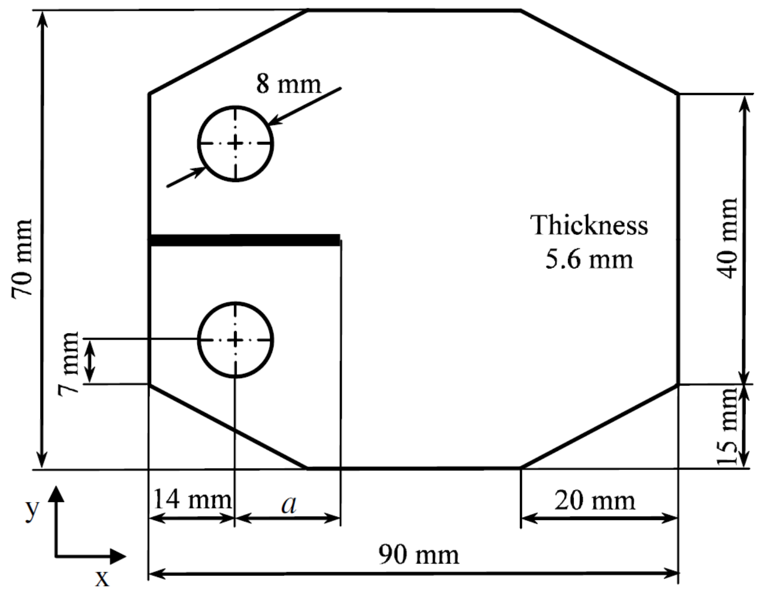

Figure A.1: Proposed 2TCT geometry, cf. [23]. $a = 20$mm

A.2.1 Specimen design

The major goal of specimen design is that no other damage mode than the desired crack propagation is induced during testing, otherwise the results would not be representative. In [23] different geometric configurations of CT specimens of carbon fabric reinforced laminates have been investigated in this regard. The most appropriate design, a so-called doubly-tapered compact tension specimen (2TCT), has been selected for testing, cf. [24]. As reported, the tests have been successfully conducted and no other damage mode than the desired crack propagation has been induced. Therefore, this configuration is proposed for determining the critical mode I intralaminar tensile energy release rate of woven laminates, the dimensions can be seen in Fig. A.1. The machined crack length of the specimen is $a = 20$mm, cf. Fig. A.1, where the last 5mm of the crack are cut using a 0.2mm thick razor blade. Considering the layup, the tows of each ply are aligned with the x and y axes, cf. Fig. A.1, where the number of plies shall be chosen in a way that the stated laminate thickness of 5.6mm is met approximately.

A.2.2 Data reduction - modified compliance calibration

The major advantage of the MCC method, cf. [82], in comparison to the other data reduction schemes is that crack growth does not have to be measured optically. This way, the scatter in the determined resistance curves (R-curves) is reduced significantly. The critical mode I tensile energy release rate, G_{Ic}, can be calculated as,

$$G_{\mathrm{Ic}} = \frac{P_{\mathrm{c}}^2}{2t}\frac{dC}{da}, \tag{A.1}$$

using the change in compliance, C, with crack length, a. P_{c} is the critical load causing crack extension and t the specimen thickness. Within the MCC method, the elastic compliance of the specimen is measured at various machined cracks of known length, where the measurements should be taken in approximately 3mm steps across the whole potential crack growth range in order to capture the compliance vs. crack length response. This response is now fitted with a function of the form

$$C = (\alpha a + \beta)^{\chi}, \tag{A.2}$$

where α, β and χ are the fitting parameters. The effective crack length, a_{eff}, during the fracture toughness test can then be determined from the load-displacement curve and Eq. (A.2) as

$$a_{\mathrm{eff}} = \frac{C_{\mathrm{m}}^{1/\chi} - \beta}{\alpha}, \tag{A.3}$$

where C_{m} is the measured compliance. Hence, the crack length during the fracture toughness test is determined with recourse to the fitted compliance vs. crack length response, Eq. (A.2), obtained from preceding tests. Finally, the critical mode I intralaminar tensile energy release rate corresponding to each measured compliance value, C_{m}, and the resulting effective crack length, a_{eff}, respectively, can be evaluated by

$$G_{\mathrm{Ic}} = \frac{P_{\mathrm{c}}^2}{2t}\,\alpha\chi(\alpha a_{\mathrm{eff}} + \beta)^{\chi-1}. \tag{A.4}$$

Hence, the R-curve behaviour can be obtained directly from Eq. (A.4).

A.3 Potential Challenges

Although the experimental determination of the critical mode I intralaminar energy release rate G_{Ic} of composite laminates seems quite straightforward according to the published literature, the described test methods do not represent standard procedures. The preparation of the crack tip requires special care and is essential for ensuring crack propagation along the desired direction. Furthermore, this work is exclusively based on literature referring to fracture toughness testing of carbon fibre reinforced polymers. The testing of more ductile materials (e.g. glass fibre reinforced polymers) may reveal some challenges, since other failure modes are more likely to occur and, thus, may distort the measured values for G_{Ic}.

Appendix B

Ply constitutive behaviour

The described constitutive model is readily available within the FEM package Abaqus/Explicit as a built-in VUMAT user subroutine and can be accessed by assigning a predefined material name (ABQ_PLY_FABRIC) in the input file, cf. [39]. In the following, a summary of the material model and the governing equations, based on [39], is given. The woven fabric reinforcement considered within the present material model is assumed to have orthogonal fibre (tow) directions. Considering the elasto-damage response, the stress-strain relation reads,

$$\begin{pmatrix} \varepsilon_{11} \\ \varepsilon_{22} \\ \varepsilon_{12}^{\mathrm{el}} \end{pmatrix} = \begin{pmatrix} \frac{1}{(1-d_1)E_1} & \frac{-\nu_{12}}{E_1} & 0 \\ & \frac{1}{(1-d_2)E_2} & 0 \\ \text{symm.} & & \frac{1}{(1-d_{12})2G_{12}} \end{pmatrix} \begin{pmatrix} \sigma_{11} \\ \sigma_{22} \\ \sigma_{12} \end{pmatrix} . \tag{B.1}$$

Plane stress conditions are assumed, where the 1 and 2 directions represent the fibre directions. The strain components are denoted as ε_{ij} whereas stress components are identified by σ_{ij}. E_1 and E_2 are the Young's moduli along the fibre directions, ν_{12} is the Poisson's ratio and G_{12} is the shear modulus. The damage variables along the fibre directions, d_1 and d_2, are further distinguished in tensile and compressive fibre failure modes as d_{1+}, d_{1-}, d_{2+} and d_{2-} where tensile or compressive states are evaluated according to the stress state in the corresponding direction. The damage variable d_{12} is related to matrix micro-cracking due to shear deformation. Note that the shear stress-strain relation in Eq. (B.1) is based on the elastic part of the shear strain, $\varepsilon_{12}^{\text{el}}$, cf. Eq. (B.8).

Considering the response along the fibre directions, the initiation and evolution of the individual damage mechanisms are described using effective stresses defined as,

$$\tilde{\sigma}_{1+} = \frac{\langle \sigma_{11} \rangle}{(1 - d_{1+})} \qquad \tilde{\sigma}_{1-} = \frac{\langle -\sigma_{11} \rangle}{(1 - d_{1-})} \quad , \tag{B.2}$$

for the 1 direction, where similar expressions are used to define the effective stresses for the 2 direction. The angle brackets $\langle \rangle$ in Eq. (B.2) represent the Macaulay operator. In the following, the fibre failure modes are represented by the index α, which may be substituted by 1+, 1-, 2+ or 2-. The elastic domain is defined in terms of damage activation functions as

$$F_\alpha = \phi_\alpha - r_\alpha \leq 0 \quad . \tag{B.3}$$

The functions ϕ_α denote the loading functions and r_α the damage thresholds which read as follows,

$$\phi_\alpha = \frac{\tilde{\sigma}_\alpha}{X_\alpha} \quad \text{and} \quad \mathrm{r}_\alpha(\mathrm{t}) = \max_{\tau \leq \mathrm{t}} \phi_\alpha(\tau) \quad , \tag{B.4}$$

where the variables X_α denote the tensile and compressive strengths along the fibre directions. The damage thresholds are initially set to one and increase according to the consistency condition $\dot{\phi}_\alpha = \dot{r}_\alpha$ upon damage activation. Furthermore, the Kuhn-Tucker conditions are assumed to hold for the damage activation functions and thresholds. Hence, the loading functions in combination with the damage thresholds describe the size of the elastic domain at a given time, t, within the loading history. Damage due to one of the failure modes, α, is assumed to propagate when the value of the corresponding loading function exceeds the one of the corresponding damage threshold. Damage propagation is modelled as exponential strain softening, where the evolution of the damage variables, d_α, is described using the relations,

$$d_\alpha = 1 - \frac{1}{r_\alpha} \exp\left(-A_\alpha (r_\alpha - 1)\right) \quad \text{and} \quad \dot{\mathrm{d}}_\alpha \geq 0 \quad . \tag{B.5}$$

The coefficients A_α are defined as,

$$A_\alpha = \frac{2g_0^\alpha L_\mathrm{c}}{G_\mathrm{Ic}^\alpha - g_0^\alpha L_\mathrm{c}} \quad \text{with} \quad \mathrm{g}_0^\alpha = \frac{\mathrm{X}_\alpha^2}{2\mathrm{E}_\alpha} \quad , \tag{B.6}$$

and relate the damage evolution, Eq. (B.5), to corresponding critical energy release rates, G_Ic^α. L_c represents a characteristic element length. Hence, mesh adjusted softening is implemented, cf. [19], ensuring that the correct amount of energy is dissipated as long as L_c is small enough so that the denominator of A_α stays positive, cf. Eq. (B.6). Considering the response under shear loading, damage initiation is modelled in a similar manner as for the response along the fibre directions, cf. Eqs. (B.2)-(B.4). The evolution of the shear damage variable, d_{12}, is defined as,

$$d_{12} = \min\left(\beta_{12} \ln\left(r_{12}\right),\ d_{12}^\mathrm{max}\right) \quad , \tag{B.7}$$

where β_{12} and d_{12}^max are material properties to be experimentally determined. Hence, it is assumed that shear damage increases proportional to the logarithm of the damage threshold until a specified maximum value is reached. Additionally, plastic behaviour under shear loading is incorporated. Therefore, the shear strain is decomposed into an elastic and a plastic part,

$$\varepsilon_{12} = \varepsilon_{12}^\mathrm{el} + \varepsilon_{12}^\mathrm{pl} \quad , \tag{B.8}$$

and the yield function,

$$F = |\tilde{\sigma}_{12}| - \tilde{\sigma}_0(\bar{\varepsilon}^\mathrm{pl}) \leq 0 \quad , \tag{B.9}$$

is introduced, where $\tilde{\sigma}_{12}$ identifies the effective shear stress, cf. Eq. (B.2), and $\tilde{\sigma}_0$ represents the hardening function which reads,

$$\tilde{\sigma}_0(\bar{\varepsilon}^\mathrm{pl}) = \tilde{\sigma}_\mathrm{y0} + (\bar{\varepsilon}^\mathrm{pl})^p C \quad . \tag{B.10}$$

As can be seen, isotropic hardening is modelled where $\tilde{\sigma}_\mathrm{y0}$ is the initial effective yield stress, $\bar{\varepsilon}^\mathrm{pl}$ the equivalent plastic strain and p and C are constants for the calibration of the hardening curve. Note that in the present case, where plastic deformations occur only due to in-plane shear loading, the equivalent plastic strain, $\overline{\varepsilon}^{\mathrm{pl}}$, is equal to the plastic shear strain, $\varepsilon_{12}^{\mathrm{pl}}$. Associated flow is assumed and the flow rule reads as,

$$\dot{\varepsilon}_{12}^{\mathrm{pl}} = \dot{\overline{\varepsilon}}^{\mathrm{pl}} \frac{\partial F}{\partial \tilde{\sigma}_{12}} = \dot{\overline{\varepsilon}}^{\mathrm{pl}} \mathrm{sign}(\tilde{\sigma}_{12}) \quad . \tag{B.11}$$

Appendix C

High velocity impact simulations

In the following, preliminary simulations of high velocity oblique impact on glass fabric reinforced laminates are presented. Thereby, the qualitative high velocity impact behaviour of laminates in an experimental gas-gun setup shall be predicted.

An illustration of the modelled setup is shown in Fig. C.1. The modelling strategy is identical to the one presented in Chapter 6. The component-scale domain is represented by a single layer of shell elements where the laminate layup is accounted for by a layered section definition. The ply-level domain is modelled using the stacked shell approach (SSA), cf. Chapter 4. The in-plane dimensions of the laminated panel are

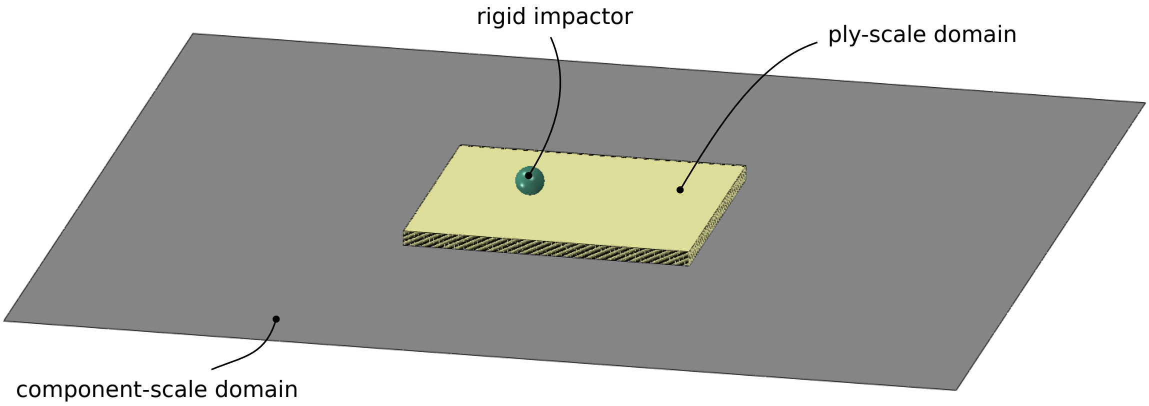

Figure C.1: Modelled experimental gas-gun setup for simulating high velocity oblique impact on glass fabric reinforced laminates.

500 mm×500 mm, where a domain of 150 mm×150 mm in the centre of the panel is modelled at the ply-level. The size of the ply-scale domain is chosen such that all occurring material nonlinearities are contained inside and decayed towards the domain transition boundary. The laminate is clamped along its perimeter and impacted by a spherical steel impactor with a diameter of 15 mm, which is considered rigid. The impact is realised at an angle of 35 ° with respect to the laminate surface, where the impact velocity magnitude is 300 m/s. The resulting impact energy is 624 J.

The discretisation of the ply-scale and the component-scale domain is identical to the one described in Section 6.4. Three different laminate configurations are considered, a 30-ply laminate, a 40-ply laminate and a 60-ply laminate. All of the laminates exhibit an alternating $[0_2/45_2]$ symmetric layup, where the tangential velocity component of the impactor is parallel to one of the tow directions of the ply at the laminates' top surface. Within the ply-scale domain the SSA is applied such that each shell layer represents two adjacent plies with equal orientation. The laminate is made up of the same glass fabric reinforced epoxy prepreg material as described in Section 6.3, cf. Tabs. 6.1 and 6.2.

Figure C.2 shows the time series of the impactor movement in steps of 0.09 ms for the 60-ply laminate configuration. The laminate is depicted in a cut-view corresponding to a state at the end of the impact event. The cutting plane corresponds to the plane of the impactor movement. It can be seen that the impactor penetrates the laminate within a region of about two impactor diameters in length, where delaminations and ply cracks occur throughout the entire laminate thickness. Thereby, the impactor gets decelerated, as indicated by the narrowing distances between the impactor depicted at subsequent states in Fig. C.2. Eventually, the impactor gets deflected.

The impact behaviour of the 40-ply laminate configuration is shown in Fig. C.3. First, the impactor penetrates the laminate whereby its normal velocity component gets significantly reduced. Then, the impactor starts to split the laminate while moving almost horizontally. Thereby, the impactor's tangential velocity component is significantly decreased, as can be seen by the narrowing distances between the

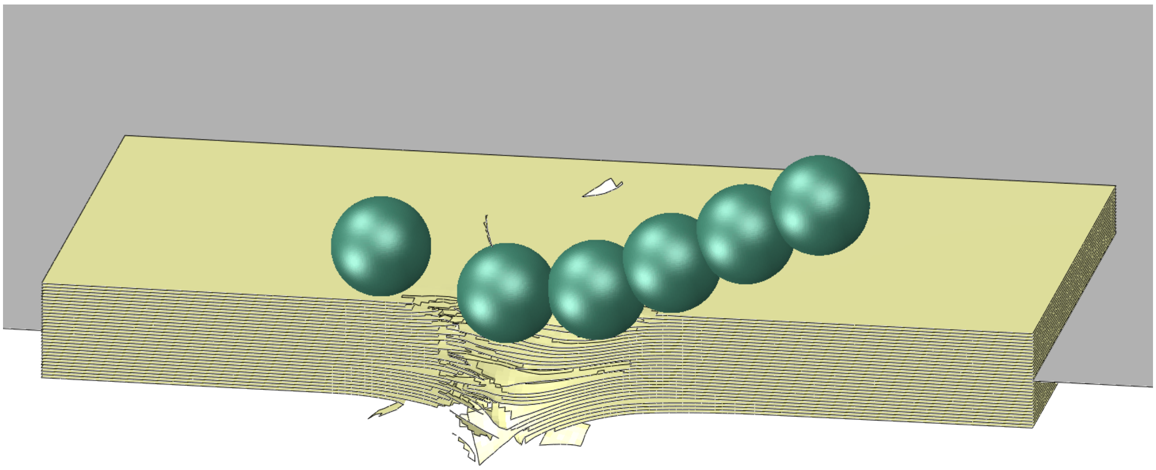

Figure C.2: Time series of the impactor movement in steps of 0.09 ms for the 60-ply laminate configuration. The laminate is shown in a cut-view where cutting plane corresponds to the plane of the impactor movement. The laminate is depicted at a state at the end of the impact event.

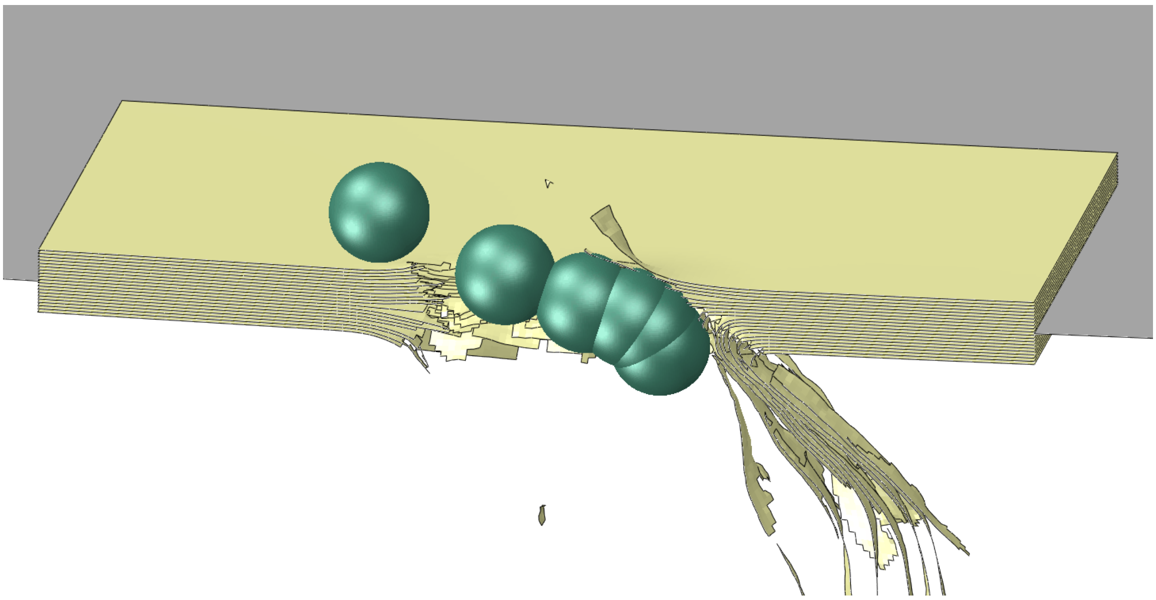

Figure C.3: Time series of the impactor movement in steps of 0.09 ms for the 40-ply laminate configuration. The laminate is shown in a cut-view where cutting plane corresponds to the plane of the impactor movement. The laminate is depicted at a state at the end of the impact event.

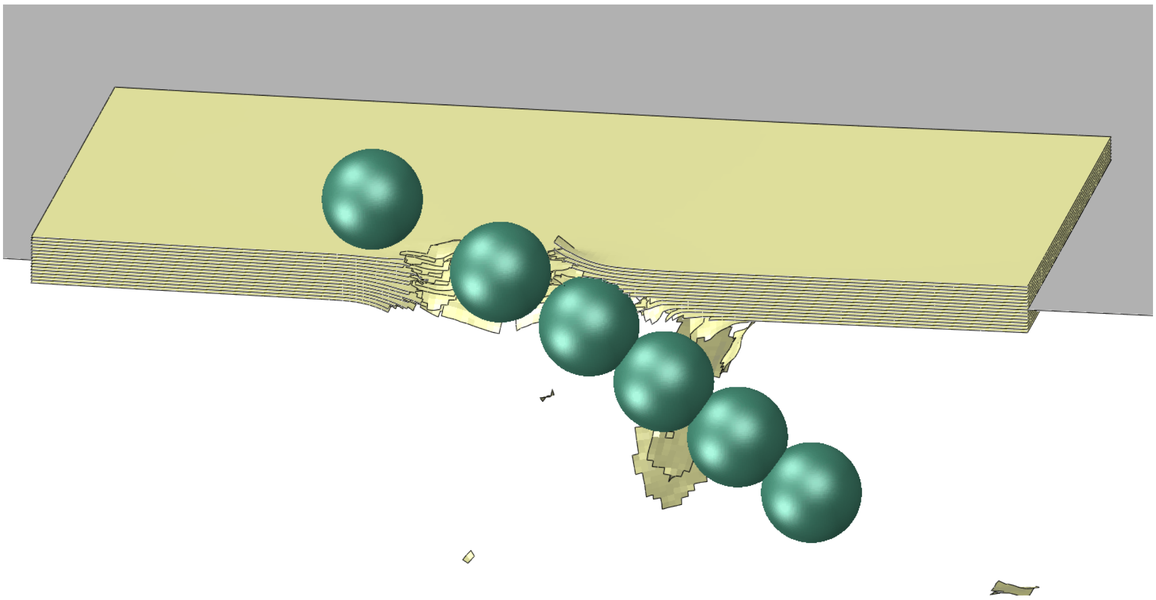

Figure C.4: Time series of the impactor movement in steps of 0.09 ms for the 30-ply laminate configuration. The laminate is shown in a cut-view where cutting plane corresponds to the plane of the impactor movement. The laminate is depicted at a state at the end of the impact event.

impactor depicted at subsequent states in Fig. C.3. Eventually the laminate is fully perforated and the impactor penetrates through the laminate.

Figure C.4 shows the impactor movement in the case of the 30-ply laminate configuration. It can be seen that the impactor penetrates through the laminate with just a slight deflection and deceleration. In contrast to the behaviour of the 40-ply configuration, cf. Fig. C.3, does not split the laminate.

Concluding, it is observed that the predicted extent of impact damaged is of the same scale as the impactor diameter. The modelling approach is found to be able to predict the varying high velocity impact behaviour of glass fabric reinforced laminates with respect to different laminate thicknesses, where the cases of impactor deflection and complete perforation can clearly be distinguished. However, it shall be noted that the applicability of the present approach to the simulation of the high velocity impact behaviour of glass fabric reinforced laminates should be verified with corresponding experiments, cf. the limitations of the SSA stated in Chapter 4. Moreover, the assumption of rate-independent material behaviour may not hold in the case of high velocity impact.

Bibliography

[1] S. Abrate. Impact on laminated composite materials. *Applied Mechanics Reviews*, 44(4):155–190, 1991.

[2] S. Abrate. Impact on laminated composites: recent advances. *Applied Mechanics Reviews*, 47(11):517–544, 1994.

[3] S. Abrate. Modeling of impacts on composite structures. *Composite Structures*, 51(2):129–138, 2001.

[4] S. Abrate. *Impact engineering of composite structures*, volume 526. Springer Science & Business Media, 2011.

[5] M. Aktaş, C. Atas, B. M. İçten, and R. Karakuzu. An experimental investigation of the impact response of composite laminates. *Composite Structures*, 87 (4):307–313, Feb 2009.

[6] G. Alfano. On the influence of the shape of the interface law on the application of cohesive-zone models. *Composites Science and Technology*, 66(6):723–730, 2006.

[7] O. Allix, P. Ladeveze, and A. Corigliano. Damage analysis of interlaminar fracture specimens. *Composite Structures*, 31(1):61–74, 1995.

[8] J. Artero-Guerrero, J. Pernas-Sánchez, J. López-Puente, and D. Varas. Experimental study of the impactor mass effect on the low velocity impact of carbon/epoxy woven laminates. *Composite Structures*, 133:774–781, 2015.

[9] ASTM E399-90. Standard test method for plane-strain fracture toughness of metallic materials. ASTM standard.

[10] C. Atas and O. Sayman. An overall view on impact response of woven fabric composite plates. *Composite Structures*, 82(3):336–345, Feb 2008.

[11] F. Aymerich, F. Dore, and P. Priolo. Prediction of impact-induced delamination in cross-ply composite laminates using cohesive interface elements. *Composites Science and Technology*, 68(12):2383–2390, 2008.

[12] E. Barbero, P. Lonetti, and K. Sikkil. Finite element continuum damage modeling of plain weave reinforced composites. *Composites Part B: Engineering*, 37(2-3):137–147, Apr 2006.

[13] G. I. Barenblatt. The mathematical theory of equilibrium cracks in brittle fracture. *Advances in Applied Mechanics*, 7:55–129, 1962.

[14] S. Bartus. A review: impact damage of composite materials. *Journal of Advanced Materials*, 39(3):3–21, 2007.

[15] S. Bartus and U. Vaidya. Performance of long fiber reinforced thermoplastics subjected to transverse intermediate velocity blunt object impact. *Composite Structures*, 67(3):263–277, 2005.

[16] K.-J. Bathe. *Finite element procedures*. Klaus-Jurgen Bathe, 2006.

[17] J. Baucom and M. Zikry. Low-velocity impact damage progression in woven E-glass composite systems. *Composites Part A: Applied Science and Manufacturing*, 36(5):658–664, May 2005.

[18] J. Baucom, M. Zikry, and A. Rajendran. Low-velocity impact damage accumulation in woven S2-glass composite systems. *Composites Science and Technology*, 66(10):1229–1238, Aug 2006.

[19] Z. P. Bažant and B. H. Oh. Crack band theory for fracture of concrete. *Matériaux et construction*, 16(3):155–177, 1983.

[20] M. Benzeggagh and M. Kenane. Measurement of mixed-mode delamination fracture toughness of unidirectional glass/epoxy composites with mixed-mode bending apparatus. *Composites Science and Technology*, 56(4):439–449, 1996.

[21] G. Bibo and P. Hogg. The role of reinforcement architecture on impact damage mechanisms and post-impact compression behaviour. *Journal of Materials Science*, 31(5):1115–1137, 1996.

[22] G. Bibo and P. Hogg. Influence of reinforcement architecture on damage mechanisms and residual strength of glass-fibre/epoxy composite systems. *Composites Science and Technology*, 58(6):803–813, 1998.

[23] N. Blanco, D. Trias, S. Pinho, and P. Robinson. Intralaminar fracture toughness characterisation of woven composite laminates. Part I: Design and analysis of a compact tension (CT) specimen. *Engineering Fracture Mechanics*, 131:349–360, 2014.

[24] N. Blanco, D. Trias, S. Pinho, and P. Robinson. Intralaminar fracture toughness characterisation of woven composite laminates. Part II: Experimental characterisation. *Engineering Fracture Mechanics*, 131:361–370, 2014.

[25] C. Bouvet, B. Castanié, M. Bizeul, and J.-J. Barrau. Low velocity impact modelling in laminate composite panels with discrete interface elements. *International Journal of Solids and Structures*, 46(14):2809–2821, 2009.

[26] C. Bouvet, S. Rivallant, and J.-J. Barrau. Low velocity impact modeling in composite laminates capturing permanent indentation. *Composites Science and Technology*, 72(16):1977–1988, 2012.

[27] P. P. Camanho and C. G. Dávila. Mixed-mode decohesion finite elements for the simulation of delamination in composite materials. *NASA-Technical paper*, 2002.

[28] P. P. Camanho and S. R. Hallett. *Numerical modelling of failure in advanced composite materials*. Woodhead Publishing, 2015.

[29] P. P. Camanho, C. Dávila, and M. De Moura. Numerical simulation of mixed-mode progressive delamination in composite materials. *Journal of Composite Materials*, 37(16):1415–1438, 2003.

[30] W. Cantwell and J. Morton. Comparison of the low and high velocity impact response of CFRP. *Composites*, 20(6):545–551, 1989.

[31] W. Cantwell and J. Morton. The impact resistance of composite materials - a review. *Composites*, 22(5):347–362, 1991.

[32] G. Caprino, V. Lopresto, C. Scarponi, and G. Briotti. Influence of material thickness on the response of carbon-fabric/epoxy panels to low velocity impact. *Composites Science and Technology*, 59(15):2279–2286, 1999.

[33] G. Caprino, V. Lopresto, A. Langella, and M. Durante. Irreversibly absorbed energy and damage in GFRP laminates impacted at low velocity. *Composite Structures*, 93(11):2853–2860, 2011.

[34] T. Ceglar. Finite element method simulations of the delamination in laminated composite structures. Master's thesis, Institute of Lightweight Design and Structural Biomechanics, Vienna University of Technology, 2016 (submitted).

[35] J.-L. Chaboche. Continuum damage mechanics: Part I - General Concepts. *Journal of Applied Mechanics*, 55(1):59–64, 1988.

[36] J.-L. Chaboche. Continuum damage mechanics: Part II - Damage growth, crack initiation, and crack growth. *Journal of Applied Mechanics*, 55(1):65–72, 1988.

[37] F.-K. Chang and K.-Y. Chang. A progressive damage model for laminated composites containing stress concentrations. *Journal of Composite Materials*, 21(9):834–855, 1987.

[38] K. M. Charlebois, R. Boukhili, O. Zebdi, F. Trochu, and A. Gasmi. Evaluation of the physical and mechanical properties of braided fabrics and their composites. *Journal of Reinforced Plastics and Composites*, 24(14):1539–1554, 2005.

[39] *VUMAT for Fabric Reinforced Composites, SIMULIA Answer 3749*. Dassault Systemes Simulia Corp., Providence, RI, USA, 2008.

[40] *Abaqus Analysis User's Guide. Version 6.14*. Dassault Systemes Simulia Corp., Providence, RI, USA, 2014.

[41] L. Daudeville, O. Allix, and P. Ladeveze. Delamination analysis by damage mechanics: some applications. *Composites Engineering*, 5(1):17–24, 1995.

[42] G. Davies and R. Olsson. Impact on composite structures. *Aeronautical Journal*, 108(1089):541–563, 2004.

[43] G. Davies and X. Zhang. Impact damage prediction in carbon composite structures. *International Journal of Impact Engineering*, 16(1):149–170, 1995.

[44] C. G. Dávila, P. P. Camanho, and A. Turon Travesa. Cohesive elements for shells. © *NASA TP Technical Reports, 2007, núm. 214869*, 2007.

[45] L. Deka, S. Bartus, and U. Vaidya. Damage evolution and energy absorption of E-glass/polypropylene laminates subjected to ballistic impact. *Journal of Materials Science*, 43(13):4399–4410, 2008.

[46] F. Dharmawan, G. Simpson, I. Herszberg, and S. John. Mixed mode fracture toughness of GFRP composites. *Composite Structures*, 75(1):328–338, 2006.

[47] M. Donadon, L. Iannucci, B. Falzon, J. Hodgkinson, and S. de Almeida. A progressive failure model for composite laminates subjected to low velocity impact damage. *Computers & Structures*, 86(11):1232–1252, Jun 2008.

[48] D. Dugdale. Yielding of steel sheets containing slits. *Journal of the Mechanics and Physics of Solids*, 8(2):100–104, 1960.

[49] A. Enfedaque, J. Molina-Aldareguía, F. Gálvez, C. González, and J. LLorca. Effect of glass fiber hybridization on the behavior under impact of woven carbon fiber/epoxy laminates. *Journal of Composite Materials*, 44(25):3051–3068, 2010.

[50] A. Faggiani and B. Falzon. Predicting low-velocity impact damage on a stiffened composite panel. *Composites Part A: Applied Science and Manufacturing*, 41 (6):737–749, 2010.

[51] B. Falzon and P. Apruzzese. Numerical analysis of intralaminar failure mechanisms in composite structures. Part I: FE implementation. *Composite Structures*, 93(2):1039–1046, 2011.

[52] B. Falzon and P. Apruzzese. Numerical analysis of intralaminar failure mechanisms in composite structures. Part II: Applications. *Composite Structures*, 93 (2):1047–1053, 2011.

[53] D. Fanteria, G. Longo, and E. Panettieri. A non-linear shear damage model to reproduce permanent indentation caused by impacts in composite laminates. *Composite Structures*, 111:111–121, 2014.

[54] D. Feng and F. Aymerich. Damage prediction in composite sandwich panels subjected to low-velocity impact. *Composites Part A: Applied Science and Manufacturing*, 52:12–22, Sep 2013.

[55] D. Feng and F. Aymerich. Finite element modelling of damage induced by low-velocity impact on composite laminates. *Composite Structures*, 108:161–171, 2014.

[56] T. Flatscher and H. E. Pettermann. A constitutive model for fiber-reinforced polymer plies accounting for plasticity and brittle damage including softening–implementation for implicit FEM. *Composite Structures*, 93(9):2241–2249, 2011.

[57] J. Gager. *Modeling and Simulation Concepts for Advanced Braided Composites*. PhD thesis, Vienna University of Technology, 2013.

[58] J. Gager and H. E. Pettermann. Numerical homogenization of textile composites based on shell element discretization. *Composites Science and Technology*, 72(7):806–812, 2012.

[59] J. Gager and H. E. Pettermann. FEM modeling of multilayered textile composites based on shell elements. *Composites Part B: Engineering*, 77:46–51, 2015.

[60] L. Gigliotti and S. Pinho. Multiple length/time-scale simulation of localized damage in composite structures using a mesh superposition technique. *Composite Structures*, 121:395–405, 2015.

[61] L. Gigliotti and S. T. Pinho. Virtual testing of large composite structures: A multiple length/time-scale framework. *Journal of Multiscale Modelling*, 6(03): 1550008, 2015.

[62] E. González, P. Maimí, A. Turon, P. Camanho, and J. Renart. Simulation of delamination by means of cohesive elements using an explicit finite element code. *Computers, Materials & Continua (CMC)*, 9(1):51–92, 2009.

[63] E. González, P. Maimí, P. Camanho, A. Turon, and J. Mayugo. Simulation of drop-weight impact and compression after impact tests on composite laminates. *Composite Structures*, 94(11):3364–3378, Nov 2012.

[64] T. Gómez-del Rio, R. Zaera, E. Barbero, and C. Navarro. Damage in cfrps due to low velocity impact at low temperature. *Composites Part B: Engineering*, 36(1):41–50, Jan 2005.

[65] C. Ha-Minh, T. Kanit, F. Boussu, and A. Imad. Numerical multi-scale modeling for textile woven fabric against ballistic impact. *Computational Materials Science*, 50(7):2172–2184, 2011.

[66] C. Ha-Minh, A. Imad, T. Kanit, and F. Boussu. Numerical analysis of a ballistic impact on textile fabric. *International Journal of Mechanical Sciences*, 69:32–39, 2013.

[67] H. Hadavinia and H. Ghasemnejad. Effects of mode-I and mode-II interlaminar fracture toughness on the energy absorption of CFRP twill/weave composite box sections. *Composite Structures*, 89(2):303–314, 2009.

[68] Z. Hashin. Failure criteria for unidirectional fiber composites. *Journal of Applied Mechanics*, 47(2):329–334, 1980.

[69] Z. Hashin and A. Rotem. A fatigue failure criterion for fiber reinforced materials. *Journal of Composite Materials*, 7(4):448–464, 1973.

[70] A. Hillerborg, M. Modéer, and P.-E. Petersson. Analysis of crack formation and crack growth in concrete by means of fracture mechanics and finite elements. *Cement and Concrete Research*, 6(6):773–781, 1976.

[71] N. Hongkarnjanakul, C. Bouvet, and S. Rivallant. Validation of low velocity impact modelling on different stacking sequences of CFRP laminates and influence of fibre failure. *Composite Structures*, 106:549–559, 2013.

[72] L. Iannucci and M. Willows. An energy based damage mechanics approach to modelling impact onto woven composite materials—Part I: Numerical models. *Composites Part A: Applied Science and Manufacturing*, 37(11):2041–2056, Nov 2006.

[73] L. Iannucci and M. Willows. An energy based damage mechanics approach to modelling impact onto woven composite materials: Part II. Experimental and numerical results. *Composites Part A: Applied Science and Manufacturing*, 38 (2):540–554, Feb 2007.

[74] A. Johnson. Modelling fabric reinforced composites under impact loads. *Composites Part A: Applied Science and Manufacturing*, 32(9):1197–1206, 2001.

[75] A. Johnson and M. Holzapfel. Influence of delamination on impact damage in composite structures. *Composites Science and Technology*, 66(6):807–815, 2006.

[76] A. Johnson and J. Simon. Modelling fabric reinforced composites under impact loads. In C. Soutis and I. Guz, editors, *EUROMECH 400: Impact and damage tolerance modelling of composite materials and structures*, 1999.

[77] A. Johnson, A. Pickett, and P. Rozycki. Computational methods for predicting impact damage in composite structures. *Composites Science and Technology*, 61(15):2183–2192, 2001.

[78] J.-K. Kim and M.-L. Sham. Impact and delamination failure of woven-fabric composites. *Composites Science and Technology*, 60(5):745–761, 2000.

[79] H. Körber. *Mechanical response of advanced composites under high strain rates*. PhD thesis, Faculdade de Engenharia. Universidade do Porto, 2010. URL `http://hdl.handle.net/10216/58350`.

[80] P. Ladevèze and E. LeDantec. Damage modelling of the elementary ply for laminated composites. *Composites Science and Technology*, 43(3):257–267, 1992.

[81] P. Ladevèze, O. Allix, J.-F. Deü, and D. Lévêque. A mesomodel for localisation and damage computation in laminates. *Computer methods in applied mechanics and engineering*, 183(1):105–122, 2000.

[82] M. Laffan, S. Pinho, P. Robinson, and L. Iannucci. Measurement of the in situ ply fracture toughness associated with mode I fibre tensile failure in FRP. Part I: Data reduction. *Composites Science and Technology*, 70(4):606–613, 2010.

[83] M. Laffan, S. Pinho, P. Robinson, and A. McMillan. Translaminar fracture toughness testing of composites: a review. *Polymer Testing*, 31(3):481–489, 2012.

[84] I. Lapczyk and J. A. Hurtado. Progressive damage modeling in fiber-reinforced materials. *Composites Part A: Applied Science and Manufacturing*, 38(11): 2333–2341, 2007.

[85] J. Lemaitre and H. Lippmann. *A course on damage mechanics*, volume 2. Springer Berlin, 1996.

[86] S. V. Lomov, D. S. Ivanov, I. Verpoest, M. Zako, T. Kurashiki, H. Nakai, and S. Hirosawa. Meso-FE modelling of textile composites: Road map, data flow and algorithms. *Composites Science and Technology*, 67(9):1870–1891, 2007.

[87] C. Lopes, P. Camanho, Z. Gürdal, P. Maimí, and E. González. Low-velocity impact damage on dispersed stacking sequence laminates. Part II: Numerical simulations. *Composites Science and Technology*, 69(7-8):937–947, Jun 2009.

[88] C. Lopes, O. Seresta, Y. Coquet, Z. Gürdal, P. Camanho, and B. Thuis. Low-velocity impact damage on dispersed stacking sequence laminates. Part I: Experiments. *Composites Science and Technology*, 69(7-8):926–936, Jun 2009.

[89] J. López-Puente, R. Zaera, and C. Navarro. An analytical model for high velocity impacts on thin CFRPs woven laminated plates. *International Journal of Solids and Structures*, 44(9):2837–2851, May 2007.

[90] J. López-Puente, R. Zaera, and C. Navarro. Experimental and numerical analysis of normal and oblique ballistic impacts on thin carbon/epoxy woven laminates. *Composites Part A: Applied Science and Manufacturing*, 39(2):374–387, 2008.

[91] P. Maimí, P. P. Camanho, J. Mayugo, and C. Dávila. A continuum damage model for composite laminates: Part I–Constitutive model. *Mechanics of Materials*, 39(10):897–908, 2007.

[92] P. Maimí, P. P. Camanho, J. Mayugo, and C. Dávila. A continuum damage model for composite laminates: Part II–Computational implementation and validation. *Mechanics of Materials*, 39(10):909–919, 2007.

[93] P. Maimí, J. Mayugo, and P. Camanho. A three-dimensional damage model for transversely isotropic composite laminates. *Journal of Composite Materials*, 42 (25):2717–2745, 2008.

[94] E. Martín-Santos, P. Maimí, E. González, and P. Cruz. A continuum constitutive model for the simulation of fabric-reinforced composites. *Composite Structures*, 111:122–129, 2014.

[95] A. Matzenmiller, J. Lubliner, and R. Taylor. A constitutive model for anisotropic damage in fiber-composites. *Mechanics of Materials*, 20(2):125–152, 1995.

[96] M. May, M. Nossek, N. Petrinic, S. Hiermaier, and K. Thoma. Adaptive multi-scale modeling of high velocity impact on composite panels. *Composites Part A: Applied Science and Manufacturing*, 58:56–64, 2014.

[97] C. Menna, D. Asprone, G. Caprino, V. Lopresto, and A. Prota. Numerical simulation of impact tests on GFRP composite laminates. *International Journal of Impact Engineering*, 38(8):677–685, 2011.

[98] S. Nemat-Nasser, W.-G. Guo, V. F. Nesterenko, S. Indrakanti, and Y.-B. Gu. Dynamic response of conventional and hot isostatically pressed Ti–6Al–4V alloys: experiments and modeling. *Mechanics of Materials*, 33(8):425–439, 2001.

[99] G. Nilakantan, M. Keefe, T. Bogetti, R. Adkinson, and J. Gillespie. On the finite element analysis of woven fabric impact using multiscale modeling techniques. *International Journal of Solids and Structures*, 47(17):2300–2315, 2010.

[100] R. Olsson. Mass criterion for wave controlled impact response of composite plates. *Composites Part A: Applied Science and Manufacturing*, 31(8):879–887, 2000.

[101] F. Pascal, P. Navarro, S. Marguet, and J. Ferrero. On the modelling of low to medium velocity impact onto woven composite materials with a 2D semi-continuous approach. *Composite Structures*, 134:302–310, 2015.

[102] M. Pasquali, C. Terra, and P. Gaudenzi. Analytical modelling of high-velocity impacts on thin woven fabric composite targets. *Composite Structures*, 131: 951–965, 2015.

[103] M. A. Pérez, X. Martínez, S. Oller, L. Gil, F. Rastellini, and F. Flores. Impact damage prediction in carbon fiber-reinforced laminated composite using the matrix-reinforced mixing theory. *Composite Structures*, 104:239–248, 2013.

[104] J. Pernas-Sánchez, J. Artero-Guerrero, J. Z. Viñuela, D. Varas, and J. López-Puente. Numerical analysis of high velocity impacts on unidirectional laminates. *Composite Structures*, 107:629–634, 2014.

[105] S. Pinho, P. Robinson, and L. Iannucci. Fracture toughness of the tensile and compressive fibre failure modes in laminated composites. *Composites Science and Technology*, 66(13):2069–2079, 2006.

[106] S. T. Pinho, C. G. Dàvila, P. P. Camanho, L. Iannucci, and P. Robinson. Failure models and criteria for FRP under in-plane or three-dimensional stress states including shear non-linearity. *NASA Technical Memorandum*, 213530:18, 2005.

[107] A. Puck and H. Schürmann. Failure analysis of FRP laminates by means of physically based phenomenological models. *Composites Science and Technology*, 58(7):1045–1067, 1998.

[108] A. Puck and H. Schürmann. Failure analysis of FRP laminates by means of physically based phenomenological models. *Composites Science and Technology*, 62(12):1633–1662, 2002.

[109] M. Quaresimin, M. Ricotta, L. Martello, and S. Mian. Energy absorption in composite laminates under impact loading. *Composites Part B: Engineering*, 44(1):133–140, 2013.

[110] L. Raimondo, L. Iannucci, P. Robinson, and P. Curtis. A progressive failure model for mesh-size-independent FE analysis of composite laminates subject to low-velocity impact damage. *Composites Science and Technology*, 72(5): 624–632, 2012.

[111] M. Richardson and M. Wisheart. Review of low-velocity impact properties of composite materials. *Composites Part A: Applied Science and Manufacturing*, 27(12):1123–1131, 1996.

[112] P. Robinson and G. A. O. Davies. Impactor mass and specimen geometry effects in low velocity impact of laminated composites. *International Journal of Impact Engineering*, 12(2):189–207, 1992.

[113] M. Schwab and H. E. Pettermann. Prediction of the energy absorption behaviour of large composite components subjected to impact loads - assessment of individual mechanisms at ply scale. In K. Drechsler, editor, *Proceedings of the 17th European Conference on Composite Materials*, 2016.

[114] M. Schwab and H. E. Pettermann. Modelling laminated composites under impact loads. In *Proceedings of the 24th International Congress of Theoretical and Applied Mechanics (extended Abstract)*, 2016.

[115] M. Schwab and H. E. Pettermann. Modelling and simulation of damage and failure in large composite components subjected to impact loads. *Composite Structures*, 158:208–216, 2016.

[116] M. Schwab, M. Todt, and H. E. Pettermann. Simulation of the intermediate velocity impact behaviour of woven composite laminates applying progressive damage models for plies and interfaces. In O. Thomsen, C. Berggreen, and B. Sørensen, editors, *Proceedings of the 20th International Conference on Composite Materials, Paper-ID 4417-4*, 2015.

[117] M. Schwab, M. Todt, and H. E. Pettermann. A multiscale modelling approach for simulating impact damage in woven composite laminates. In S. R. Hallett and J. J. C. Remmers, editors, *Proceedings of the 5th ECCOMAS Thematic Conference on the Mechanical Response of Composites*, 2015.

[118] M. Schwab, M. Todt, M. Wolfahrt, and H. E. Pettermann. Failure mechanism based modelling of impact on fabric reinforced composite laminates based on shell elements. *Composites Science and Technology*, 128:131–137, 2016.

[119] E. Sevkat, B. Liaw, F. Delale, and B. B. Raju. Drop-weight impact of plain-woven hybrid glass–graphite/toughened epoxy composites. *Composites Part A: Applied Science and Manufacturing*, 40(8):1090–1110, 2009.

[120] Y. Shi, T. Swait, and C. Soutis. Modelling damage evolution in composite laminates subjected to low velocity impact. *Composite Structures*, 94(9):2902–2913, Sep 2012.

[121] Y. Shi, C. Pinna, and C. Soutis. Modelling impact damage in composite laminates: A simulation of intra-and inter-laminar cracking. *Composite Structures*, 114:10–19, 2014.

[122] M. M. Shokrieh and M. J. Omidi. Tension behavior of unidirectional glass/epoxy composites under different strain rates. *Composite Structures*, 88 (4):595–601, 2009.

[123] T.-W. Shyr and Y.-H. Pan. Impact resistance and damage characteristics of composite laminates. *Composite Structures*, 62(2):193–203, Nov 2003.

[124] L. Sutherland and C. G. Soares. Impact on low fibre-volume, glass/polyester rectangular plates. *Composite Structures*, 68(1):13–22, 2005.

[125] D. D. Symons. Characterisation of indentation damage in 0/90 lay-up T300/914 CFRP. *Composites Science and Technology*, 60(3):391–401, 2000.

[126] M. Todt, M. Schwab, and H. E. Pettermann. Modeling of transverse shear in layered composite structures with cohesive elements. Technical report, Institute of Lightweight Design and Structural Biomechanics, Vienna University of Technology, 2014.

[127] A. Turon, P. P. Camanho, J. Costa, and C. Dávila. A damage model for the simulation of delamination in advanced composites under variable-mode loading. *Mechanics of Materials*, 38(11):1072–1089, 2006.

[128] A. Turon, C. G. Davila, P. P. Camanho, and J. Costa. An engineering solution for mesh size effects in the simulation of delamination using cohesive zone models. *Engineering fracture mechanics*, 74(10):1665–1682, 2007.

[129] A. Turon, P. Camanho, J. Costa, and J. Renart. Accurate simulation of delamination growth under mixed-mode loading using cohesive elements: definition of interlaminar strengths and elastic stiffness. *Composite Structures*, 92(8): 1857–1864, 2010.

[130] B. Vieille, V. Casado, and C. Bouvet. About the impact behavior of woven-ply carbon fiber-reinforced thermoplastic- and thermosetting-composites: A comparative study. *Composite Structures*, 101:9–21, Jul 2013.

[131] M. Will, T. Franz, and G. Nurick. The effect of laminate stacking sequence of CFRP filament wound tubes subjected to projectile impact. *Composite Structures*, 58(2):259–270, 2002.

[132] Q. Yang and B. Cox. Cohesive models for damage evolution in laminated composites. *International Journal of Fracture*, 133(2):107–137, 2005.

[133] S. Yashiro, K. Ogi, T. Nakamura, and A. Yoshimura. Characterization of high-velocity impact damage in CFRP laminates: Part I–Experiment. *Composites Part A: Applied Science and Manufacturing*, 48:93–100, 2013.

[134] H. Zabala, L. Aretxabaleta, G. Castillo, J. Urien, and J. Aurrekoetxea. Impact velocity effect on the delamination of woven carbon–epoxy plates subjected to low-velocity equienergetic impact loads. *Composites Science and Technology*, 94:48–53, 2014.

[135] O. C. Zienkiewicz, R. L. Taylor, O. C. Zienkiewicz, and R. L. Taylor. *The finite element method*, volume 3. McGraw-hill London, 1977.